Inhibitory Control of Synaptic Plasticity in the Mouse Hippocampus

By

F. Clifford Rodgers

A dissertation submitted in partial fulfillment of
the requirements for the degree of

Doctor of Philosophy
(Neuroscience)

at the

UNIVERSITY OF WISCONSIN-MADISON

2014

Date of final oral examination: 12/10/14

The dissertation is approved by the following members of the Final Oral Committee:

Robert A. Pearce, Professor, Anesthesiology
Matthew I. Banks, Associate Professor, Anesthesiology
Mathew V. Jones, Associate Professor, Neuroscience
Peter Lipton, Professor, Neuroscience
Donata Oertel, Professor, Neuroscience
Misha Perouansky, Professor, Anesthesiology

Dedication

This work is dedicated to my great grandfather, and namesake, Frank Leigh Robeson, Ph.D.

Acknowledgements

Science is never conducted alone. A large number of people have assisted me in producing this thesis both directly in conducting and interpreting the research presented here, and indirectly in with moral support.

Thank you to my committee collectively and individually for many rousing debates. You all have supported my education as a scientist before and during my doctoral work. I know that interactions with you at conferences and journal clubs in the future will continue to enrich my perspective on science and society.

Thank you to my lab members for training, assisting, and encouraging me in this research. Your support is reflected throughout this work in the shared authorship and acknowledgments of the data chapters within, and it is also reflected in the sometimes jury-rigged systems and structures that we have built. I hope those continue to remain useful long after I leave. Thank you especially to my advisor, Bob Pearce, for giving me the chance to pursue this degree, and for supporting me through it.

Additional thanks go out to all of my friends and family who provided moral support over the years spent carrying out this research. Thanks to my parents and brother for daring to visit me, occasionally, during Wisconsin winters. Most of all, thanks to my partner, Martina, for putting up with me.

Table of Contents

Abstract

The hippocampus is one of the most studied structures in the brain. It is known to participate in the formation of declarative memories, and has more recently been implicated in the cognitive representation of space and spatial memory. Our understanding of the function of the hippocampus is intimately tied to experiments measuring amnesia caused by impairment or ablation of the brain structure. The focus of this work seeks to investigate the inhibitory control of synaptic plasticity, a commonly used cellular model for learning and memory, in mouse hippocampus by using etomidate, an anesthetic with a well-characterized pharmacology for γ-aminobutyric acid type A receptors ($GABA_A$Rs) to induce amnesia.

The $GABA_A$Rs, a family of heteropentameric ligand-gated anion channels most commonly composed of two α, two β and one γ subunit, mediate the majority of inhibition in the central nervous system. Previous experiments have shown that etomidate suppresses long-term potentiation (LTP) by enhancing tonic inhibition in CA1 pyramidal cells mediated by α5-subunit containing $GABA_A$Rs. My thesis presents evidence characterizing the likely β subunit partners (possibly β1 or β2) for the α5-containing $GABA_A$Rs targeted by etomidate and that α5-containing $GABA_A$Rs on non-pyramidal cells are sufficient to mediate the inhibition necessary for etomidate to suppress synaptic plasticity.

Additionally I present evidence that a custom-manufactured *in vitro* recording chamber mimicking *in vivo* electrode placement allows for robust characterization of current source densities (CSDs) via simultaneous acquisition. By acquiring data from all *strata* of CA1 simultaneously we were able to characterize CSD during the induction phase of LTP. I also show for the first time that amnestic concentrations of anesthetics suppress synaptic plasticity as measured by CSD. These results contribute to a more precise understanding of the type of inhibition that controls synaptic plasticity.

CHAPTER 1

Introduction

Introduction

Preface

In this thesis I present data collected from *in vitro* slice electrophysiology experiments that were prepared for publication in four manuscripts. I present the relevant background on the inhibition mediated by the γ-aminobutyric acid type A receptor that I study by using the effects of the anesthetic etomidate to perturb a commonly used cellular model of learning and memory. I endeavor to summarize the relevant information in a format that could be used to design a curriculum for teaching the background material, explaining terminology and pointing out where explanations have been simplified for the sake of argument or brevity. At several points in the background review, I compare data from my experiments to previously published accounts. I then present four manuscripts in the following chapters. Subsequently, I summarize the conclusions from these four studies and propose future directions for the work that contributes to my doctoral thesis.

Background

What receptors mediate inhibition that controls learning and memory in hippocampus?

The γ-aminobutyric acid type A receptor ($GABA_AR$) is a membrane-spanning protein made up of a combination five heterogeneous subunits arranged around a central pore, forming an ion channel. Each subunit consists of a large N-terminal extracellular domain, four transmembrane (TM) segments, a large intracellular loop between TM3 and TM4, and an extracellular C-terminal domain (Schofield et al., 1987). The $GABA_ARs$ function as the primary mediators of inhibition in the central nervous system (CNS).

The $GABA_AR$ is a member of the Cys-loop family of genes[1] coding for such receptors as the nicotinic acetylcholine receptor (nAChR; Lindstrom et al., 1995; Gotti et al., 2006), the glycine receptor (Vannier and Triller, 1997; Lynch, 2009), and the serotonin receptor subtype, $5\text{-}HT_3$ (Maricq et al., 1991; Reeves and Lummis, 2002). $GABA_ARs$ are assembled from a pool of at least 19 different subunits comprised of 8 different types: α1-6, β1-3, γ1-3, δ, ε, π, θ, and ρ1-3 (Whiting et al., 1999; Olsen and Sieghart, 2009).

Native CNS $GABA_AR$ structure

Several avenues of inquiry contribute to the ability to discriminate individual pentameric subtypes of the $GABA_AR$ in intact animals. In a 2008 review, Richard Olsen and Werner Sieghart define several criteria for qualification as native

[1] Named for a conserved extracellular motif consisting of two cysteine residues separated by 13 amino acids near the N-terminus.

receptor subtypes broadly based on structure, pharmacology, and function in recombinant[2] and native studies:

1) Colocalization of subunits: in tissue, in individual cells (*in situ* or via single-cell reverse transcription polymerase chain reaction (RT-PCR)), and at a subcellular level (via light and electron microscopy).
2) Physical evidence of subunit interactions: coimmunoprecipitation, for example.
3) Functional evidence: demonstrating pharmacological properties of receptors in real neurons, corresponding to evidence from recombinant studies; genetic modification of a subunit affects specific functions *in vitro* and/or *in vivo*.

Extensive immunoaffinity chromatography, immunocytochemical, immunoprecipitation, and immunodepletion studies have revealed the most likely stoichiometric composition of native $GABA_A$Rs in the central nervous system (CNS) to be two α, two β, and one γ arranged in the sequence γ-β-α-β-α, anti-clockwise when viewed from the perspective of the presynaptic terminal looking "down" across the synaptic cleft (Sieghart et al., 1999; Pirker et al., 2000; Sieghart and Sperk, 2002; Farrant and Nusser, 2005; Olsen and Sieghart, 2008).

[2] Recombinant, expressed receptor studies often require, e.g., artificial conditions to achieve desired levels of protein expression, making them an insufficient preparation to faithfully mimic native receptors. However, despite their artificial nature, recombinant tools can be critically useful in terms of quantifying receptor properties, as I illustrate below.

While there are copious varieties of $GABA_AR$ subunits, *in vitro* expressed receptor studies in *Xenopus* oocytes (α1β1γ2, Pritchett et al., 1989) and HEK 293 cells (α1β1γ2L, Ueno et al., 1996; α1β3γ2, Tretter et al., 1997)[3] have shown that coexpression of α, β, and γ subunits is sufficient to replicate native receptor properties. One possible complication in interpreting the relevance of expressed receptor systems to native receptors is that the cells in which the genes of interest are expressed could themselves contain endogenous systems and substances that influence the characteristics of expressed receptors. For instance, transfected QT6 quail fibroblasts do not express receptors with native $GABA_AR$ properties, while HEK 293 cells transfected with the same genetic material coding for the same subunits (α1, β1, γ2L) did express receptors with properties similar to native receptors (Ueno et al., 1996). The receptors in the QT6 quail fibroblasts either have altered pharmacology or do not express on the surface of the cell.

So, it is worth scrutinizing the particular expression system employed, when interpreting the results of expressed receptor experiments with respect to their greater relevance to the intact organism they are meant to model.

---

[3] The γ subunit has multiple RNA splice variants (Whiting et al., 1990), which are distributed differently in the brain (Miralles et al., 1994) and confer unique functional properties to receptors that incorporate these subunits (Boileau et al., 2010). In this case γ2L refers to the long splice variant, which includes eight more amino acids in the resulting protein's large intracellular loop than γ2S, the short splice variant.

I have previously noted that the most common stoichiometry of the $GABA_AR$ is as a heteropentamer composed of two α, two β, and one γ subunit (see above). But which of the 12 types of these subunits (α1-6, β1-3, and γ1-3; Whiting et al., 1999; Olsen and Sieghart, 2009) are expressed most abundantly in the brain, and in the hippocampus proper?

Ignoring, for a moment, the most common subunits in native $GABA_ARs$, and whether or not, in the case of ρ $GABA_ARs$, these subunits comingle at all in native receptors (Bormann, 2000; Pirker et al., 2000; Sieghart and Sperk, 2002; Olsen and Sieghart, 2008), it is clear that the diversity of known subunits supports a potentially huge variety of receptors: there are many thousands of possible subunit combinations, given 19 $GABA_AR$ subunit types arranged into pentamers (Olsen and Sieghart, 2008). Restricting the pool of potential receptors to pentamers incorporating at least one α, one β, and one γ from a library of 13 receptors common in the rodent brain (Pirker et al., 2000), α1-6, β1-3, γ1-3, and δ1,[4] results in more than 10,000 possible pentameric subunit combinations (McKernan and Whiting, 1996). Reducing the possibility space of $GABA_AR$ subunit combinations to the combinations that are expressed in native receptors

[4] Curiously, they allow for the possibility of a receptor incorporating both γ and δ or multiple γ subunits in the same receptor, both of which possibilities do not apparently occur in nature (Olsen and Sieghart, 2009). But I imagine the intent is simply to illustrate that there many possible receptors can be constructed from these subunits.

is not a trivial exercise. It has been hypothesized that more than 800 distinct $GABA_AR$ subtypes exist in the brain (Barnard et al., 1998).

The term subtype has been used previously in this work, but here it is meant to denote a particular combination of subunits contributing to a distinct and meaningful population of $GABA_ARs$ expressed in a certain region of the CNS. It is conventional to list only the distinct subunits contributing to the pentamer, rather than each of the five individual subunits. When multiple subunits are not listed, one can assume that the pentamer is composed of the usual two αX, two βY, and one γZ subunit combination (see above), where the letters X, Y, and Z denote the particular type of subunit. The most abundant subtype of the $GABA_AR$ seems to be α1β2γ2 (McKernan and Whiting, 1996; Pirker et al., 2000; Olsen and Sieghart, 2008, 2009). In their 2002 review, Sieghart and Sperk also identify several $GABA_AR$ subtypes that appear to be common in a variety of brain areas: α2βγ2, α3βγ2, α4βγ2, α5βγ2, α6βγ2, α6βδ, and α4βδ. Sieghart and Sperk (2002) do not characterize the type of β subunit contributing to this most abundant subtype of $GABA_AR$ in the brain because previous studies did not have antibodies able to differentiate among β subunits available, indicating that receptors incorporating β1 or β3 subunits are possibly common as well, although not the most abundant. More recently definitive evidence has been found for α4β2δ, α4β3δ, α6β2δ, and α6β3δ, as well as the likely native subtypes α1β3γ2, α5β3γ2, αβ1γ/δ, and α1βδ (Olsen and Sieghart, 2008).

Which subunits and subtypes of the $GABA_AR$ are most common in the hippocampus? Immunocytochemical studies indicate that α5 subunits make up ~7-8% of whole brain, they are especially enriched in the hippocampus, where they are present in ~30% of the $GABA_ARs$ (McKernan et al., 1991; Sieghart and Sperk, 2002). So, those subtypes that occur with certain frequencies in the brain, as a whole, may be present in greater quantities in hippocampus proper or, conversely, may be absent. It is necessary to examine the hippocampus as a separate and unique structure, rather than assuming that the $GABA_AR$ subunit and subtype distributions present in the CNS as a whole are reproduced in the hippocampus. I will review the structural and physical evidence for hippocampal native receptor subtypes before diving into the functional evidence for two specific subunits of interest for my work.

Anatomy of the hippocampal formation

Briefly, I'd like to provide a bit of historical perspective to explain the nomenclature used in the present work. The term hippocampus originated in the sixteenth century from the anatomist Arantius (1584; Andersen, 2007), based on the Greek word for sea horse, to which he thought the structure of the dissected human hippocampus bore resemblance. A more general term, hippocampal formation, as well as functionally and cytoarchitectonically distinct Cornu Ammonis (CA) subfields (e.g. CA1) were contributed by the twentieth century

neuroanatomist Rafael Lorente de Nó (1933; 1934), building off of the pioneering work of Santiago Ramón y Cajal (1893, 1968), and further clarified by Theodor Blackstad (1956) and David Amaral (1978). In this work, for simplicity's sake, the term hippocampus is, in principle, meant to include those areas typically excluded from the hippocampus proper, but included in the hippocampal formation (i.e. dentate gyrus, hippocampus, subiculum, parasubiculum, presubiculum, and entorhinal cortex). The information processing circuitry of the hippocampus was later enshrined as the "trisynaptic circuit," a collection of pathways (including the perforant path, mossy fibers, and Schaffer Collaterals) arising in entorhinal cortex (EC), filtering through the DG, CA3, and CA1, before flowing back to the EC (Andersen et al., 1971).

The hippocampus is a laminar structure, like the cortex and other brain areas (Andersen, 2007; Shepherd, 2011), consisting of clearly defined borders (hence, *strata*) between, for example, dendrites, somata, and efferent axons efficiently organized into distinct functional circuits. From the cortical surface toward the hippocampal fissure in CA1 of mouse hippocampus, the layers are *stratum oriens* (SO), *stratum pyramidale* (SP), *stratum radiatum* (SR), and *stratum lacunosum-moleculare* (SLM). Counterintuitively (at least in my opinion), "superficial" in conventional anatomical terms refers to those structures of the hippocampus that are closer to the fissure, whereas "deep" refers to structures closer to the alveus, SO, and the cortical surface. This convention is

intended to keep hippocampal orientation consistent with the conventions for the cerebral cortex, where the white matter is buried several layers beneath the pial surface. It also reflects the developmental folding of the hippocampus into its final configuration.

Layer-specific $GABA_AR$ subunit distribution

At least two groups have investigated the layer-specific distribution of $GABA_AR$ subunits (Sperk et al., 1997; Pirker et al., 2000). My goal in this section is to develop a concordance mapping the likely distribution of $GABA_AR$ subunits in order to inform the investigation and interpretation of targets of anesthetics in CA1.

Susanne Pirker and colleagues (2000) measured layer-specific $GABA_AR$ subunit immunoreactivity (IR) in the hippocampal subfields. I will focus on their results in CA1. They quantified staining intensity over five levels: unstained, sparse staining, moderate staining, strong staining, and maximal staining. Staining density, when reported, was quantified over three levels: individual, moderate, and dense.

In *strata oriens* and *radiatum* (likely lumped together because they contain apical, basal, and oblique dendrites of CA1 pyramidal cells) of CA1 they found IR staining for β1 (moderate diffuse staining), β2 (moderate diffuse staining and moderate staining on moderately densely labeled processes), β3 (strong diffuse

staining), γ2 (moderate diffuse staining and strong staining on moderately densely labeled processes), γ3 (sparse diffuse staining), α1 (moderate diffuse staining and strongly labeled processes of moderate density), α2 (moderate diffuse staining), α4 (moderate diffuse staining), and α5 subunits (strong diffuse staining) of the $GABA_AR$. These data are consistent with findings from Sperk and coauthors (1997), except that Sperk and colleagues found "weak" staining for α3 and δ in *strata oriens* and *radiatum.*

In SP of CA1 Susanne Pirker and colleagues (2000) found IR staining for β1 (mild staining on numerous somata), β2 (moderate staining on moderately densely labeled processes), γ2 (strong staining on individually labeled processes), α1 (strong staining on individually labeled processes), and δ-subunits (sparse staining on dense networks of processes) of the $GABA_AR$. These data are consistent with findings from Sperk and coauthors (1997), except that they found "weak" staining for γ1 subunits and did not observe any immunoreactivity for δ subunits.

In SLM of CA1 Susanne Pirker and colleagues (2000) found IR staining for β1 (moderate diffuse staining), β2 (moderate diffuse staining and moderate staining on moderately densely labeled processes), β3 (strong diffuse staining), γ2 (strong diffuse staining), α1 (moderate diffuse staining), α2 (moderate diffuse staining), α4 (moderate diffuse staining), and α5 subunits (strong diffuse staining) of the $GABA_AR$. These data are consistent with findings from the Sperk group

(1997), except that they found "weak" staining for γ1 subunits and did not observe any immunoreactivity for α4 subunits.

Susanne Pirker and colleagues (2000) looked at interneurons in hippocampus, without regard to their locations in the CA1 and CA3 hippocampal subfields. They found IR staining for β1 (mild diffuse staining on individual cell bodies), β2 (moderate diffuse staining on individual cell bodies), γ2 (maximal diffuse staining on individual cell bodies), α1 (moderate diffuse staining on numerous somata), α3 (sparse staining on moderately densely labeled somata), and δ subunits (moderate staining on individual cell bodies) of the $GABA_AR$. These data are consistent with findings from the Sperk group (1997), except they did not observe β1 subunit or α4 subunit immunoreactivity.

Overall, the reports from the Sperk group (1997) and the Pirker group (2000) were largely consistent. Susanne Pirker and coauthors do not offer an explanation for the previously mentioned exceptions in immunoreactivity for particular subunits that are inconsistent with data from the Sperk group. Given the relatively subjective nature of classifying staining on a five-point scale, such inconsistencies may be trivial.

It is worth mentioning here that, in all of these cases, there is a possibility that some or all of the staining observed could come from non-neuronal cells (Sperk et al., 1997; Pirker et al., 2000). Steps can be taken to identify glial cells based on their morphology, but the $GABA_AR$ subunits they express are sensitive to the

same antibodies and antigens as those expressed in neurons (Sperk et al., 1997). Specifically, Sperk and colleagues observe “faint” β1, γ1, and “possibly” α4 staining in “astrocyte-like structures.” Another report found transient increases in staining, following kainic acid injection, for α3-, α4-, α5-, γ1-, γ3-, and δ-immunoreactivity in astrocytes in hippocampus (Schwarzer et al., 1997).

As previously mentioned, α1β2γ2 $GABA_AR$s are likely the most abundant in the brain (McKernan and Whiting, 1996; Pirker et al., 2000; Olsen and Sieghart, 2009). Therefore, it comes as no surprise that studies have found extensive colocalization of α1, β2, and γ2 in hippocampus, via immunocytochemistry (Fritschy et al., 1992) and immunogold-labeled electron microscopic studies (Nusser et al., 1995; Somogyi et al., 1996). Taking into account the above-mentioned layer-specific distribution of $GABA_AR$ subunit immunoreactivity (Sperk et al., 1997; Pirker et al., 2000), it is likely that α1β2γ2 are expressed across all of the hippocampal layers in CA1, in SO, SR, SP, and SLM; and on interneurons.

Cross-referencing the identified $GABA_AR$ subtypes with the layer-specific immunoreactivity, I can begin to construct a list of the probable distributions of native receptors in CA1. The α2βγ2[5] and α1β3γ2 $GABA_AR$ subtypes are likely

[5] In a 1998 review, Eric Barnard and coauthors identify α2β3γ2 as a native subtype of the $GABA_AR$ in hippocampal pyramidal cells based on evidence coexpression based on multiple staining (Benke et al., 1994; Mohler et al., 1996). Dietmar Benke and coauthors were able to discriminate between antibodies staining for β2 and β2/β3 $GABA_AR$ subunits. Perhaps they are reasoning from prior work on the mRNA distributions for these subunits in hippocampus (Wisden et al., 1992). However they did not see definitive staining for β3, possibly

present in SO, SR, and SLM. The α3βγ2 $GABA_AR$ subtype is likely present in SO and SR, and interneurons. The α4βγ2, α5βγ2, and α5β3γ2 $GABA_AR$ subtypes are likely present in SLM. The αβ1γδ, αβ1δ, and α1βδ are likely present in SO, SR, and SP, and interneurons. And the α4βδ, α4β2δ, and α4β3δ $GABA_AR$ subtypes are inconsistent with the reported layer-specific IR distributions[6].

The project of determining conclusively which subtypes of the $GABA_AR$ are expressed in hippocampus is a murky task that will not be finished any time soon. But I hope that I have demonstrated the progress that has been made, and have convincingly shown that we have some understanding of the diversity of native receptors in hippocampus specifically, and the brain in general.

Location of α5- and β3-containing $GABA_ARs$

At this point, I will begin to narrow my focus to those subunits that I have studied in my thesis work. Namely, I will focus on α5- and β3-containing $GABA_ARs$ as critical participants in the control of learning and memory. I use the term critical participants to mean that these subunits seem to be required for normal learning and memory function. I will review the evidence to support this claim below. By necessity, given the relative lack of specificity in antibody

---

restricting Olsen and Sieghart (2009) from specifying α2β3γ2 as an identified native receptor. Olsen and Sieghart do not address this point.

[6] However, evidence for the presence of α4β2δ and α4βδ $GABA_AR$ subtypes in CA1 of hippocampus has been demonstrated in female mice (Sabaliauskas et al., 2012).

staining and the overlap in pharmacological sensitivities, I will also include some mention of β1 and β2 subunits.

In CA1 hippocampus, $GABA_A$Rs containing α5 subunits do not colocalize with gephyrin, a postsynaptic marker for inhibitory synapses, indicating that they are likely distributed extrasynaptically on the dendrites of pyramidal cells in CA1 SR (Crestani et al., 2002). Given the typical α5 subunit pentameric partners, it seems likely that these are receptors of the α5βγ2 subtype (McKernan et al., 1991; Mertens et al., 1993; McKernan and Whiting, 1996; Semyanov et al., 2004). It is important to note that other $GABA_A$Rs composed of other subunits (e.g. those incorporating δ-subunits) may contribute to nonsynaptic GABAergic transmission in CA1 (as indicated by immunocytochemistry, Sperk et al., 1997; Pirker et al., 2000), and certainly elsewhere in the brain (Nusser and Mody, 2002; Farrant and Nusser, 2005). $GABA_A$Rs incorporating α5 subunits are slow desensitizing and display high affinity for GABA (Capogna and Pearce, 2011). As a consequence of the large cellular surface area covered by these $GABA_A$Rs, they carry significant charge that can affect cellular activity, despite the low concentration of agonist present (Nusser and Mody, 2002; Olsen and Sieghart, 2009). It is likely that α5-containing $GABA_A$Rs contribute to slow phasic inhibitory conductance and tonic inhibitory conductance. In fact, a role for α5-containing $GABA_A$Rs in mediating slow phasic inhibition and tonic inhibition has been shown in recent reports (Caraiscos et al., 2004; Zarnowska et al., 2009).

There is evidence that α5βγ2 $GABA_A$Rs are a native receptor subtype in the hippocampus, comprising 4% of the total $GABA_A$Rs in rat brain (McKernan et al., 1991; Mertens et al., 1993; McKernan and Whiting, 1996; Semyanov et al., 2004). However, due to difficulties discriminating between β1-, β2-, and β3-containing $GABA_A$Rs, it is not clear which of these subunits is most abundant in native hippocampal receptors. Of these three subtypes, the β3 messenger ribonucleic acid (mRNA)[7] and β1 mRNA are present in higher levels in hippocampus than β2 mRNA (Wisden et al., 1992), indicating that these subunits are likely being synthesized in hippocampal cells, however telling nothing about whether they form working, expressible receptors. Pharmacological evidence also indicates that α5βγ2 $GABA_A$Rs are present on interneurons in SO (Patenaude et al., 2001). Immunodepletion and pharmacological studies suggest that α5β3γ2 have a high probability of existence as a native $GABA_A$R subtype because α5 and β3 subunits are co-depleted, indicating that they likely exist in the same receptor pentamer, and expressed recombinant α5β3γ2 $GABA_A$Rs have similar properties to those in a subset of CA1 hippocampal pyramidal cells (McKernan et al., 1991; Mertens et al., 1993; Burgard et al., 1996; Sur et al., 1998; Olsen and Homanics, 2000; Caraiscos et al., 2004). This evidence does

[7] mRNA is a chemical code that transmits a signal from the genetic information in the deoxyribonucleic acid (DNA) in the nucleus of the cell to the ribosomal machinery that will eventually synthesize a protein (in this case, the β3 $GABA_A$R subunit).

not conclusively rule out the possibility of native α5β2γ2 $GABA_A$Rs. It must also be noted that subtypes of $GABA_A$R incorporating both subunits may exist (i.e. α5β3γ2 and α5β2γ2 $GABA_A$Rs) natively in hippocampus, but may differ in the nature of their functional roles in the native neural network. It should also be mentioned that these subunits do not need to be incorporated into the same receptor to critically (and potentially synergistically) affect the function of inhibition in hippocampus.

Specifically, evidence from recombinant expressed receptors (Burgard et al., 1996) indicates that, while they have similar sensitivity for GABA, α5β3γ2L and α5β2γ2L $GABA_A$Rs differ in current-voltage response showing outward rectifying and nonrectifying (i.e. linear) relationships, respectively. These receptor subtypes also differ in terms of desensitization to GABA at high concentrations (300 μM), with β3 subtype-containing receptors showing less desensitization at depolarized membrane potentials than β2 subtype-containing receptors.

Ionic basis of GABAergic inhibition

$GABA_A$Rs form ion channels permeable to Cl^- and bicarbonate anions in the membranes of CNS cells and they are responsible for mediating the majority of fast inhibitory transmission in the CNS (Whiting et al., 1999; Farrant and Nusser, 2005). The $GABA_A$R is named for its ligand, γ-aminobutyric acid (GABA). When

bound GABA causes a conformational change in the $GABA_AR$ protein, opening a pore in the neuronal membrane, allowing Cl^- to flow.

In the resting state, adult neurons have a negative electrical potential across their cellular membranes. Neurons tend to have higher intracellular concentration of K ions, and lower intracellular concentrations of Na^+ and Cl^-, in respect to the extracellular milieu. These gradients set-up a driving force for ionic movement against electromagnetic repulsion, and because the cellular membrane is selectively permeable to these ions via pores, such as the Cl^--fluxing pore in the $GABA_AR$. Also critical for maintaining cellular membrane potential are ion pumps and transporters, proteins that move ions against their concentration gradients (Farrant and Nusser, 2005). Otherwise in adult neurons, Na^+ would constantly move into the cell and K^+ would constantly leak out via passive flux through the permeable cell membrane until the concentration of ions inside and outside the cell reached equilibrium. The equilibrium potential for each ion refers to the cellular membrane potential that results in no net ionic movement across the membrane despite the presence of conductance for that ion[8]. Under normal conditions, when the cell generates a conductance for a particular ion, it will drive the cellular membrane potential toward the equilibrium potential, or reversal potential, of that ion.

---

[8] The Nernst equation models reversal potential for a single ion. In cells that are permeable to multiple ions, the Goldman-Hodgkin-Katz equation models the reversal potentials, and can be used to calculate resting membrane potential *a priori*.

Manipulating equilibrium potentials by changing the ionic milieu outside the cell (as in cell-attached recordings) and inside the cell (via dialysis, as in whole-cell recordings) are core techniques to isolate and measure ionic currents, ionic conductances, and dynamic membrane potentials in patch clamp electrophysiology recordings.

The K^+ and Na^+ ionic conductances are critical to generating action potentials, the all-or-none electrical signals that constitute the output of neuronal computation. The Cl^- conductance, on the other hand, acts as a sort of brake on the system through two primary means: phasic and tonic inhibition. Cl^- transporter proteins (KCC2, the K-Cl co-transporter, e.g., Farrant and Nusser, 2005; Chamma et al., 2012)[9] play a critical role in determining the effect Cl^- flux will have on the membrane potential, with Cl^- possibly depolarizing younger neurons (thus, in young neurons, GABA is an excitatory neurotransmitter), which have higher intracellular Cl^- due, in part, to relatively low levels of Cl^- transporter protein expression (Khalilov et al., 2005; Andersen, 2007). However this is a slight simplification, since it is still possible for net inhibition to occur as the cell becomes leakier (via shunting inhibition), and as a function of the spatiotemporal dynamics of the incoming excitation and fluctuating membrane conductance and voltage (Farrant and Nusser, 2005).

---

[9] The K-Cl co-transporter moves Cl^- against its electrochemical gradient (i.e. toward a higher concentration outside the cell, $[Cl^-_O]$) using energy from the K^+ gradient, which has been set up by activity of adenosine triphosophate (ATP) at the Na-K ATPase membrane transport protein (Chamma et al., 2012).

Types of GABAergic inhibition

As stated previously, the $GABA_AR$ can mediate a type of inhibition called shunting inhibition, which hyperpolarizes the membrane potential toward resting potential when the membrane is depolarized and depolarizes the membrane toward resting potential when the membrane is hyperpolarized. This has the effect of decreasing input resistance locally, and blunts the amplitude of any excitatory post-synaptic potentials (EPSPs) coming in near the source of shunting inhibition (Andersen, 2007).

Inhibition mediated by $GABA_ARs$ takes primarily two major forms: phasic and tonic (Farrant and Nusser, 2005). Phasic inhibition is activated in a temporally precise manner, marked by periods of active inhibition when presynaptic GABAergic cells fire, releasing GABA, and increasing the concentration of GABA to a high level (approximately 3mM) for a brief period of time before GABA diffuses away from the synaptic cleft (with a decay time constant (τ_{decay}) of approximately 100 μs, Mozrzymas et al., 2003)[10]. Tonic GABAergic inhibition arises from action-potential-independent sources outside of the classical synapse between two neurons (Semyanov et al., 2004). As such, extrasynaptic inhibition

[10] These numbers reflect parameters in a model used to explain observed effects of pH on GABAergic transmission. There are many other ways to derive values for the concentration of GABA at the synapse, as direct measurement is exceedingly difficult at present. So, far from definitive, these values are meant to serve as a gross approximation of scale (Mozrzymas et al., 2003).

must arise from lower concentrations of neurotransmitter than locally high concentrations within the synaptic cleft at a GABAergic synapse. These types of inhibition exist throughout the CNS (Farrant and Nusser, 2005; Capogna and Pearce, 2011), but in this work, when possible, I will focus on CA1 of the hippocampus.

Phasic GABAergic transmission is likely affected by a number of different parameters, including: vesicle size, quantal release size, vesicle fusion, synaptic geometry, and the location and quantity of both $GABA_A$Rs and transporters (Farrant and Nusser, 2005). The kinetics of conformational changes of individual $GABA_A$Rs, modeled by transitions between open, closed, and desensitized states, also play a large role in determining macroscopic characteristics of GABAergic transmission. The onset time course of fast phasic inhibition measured by recording miniature inhibitory postsynaptic currents (mIPSCs) in the presence of the fast, voltage-gated Na^+ channel blocker tetrodotoxin (TTX; i.e. action-potential independent), thought to arise from the spontaneous quantal release of a single presynaptic vesicle (Otis and Mody, 1992), is around 100 μs, which depends on the kinetic rate of receptor opening and the proximity to the presynaptic site of release (Farrant and Nusser, 2005). The phasic GABAergic response then decays, undergoing a macroscopic process called deactivation, which is composed of interactions between multiple conformational state changes in multiple $GABA_A$Rs (Jones and Westbrook, 1995; Farrant and Nusser,

2005). The previous example illustrates a simple case of phasic GABAergic transmission. Action-potential dependent phasic inhibition can involve asynchronous release from multiple spatially segregated presynaptic sites, with diffusion of GABA to perisynaptic, extrasynaptic and presynaptic receptors (Farrant and Nusser, 2005).

I see evidence that fast phasic inhibition is present in my extracellular recordings from CA1 hippocampus because I see clear single population spikes (PS) evoked upon SC stimulation, rather than multiple PS, as in the presence of bicuculline (e.g., Pearce, 1993). As detailed further below, it is likely that this inhibition is mediated directly or indirectly by interneurons (e.g. BCs) contributing to fast feedforward inhibition[11] at the basal pyramidal cell dendrites or at pyramidal cell bodies.

There is another form of phasic GABAergic synaptic transmission called $GABA_{A,slow}$ (Pearce, 1993) with IPSCs characterized by slow rise and decay kinetics, which distinguish it from faster currents mediated by $GABA_{A,fast}$ (also referred to as fast phasic GABAergic inhibition) and slower inhibition mediated by $GABA_BRs$[12] (Capogna and Pearce, 2011). $GABA_{A,slow}$ currents have τ_{decay} greater

[11] The terms feedforward and feedback inhibition refer to the source of synaptic activation that elicits inhibition. For the purposes of this work, in CA1 pyramidal cells feedforward inhibition is typically activated by glutamate release from SC axons. Feedback inhibition is typically activated by local glutamate release from CA1 pyramidal cell axons.

[12] $GABA_BRs$ are metabotropic receptors, which affect Ca^{2+} and K^+ channels via G proteins and second messenger systems (Bormann, 2000). Controlling for

than 30 ms, which refers to a parameter used to characterize a linear time invariant system (typically it involves an exponential function) that models the dynamics of the measured current. Although there is usually slight variation of decay time among phasic GABAergic IPSCs, $GABA_{A,fast}$ and $GABA_{A,slow}$ arise from different presynaptic populations and likely involve distinct biophysical mechanisms (Capogna and Pearce, 2011).

$GABA_{A,fast}$ is blocked by the noncompetitive, reversible $GABA_A$ channel blocker furosemide at a concentration of 600 μM, which leaves $GABA_{A,slow}$ intact (Pearce, 1993; Banks et al., 1998). Similarly, NO-711, a GABA uptake inhibitor, prolongs the τ_{decay} of evoked $GABA_{A,slow}$ 2-fold without altering the peak amplitude of the IPSC, while leaving spontaneous $GABA_{A,fast}$ unaffected (Banks et al., 2000). $GABA_{A,fast}$ is more sensitive to the volatile anesthetic enflurane, than $GABA_{A,slow}$, which, in contrast, is more sensitive to the volatile anesthetic halothane (Pearce, 1996).

It is likely that distinct populations of interneurons give rise to $GABA_{A,slow}$ and $GABA_{A,fast}$ IPSCs (Szabadics et al., 2007). One line of evidence supporting this claim is that action-potential dependent spontaneous IPSCs (sIPSCs) in CA1 pyramidal cells do not display mixed $GABA_{A,fast}$ and $GABA_{A,slow}$ kinetics (Otis and Mody, 1992; Banks et al., 1998; Banks et al., 2000). The lack of mixed kinetics

---

inhibition mediated by $GABA_B$Rs, for instance by blocking it with the competitive antagonist saclofen, is an important test when trying to practically determining whether recorded phasic inhibition is truly $GABA_{A,slow}$.

also discounts involvement of $GABA_BRs$ in mediating $GABA_{A,slow}$ inhibition (Price et al., 2005); although they are likely present on presynaptic terminals due to their involvement in paired-pulse depression of $GABA_{A,slow}$ IPSCs, but not suppression of fast inhibition (SFI; Banks et al., 2000; Capogna and Pearce, 2011). If sIPSCs showed mixed kinetics for $GABA_{A,fast}$ and $GABA_{A,slow}$, it would be consistent with action-potential dependent generation of both types of sIPSC kinetics in a single interneuron. Specifically, in hippocampus, the current wisdom states that dendrite-targeting neurogliaform cells (Price et al., 2005; Price et al., 2008) and Ivy cells (Fuentealba et al., 2008) give rise to $GABA_{A,slow}$ in CA1 pyramidal neurons (Klausberger and Somogyi, 2008; Capogna and Pearce, 2011), whereas somatic basket cells primarily mediate $GABA_{A,fast}$ (Buhl et al., 1995; Banks et al., 1998; Klausberger and Somogyi, 2008). It is unclear whether populations of oriens lacunosum-moleculare (OLM) cells, interneurons located in SO, give rise to IPSCs with characteristics that are primarily $GABA_{A,fast}$ (Ali and Thomson, 1998; Pouille and Scanziani, 2004; Biro et al., 2005; Andersen, 2007), $GABA_{A,slow}$ (Pouille and Scanziani, 2004; Hentschke et al., 2009) or some combination of the two.

Another piece of evidence supporting separate populations mediating $GABA_{A,fast}$ and $GABA_{A,slow}$ in CA1 is the previously mentioned phenomenon known as SFI. When $GABA_{A,slow}$ IPSCs are evoked in hippocampal slices via electrical stimulation in SLM of CA1, there is an action-potential dependent

(meaning the phenomenon is blocked by the application of TTX) suppression of ongoing spontaneous $GABA_{A,fast}$ IPSCs recorded in pyramidal cells (Banks et al., 2000), indicating that $GABA_{A,slow}$ inhibition affects both pyramidal cells and interneurons that mediate $GABA_{A,fast}$ IPSCs. Furthermore, the GABA reuptake inhibitor NO-711, which selectively prolongs $GABA_{A,slow}$ IPSCs while leaving $GABA_{A,fast}$ IPSCs unaffected, prolongs SFI (Banks et al., 2000).

These data, as well as the data highlighted above, indicate that there are separate cellular networks and mechanisms that mediate $GABA_{A,slow}$ and $GABA_{A,fast}$.

However, it is worth acknowledging a caveat here. There is a possibility that the slower $GABA_{A,slow}$ IPSC kinetics arise as an artifact of imperfect voltage-clamp in the dendrites of hippocampal pyramidal cells, which manifests as slower measured currents at the soma than the true time-course for underlying conductances in the dendrites because the capacitative charge accumulates in the distal dendrites (Spruston et al., 1993; Golding et al., 2005). One approach to counteract the buildup of charge that results in the dendritic filtering phenomenon called voltage jump involves holding the cell at the reversal potential for synaptic Cl^- currents, thus preventing the flow of current during stimulation, even though $GABA_A$Rs bind GABA and their channels open (Pearce, 1993; Capogna and Pearce, 2012). The voltage jump approach demonstrates that the underlying conductances for $GABA_{A,fast}$ and $GABA_{A,slow}$ are compatible with different

synaptic currents. Evidence demonstrates kinetically similar $GABA_{A,slow}$ IPSCs in electrotonically smaller compartments, including interneurons, synapses on pyramidal cell soma instead of dendrite, and in neurogliaform autapses[13] (Price et al., 2005; Price et al., 2008; Capogna and Pearce, 2011). The axons of OLM cells synapse with pyramidal cell dendrites at a similarly distal location, but give rise to IPSCs with faster kinetics (Ali et al., 1998; Pouille and Scanziani, 2004; Andersen, 2007; Klausberger and Somogyi, 2008). So it is likely that $GABA_{A,slow}$ represents a truly different mode of inhibitory synaptic transmission in the CNS.

Synaptic plasticity

Synaptic plasticity at excitatory synapses on hippocampal pyramidal cells is a commonly used model for learning and memory (Hebb, 1949; Andersen et al., 1980; Bliss and Collingridge, 1993; Martin et al., 2000; Martin and Morris, 2002; Andersen, 2007). Long-term potentiation is a type of synaptic plasticity that has been studied extensively in the hippocampus (Bliss and Collingridge, 1993). LTP can typically be characterized, to paraphrase Donald Hebb, by the rule of thumb: "Neurons that fire together, wire together," which means that the conditional and coincidental spiking of two cells will tend to increase the likelihood of their conditional firing, via "some growth process or metabolic change" (Hebb, 1949).

[13] Autapses are synapses of a cell's axon onto its own dendrites.

LTP can be evoked *in vitro* through a variety of means in slice preparations. The most commonly studied variety of LTP induction is the means I will use in my experiments: electrical stimulation of presynaptic axons to depolarize presynaptic terminals at high frequency. A common approach consists of inducing LTP by delivering a tetanus, or train of specific duration or stimulus number, of electrical stimuli at a particular frequency, such as 100 Hz (Bliss and Lomo, 1973; Collingridge et al., 1983), or as a series of bursts with an interburst frequency meant to mimic oscillations in cellular firing patterns (Larson et al., 1986; Buzsaki et al., 2003; Hyman et al., 2003; Martin et al., 2010). Spike timing-dependent plasticity is a temporally atypical form LTP in which the presynaptic cell is stimulated slightly before or coincident to an artificial action potential is evoked via current injection in the postsynaptic cell, resulting in LTP without the normal somatic integration of dendritically filtered signals, illustrating the potential for dendritically mediated LTP (Markram et al., 1997). The application of substances (e.g., forskolin) can bring cells to a high level of activity, which evokes LTP without the necessity of the typical electrical stimulation of presynaptic inputs (Otmakhov et al., 2004).

In the prototypical case: high frequency synaptic transmission leads to activation of *N*-methyl-D-aspartate receptors (NMDARs), which mediate a large influx of Ca^{2+} into the postsynaptic terminal. This elevation of [Ca^{2+}] in the

postsynaptic cell is necessary for the induction of LTP (Collingridge et al., 1983; Tsien et al., 1996; Volianskis and Jensen, 2003; MacDonald et al., 2006).

A variety of intracellular signaling molecules and pathways contribute to the induction, maintenance, and expression of electrically evoked LTP (Harris et al., 1984; Newton, 2001; Winder and Sweatt, 2001; Xia and Storm, 2005; Lauri et al., 2007; Ho et al., 2011). Furthermore, it is not known whether the site of expression for LTP is generally presynaptic or postsynaptic, and individual cases will vary (Kullmann, 2012). My research cannot speak directly to the mechanisms or locus of expression of LTP engaged in the cells from which I record.

There are several reports that classical benzodiazepines and anesthetics can affect learning and memory in humans and mice (Arolfo and Brioni, 1991; Buffett-Jerrott and Stewart, 2002; Rudolph and Knoflach, 2011), as well as LTP in CA1 of mouse hippocampus (Seabrook et al., 1997), suggesting that $GABA_A$Rs play a role in regulating learning and memory. Additionally, knocking out the gene coding for the α5 subunit of the $GABA_A$R has been shown to enhance learning and memory and alter GABAergic synaptic transmission in mice (Collinson et al., 2002), making it a likely target in the inhibitory control of learning and memory. My research seeks to use anesthetics as a tool to perturb synaptic plasticity in order to learn about the function of the CA1 hippocampal circuit as a whole.

References

Ali AB, Thomson AM (1998) Facilitating pyramid to horizontal oriens-alveus interneurone inputs: dual intracellular recordings in slices of rat hippocampus. J Physiol 507 (Pt 1):185-199.

Ali AB, Deuchars J, Pawelzik H, Thomson AM (1998) CA1 pyramidal to basket and bistratified cell EPSPs: dual intracellular recordings in rat hippocampal slices. J Physiol 507 (Pt 1):201-217.

Amaral DG (1978) A Golgi study of cell types in the hilar region of the hippocampus in the rat. J Comp Neurol 182:851-914.

Andersen P (2007) The hippocampus book. Oxford ; New York: Oxford University Press.

Andersen P, Bliss TV, Skrede KK (1971) Lamellar organization of hippocampal pathways. Exp Brain Res 13:222-238.

Andersen P, Sundberg SH, Sveen O, Swann JW, Wigstrom H (1980) Possible mechanisms for long-lasting potentiation of synaptic transmission in hippocampal slices from guinea-pigs. J Physiol 302:463-482.

Arantius JC (1584) De humano foetu libellus. In: ex officinâ Felicis de Haro, 1664.

Arolfo MP, Brioni JD (1991) Diazepam impairs place learning in the Morris water maze. Behav Neural Biol 55:131-136.

Banks MI, Li TB, Pearce RA (1998) The synaptic basis of GABAA,slow. J Neurosci 18:1305-1317.

Banks MI, White JA, Pearce RA (2000) Interactions between distinct GABA(A) circuits in hippocampus. Neuron 25:449-457.

Barnard EA, Skolnick P, Olsen RW, Mohler H, Sieghart W, Biggio G, Braestrup C, Bateson AN, Langer SZ (1998) International Union of Pharmacology. XV. Subtypes of gamma-aminobutyric acidA receptors: classification on the basis of subunit structure and receptor function. Pharmacol Rev 50:291-313.

Benke D, Mertens S, Trzeciak A, Gillessen D, Mohler H (1991) GABAA receptors display association of gamma 2-subunit with alpha 1- and beta 2/3-subunits. J Biol Chem 266:4478-4483.

Benke D, Fritschy JM, Trzeciak A, Bannwarth W, Mohler H (1994) Distribution, prevalence, and drug binding profile of gamma-aminobutyric acid type A receptor subtypes differing in the beta-subunit variant. J Biol Chem 269:27100-27107.

Biro AA, Holderith NB, Nusser Z (2005) Quantal size is independent of the release probability at hippocampal excitatory synapses. J Neurosci 25:223-232.

Blackstad TW (1956) Commissural connections of the hippocampal region in the rat, with special reference to their mode of termination. J Comp Neurol 105:417-537.

Bliss TV, Lomo T (1973) Long-lasting potentiation of synaptic transmission in the dentate area of the anaesthetized rabbit following stimulation of the perforant path. J Physiol 232:331-356.

Bliss TV, Collingridge GL (1993) A synaptic model of memory: long-term potentiation in the hippocampus. Nature 361:31-39.

Boileau AJ, Pearce RA, Czajkowski C (2010) The short splice variant of the gamma 2 subunit acts as an external modulator of GABA(A) receptor function. J Neurosci 30:4895-4903.

Bormann J (2000) The 'ABC' of GABA receptors. Trends Pharmacol Sci 21:16-19.

Buffett-Jerrott SE, Stewart SH (2002) Cognitive and sedative effects of benzodiazepine use. Curr Pharm Des 8:45-58.

Buhl EH, Cobb SR, Halasy K, Somogyi P (1995) Properties of unitary IPSPs evoked by anatomically identified basket cells in the rat hippocampus. Eur J Neurosci 7:1989-2004.

Burgard EC, Tietz EI, Neelands TR, Macdonald RL (1996) Properties of recombinant gamma-aminobutyric acid A receptor isoforms containing the alpha 5 subunit subtype. Mol Pharmacol 50:119-127.

Buzsaki G, Buhl DL, Harris KD, Csicsvari J, Czeh B, Morozov A (2003) Hippocampal network patterns of activity in the mouse. Neuroscience 116:201-211.

Cajal SR (1893) Estructura del asta de Ammon y fascia dentata: tip. de Fortanet.

Cajal SR (1968) The structure of Ammon's horn: C. C. Thomas.

Capogna M, Pearce RA (2011) GABA A,slow: causes and consequences. Trends Neurosci 34:101-112.

Caraiscos VB, Elliott EM, You-Ten KE, Cheng VY, Belelli D, Newell JG, Jackson MF, Lambert JJ, Rosahl TW, Wafford KA, MacDonald JF, Orser BA (2004) Tonic inhibition in mouse hippocampal CA1 pyramidal neurons is mediated by alpha5 subunit-containing gamma-aminobutyric acid type A receptors. Proc Natl Acad Sci U S A 101:3662-3667.

Chamma I, Chevy Q, Poncer JC, Levi S (2012) Role of the neuronal K-Cl co-transporter KCC2 in inhibitory and excitatory neurotransmission. Front Cell Neurosci 6:5.

Collingridge GL, Kehl SJ, McLennan H (1983) Excitatory amino acids in synaptic transmission in the Schaffer collateral-commissural pathway of the rat hippocampus. J Physiol 334:33-46.

Collinson N, Kuenzi FM, Jarolimek W, Maubach KA, Cothliff R, Sur C, Smith A, Otu FM, Howell O, Atack JR, McKernan RM, Seabrook GR, Dawson GR, Whiting PJ, Rosahl TW (2002) Enhanced learning and memory and altered GABAergic synaptic transmission in mice lacking the alpha 5 subunit of the GABAA receptor. J Neurosci 22:5572-5580.

Farrant M, Nusser Z (2005) Variations on an inhibitory theme: phasic and tonic activation of GABA(A) receptors. Nat Rev Neurosci 6:215-229.

Fritschy JM, Benke D, Mertens S, Oertel WH, Bachi T, Mohler H (1992) Five subtypes of type A gamma-aminobutyric acid receptors identified in neurons by double and triple immunofluorescence staining with subunit-specific antibodies. Proc Natl Acad Sci U S A 89:6726-6730.

Golding NL, Mickus TJ, Katz Y, Kath WL, Spruston N (2005) Factors mediating powerful voltage attenuation along CA1 pyramidal neuron dendrites. J Physiol 568:69-82.

Gotti C, Zoli M, Clementi F (2006) Brain nicotinic acetylcholine receptors: native subtypes and their relevance. Trends Pharmacol Sci 27:482-491.

Harris EW, Ganong AH, Cotman CW (1984) Long-term potentiation in the hippocampus involves activation of N-methyl-D-aspartate receptors. Brain Res 323:132-137.

Hebb DO (1949) The organization of behavior; a neuropsychological theory. New York,: Wiley.

Hentschke H, Benkwitz C, Banks MI, Perkins MG, Homanics GE, Pearce RA (2009) Altered GABAA,slow inhibition and network oscillations in mice lacking the GABAA receptor beta3 subunit. J Neurophysiol 102:3643-3655.

Ho VM, Lee JA, Martin KC (2011) The cell biology of synaptic plasticity. Science 334:623-628.

Hyman JM, Wyble BP, Goyal V, Rossi CA, Hasselmo ME (2003) Stimulation in hippocampal region CA1 in behaving rats yields long-term potentiation when delivered to the peak of theta and long-term depression when delivered to the trough. J Neurosci 23:11725-11731.

Jones MV, Westbrook GL (1995) Desensitized states prolong GABAA channel responses to brief agonist pulses. Neuron 15:181-191.

Khalilov I, Le Van Quyen M, Gozlan H, Ben-Ari Y (2005) Epileptogenic actions of GABA and fast oscillations in the developing hippocampus. Neuron 48:787-796.

Klausberger T, Somogyi P (2008) Neuronal diversity and temporal dynamics: the unity of hippocampal circuit operations. Science 321:53-57.

Kullmann DM (2012) The Mother of All Battles 20 years on: is LTP expressed pre- or postsynaptically? J Physiol 590:2213-2216.

Larson J, Wong D, Lynch G (1986) Patterned Stimulation at the Theta-Frequency Is Optimal for the Induction of Hippocampal Long-Term Potentiation. Brain Res 368:347-350.

Lauri SE, Palmer M, Segerstrale M, Vesikansa A, Taira T, Collingridge GL (2007) Presynaptic mechanisms involved in the expression of STP and LTP at CA1 synapses in the hippocampus. Neuropharmacology 52:1-11.

Lindstrom J, Anand R, Peng X, Gerzanich V, Wang F, Li Y (1995) Neuronal nicotinic receptor subtypes. Ann N Y Acad Sci 757:100-116.

Lorente de Nó R (1933) Studies on the structure of the cerebral cortex I. The area entorhinalis. J Psychol Neurol 45:381-438.

Lorente de Nó R (1934) Studies on the structure of the cerebral cortex. II. Continuation of the study of the ammonic system. J Psychol Neurol 46:113-177.

Lynch JW (2009) Native glycine receptor subtypes and their physiological roles. Neuropharmacology 56:303-309.

MacDonald JF, Jackson MF, Beazely MA (2006) Hippocampal long-term synaptic plasticity and signal amplification of NMDA receptors. Crit Rev Neurobiol 18:71-84.

Maricq AV, Peterson AS, Brake AJ, Myers RM, Julius D (1991) Primary structure and functional expression of the 5HT3 receptor, a serotonin-gated ion channel. Science 254:432-437.

Markram H, Lubke J, Frotscher M, Sakmann B (1997) Regulation of synaptic efficacy by coincidence of postsynaptic APs and EPSPs. Science 275:213-215.

Martin LJ, Zurek AA, MacDonald JF, Roder JC, Jackson MF, Orser BA (2010) Alpha5GABAA receptor activity sets the threshold for long-term potentiation and constrains hippocampus-dependent memory. J Neurosci 30:5269-5282.

Martin SJ, Morris RG (2002) New life in an old idea: the synaptic plasticity and memory hypothesis revisited. Hippocampus 12:609-636.

Martin SJ, Grimwood PD, Morris RG (2000) Synaptic plasticity and memory: an evaluation of the hypothesis. Annu Rev Neurosci 23:649-711.

McKernan RM, Whiting PJ (1996) Which GABAA-receptor subtypes really occur in the brain? Trends Neurosci 19:139-143.

McKernan RM, Quirk K, Prince R, Cox PA, Gillard NP, Ragan CI, Whiting P (1991) GABAA receptor subtypes immunopurified from rat brain with alpha subunit-specific antibodies have unique pharmacological properties. Neuron 7:667-676.

Mertens S, Benke D, Mohler H (1993) GABAA receptor populations with novel subunit combinations and drug binding profiles identified in brain by alpha 5- and delta-subunit-specific immunopurification. J Biol Chem 268:5965-5973.

Miralles CP, Gutierrez A, Khan ZU, Vitorica J, De Blas AL (1994) Differential expression of the short and long forms of the gamma 2 subunit of the GABAA/benzodiazepine receptors. Brain Res Mol Brain Res 24:129-139.

Mohler H (2006) GABA(A) receptor diversity and pharmacology. Cell Tissue Res 326:505-516.

Mohler H, Fritschy JM, Luscher B, Rudolph U, Benson J, Benke D (1996) The GABAA receptors. From subunits to diverse functions. Ion Channels 4:89-113.

Mozrzymas JW, Zarnowska ED, Pytel M, Mercik K (2003) Modulation of GABA(A) receptors by hydrogen ions reveals synaptic GABA transient and a crucial role of the desensitization process. J Neurosci 23:7981-7992.

Newton AC (2001) Protein kinase C: structural and spatial regulation by phosphorylation, cofactors, and macromolecular interactions. Chem Rev 101:2353-2364.

Nusser Z, Mody I (2002) Selective modulation of tonic and phasic inhibitions in dentate gyrus granule cells. J Neurophysiol 87:2624-2628.

Nusser Z, Roberts JD, Baude A, Richards JG, Sieghart W, Somogyi P (1995) Immunocytochemical localization of the alpha 1 and beta 2/3 subunits of the GABAA receptor in relation to specific GABAergic synapses in the dentate gyrus. Eur J Neurosci 7:630-646.

Olsen RW, Homanics GE (2000) Function of GABAA receptors: insights from mutant and knockout mice. In: GABA in the Nervous System: The View at 50 Years (Martin DL, Olsen RW, eds), pp 81-96. Philadelphia: Lippincott, Williams & Wilkins.

Olsen RW, Sieghart W (2008) International Union of Pharmacology. LXX. Subtypes of gamma-aminobutyric acid(A) receptors: classification on the basis of subunit composition, pharmacology, and function. Update. Pharmacol Rev 60:243-260.

Olsen RW, Sieghart W (2009) GABA A receptors: subtypes provide diversity of function and pharmacology. Neuropharmacology 56:141-148.

Otis TS, Mody I (1992) Modulation of decay kinetics and frequency of GABAA receptor-mediated spontaneous inhibitory postsynaptic currents in hippocampal neurons. Neuroscience 49:13-32.

Otmakhov N, Khibnik L, Otmakhova N, Carpenter S, Riahi S, Asrican B, Lisman J (2004) Forskolin-induced LTP in the CA1 hippocampal region is NMDA receptor dependent. J Neurophysiol 91:1955-1962.

Patenaude C, Nurse S, Lacaille JC (2001) Sensitivity of synaptic GABA(A) receptors to allosteric modulators in hippocampal oriens-alveus interneurons. Synapse 41:29-39.

Pearce RA (1993) Physiological evidence for two distinct GABAA responses in rat hippocampus. Neuron 10:189-200.

Pearce RA (1996) Volatile anaesthetic enhancement of paired-pulse depression investigated in the rat hippocampus in vitro. J Physiol 492 (Pt 3):823-840.

Pirker S, Schwarzer C, Wieselthaler A, Sieghart W, Sperk G (2000) GABA(A) receptors: immunocytochemical distribution of 13 subunits in the adult rat brain. Neuroscience 101:815-850.

Pouille F, Scanziani M (2004) Routing of spike series by dynamic circuits in the hippocampus. Nature 429:717-723.

Price CJ, Scott R, Rusakov DA, Capogna M (2008) GABA(B) receptor modulation of feedforward inhibition through hippocampal neurogliaform cells. J Neurosci 28:6974-6982.

Price CJ, Cauli B, Kovacs ER, Kulik A, Lambolez B, Shigemoto R, Capogna M (2005) Neurogliaform neurons form a novel inhibitory network in the hippocampal CA1 area. J Neurosci 25:6775-6786.

Pritchett DB, Sontheimer H, Shivers BD, Ymer S, Kettenmann H, Schofield PR, Seeburg PH (1989) Importance of a novel GABAA receptor subunit for benzodiazepine pharmacology. Nature 338:582-585.

Reeves DC, Lummis SC (2002) The molecular basis of the structure and function of the 5-HT3 receptor: a model ligand-gated ion channel (review). Mol Membr Biol 19:11-26.

Rudolph U, Knoflach F (2011) Beyond classical benzodiazepines: novel therapeutic potential of GABAA receptor subtypes. Nat Rev Drug Discov 10:685-697.

Sabaliauskas N, Shen H, Homanics GE, Smith SS, Aoki C (2012) Knockout of the gamma-aminobutyric acid receptor subunit alpha4 reduces functional delta-containing extrasynaptic receptors in hippocampal pyramidal cells at the onset of puberty. Brain Res 1450:11-23.

Schofield PR, Darlison MG, Fujita N, Burt DR, Stephenson FA, Rodriguez H, Rhee LM, Ramachandran J, Reale V, Glencorse TA, et al. (1987) Sequence and functional expression of the GABA A receptor shows a ligand-gated receptor super-family. Nature 328:221-227.

Schwarzer C, Tsunashima K, Wanzenbock C, Fuchs K, Sieghart W, Sperk G (1997) GABA(A) receptor subunits in the rat hippocampus II: altered distribution in kainic acid-induced temporal lobe epilepsy. Neuroscience 80:1001-1017.

Seabrook GR, Easter A, Dawson GR, Bowery BJ (1997) Modulation of long-term potentiation in CA1 region of mouse hippocampal brain slices by GABAA receptor benzodiazepine site ligands. Neuropharmacology 36:823-830.

Semyanov A, Walker MC, Kullmann DM, Silver RA (2004) Tonically active GABA A receptors: modulating gain and maintaining the tone. Trends Neurosci 27:262-269.

Shen H, Gong QH, Aoki C, Yuan M, Ruderman Y, Dattilo M, Williams K, Smith SS (2007) Reversal of neurosteroid effects at alpha4beta2delta GABAA receptors triggers anxiety at puberty. Nat Neurosci 10:469-477.

Shepherd GM (2011) The microcircuit concept applied to cortical evolution: from three-layer to six-layer cortex. Front Neuroanat 5:30.

Sieghart W, Sperk G (2002) Subunit composition, distribution and function of GABA(A) receptor subtypes. CurrTopMedChem 2:795-816.

Sieghart W, Fuchs K, Tretter V, Ebert V, Jechlinger M, Hoger H, Adamiker D (1999) Structure and subunit composition of GABA(A) receptors. Neurochem Int 34:379-385.

Somogyi P, Fritschy JM, Benke D, Roberts JD, Sieghart W (1996) The gamma 2 subunit of the GABAA receptor is concentrated in synaptic junctions containing the alpha 1 and beta 2/3 subunits in hippocampus, cerebellum and globus pallidus. Neuropharmacology 35:1425-1444.

Sperk G, Schwarzer C, Tsunashima K, Fuchs K, Sieghart W (1997) GABA(A) receptor subunits in the rat hippocampus I: immunocytochemical distribution of 13 subunits. Neuroscience 80:987-1000.

Spruston N, Jaffe DB, Williams SH, Johnston D (1993) Voltage- and space-clamp errors associated with the measurement of electrotonically remote synaptic events. J Neurophysiol 70:781-802.

Sur C, Quirk K, Dewar D, Atack J, McKernan R (1998) Rat and human hippocampal alpha5 subunit-containing gamma-aminobutyric AcidA receptors have alpha5 beta3 gamma2 pharmacological characteristics. Mol Pharmacol 54:928-933.

Szabadics J, Tamas G, Soltesz I (2007) Different transmitter transients underlie presynaptic cell type specificity of GABAA,slow and GABAA,fast. Proc Natl Acad Sci U S A 104:14831-14836.

Tretter V, Ehya N, Fuchs K, Sieghart W (1997) Stoichiometry and assembly of a recombinant GABAA receptor subtype. J Neurosci 17:2728-2737.

Tsien JZ, Huerta PT, Tonegawa S (1996) The essential role of hippocampal CA1 NMDA receptor-dependent synaptic plasticity in spatial memory. Cell 87:1327-1338.

Ueno S, Zorumski C, Bracamontes J, Steinbach JH (1996) Endogenous subunits can cause ambiguities in the pharmacology of exogenous gamma-aminobutyric acidA receptors expressed in human embryonic kidney 293 cells. Mol Pharmacol 50:931-938.

Vannier C, Triller A (1997) Biology of the postsynaptic glycine receptor. Int Rev Cytol 176:201-244.

Volianskis A, Jensen MS (2003) Transient and sustained types of long-term potentiation in the CA1 area of the rat hippocampus. J Physiol 550:459-492.

Whiting P, McKernan RM, Iversen LL (1990) Another mechanism for creating diversity in gamma-aminobutyrate type A receptors: RNA splicing directs expression of two forms of gamma 2 phosphorylation site. Proc Natl Acad Sci U S A 87:9966-9970.

Whiting PJ, Bonnert TP, McKernan RM, Farrar S, Le Bourdelles B, Heavens RP, Smith DW, Hewson L, Rigby MR, Sirinathsinghji DJ, Thompson SA, Wafford KA (1999) Molecular and functional diversity of the expanding GABA-A receptor gene family. Ann N Y Acad Sci 868:645-653.

Winder DG, Sweatt JD (2001) Roles of serine/threonine phosphatases in hippocampal synaptic plasticity (vol 2, pg 461, 2001). Nature Reviews Neuroscience 2:670-670.

Wisden W, Laurie DJ, Monyer H, Seeburg PH (1992) The distribution of 13 GABAA receptor subunit mRNAs in the rat brain. I. Telencephalon, diencephalon, mesencephalon. J Neurosci 12:1040-1062.

Xia Z, Storm DR (2005) The role of calmodulin as a signal integrator for synaptic plasticity. Nat Rev Neurosci 6:267-276.

Zarnowska ED, Keist R, Rudolph U, Pearce RA (2009) GABAA receptor alpha5 subunits contribute to GABAA,slow synaptic inhibition in mouse hippocampus. J Neurophysiol 101:1179-1191.

CHAPTER 2

A microfluidic brain slice perfusion chamber for multisite recording using penetrating electrodes

A microfluidic brain slice perfusion chamber for multisite recording using penetrating electrodes

Alexander J. Blake[1], Frank C. Rodgers[2], Anna Bassuener[2], Joseph A. Hippensteel[1], Thomas M. Pearce[1,3], Timothy R. Pearce[1], Ewa D. Zarnowska[2], Robert A. Pearce[2], Justin C. Williams[1]

[1]Department of Biomedical Engineering, University of Wisconsin, Madison, WI 53705

[2]Department of Anesthesiology, University of Wisconsin, Madison, WI 53711

[3]Current address: Department of Anatomy and Neurobiology, Washington University in St Louis School of Medicine, St. Louis, MO 63130

Corresponding author:

Dr. Justin C. Williams
Assistant Professor
University of Wisconsin
Department of Biomedical Engineering #2150 Engineering Centers Building 1550 Engineering Drive
Madison, WI 53706, USA jwilliams@engr.wisc.edu office 608 265 3952
fax 608 265 9239

Acknowledgements
The authors would like to thank Luke Bassuener for providing the drawing in Fig. 1C, and Mark Perkins for excellent technical assistance. This research was supported by National Institutes of Health grants P01-GM47818 and R01-NS56411 to R.A. Pearce and by National Institutes of Health grants KL2-RR025012 and R21-NS051580 to J.C. Williams.

AJB, TMP, TRP, and JCW designed and fabricated the perfusion chambers; FCR, AB, EDZ, and RAP performed electrophysiological experiments; FCR, JAH, and AJB analyzed electrophysiological data; and AJB, FCR, EDZ, RAP, and JCW wrote the manuscript.

Abstract

To analyze the spatiotemporal dynamics of network activity in a brain tissue slice, it is useful to record simultaneously from multiple locations. When obtained from laminar structures such as the hippocampus or neocortex, multisite recordings also yield information about subcellular current distributions via current source density analysis. Multisite probes developed for *in vivo* recordings could serve these purposes *in vitro*, allowing recordings to be obtained from brain slices at sites deeper within the tissue than currently available surface recording methods permit. However, existing recording chambers do not allow for the insertion of lamina-spanning probes that enter through the edges of brain slices. Here, we present a novel brain slice recording chamber design that accomplishes this goal. The device provides a stable microfluidic perfusion environment in which tissue health is optimized by superfusing both surfaces of the slice. Multichannel electrodes can be inserted parallel to the surface of the slice, at any depth relative to the surface. Access is also provided from above for the insertion of additional recording or stimulating electrodes. We illustrate the utility of this recording configuration by measuring current sources and sinks during theta burst stimuli that lead to the induction of long-term potentiation in hippocampal slices.

Keywords

microfluidics, hippocampus, field potentials, action potential, long-term potentiation (LTP), current source density (CSD), multisite recording electrodes

Introduction

The brain is composed of ensembles of small- and large-scale neuronal networks that, spontaneously or upon stimulation, generate coordinated activity patterns. In order to acquire information about the underlying spatiotemporal dynamics it is useful to record activity simultaneously at multiple locations (Csicsvari et al., 2003B). In laminated neural structures, additional information can be obtained by using current source density (CSD) analysis to derive the distribution of synchronous membrane events that give rise to the measured voltage fluctuations (Freeman and Nicholson, 1975; Mitzdorf, 1985; Buzsáki et al., 1986; Taube and Schwartzkroin, 1988; Vida et al., 1995). Penetrating multisite linear recording arrays have been developed that can be used for these purposes in vivo. The electrode sites are configured for specific electrophysiological applications by roughly matching them with the tissue cytoarchitecture (Buzsáki et al., 2004).

Brain slice preparations offer an alternative recording environment. For investigations of network patterns of activity, they provide a number of advantages over in vivo preparations, including the ability to record from discrete brain regions that maintain cytoarchitecturally preserved units of neuronal networks removed from the influence of afferent pathways (Sarvey et al., 1989; Traub et al., 1989). More importantly, in vitro brain slice recording methods offer a substantially greater control over certain experimental parameters (e.g.

temperature, pH, pharmacological modulation), greatly facilitating investigations into the cellular mechanisms that underlie network activity.

A number of in vitro recording devices have been developed that incorporate multiple recording sites, including planar and three-dimensional microelectrode arrays (MEAs), which are capable of recording and stimulating at the sub-millimeter scale (Boppart et al., 1992; Csicsvari et al., 2003A; Gholmieh et al., 2006; Berdichevsky et al., 2009). Unfortunately, signals that originate from intact networks within the interior of slices are degraded at the injured tissue surfaces (Aitken et al., 1995), and this adversely affects the signal-to-noise ratio in recordings obtained from planar MEA recordings. This problem can be partially overcome using three-dimensional MEAs that penetrate the injured surface (Heuschkel et al., 2002; Nam et al., 2006), but this approach itself suffers from a combination of a limited recording depth and the need to obtain recordings near the non-perfused surface of the brain slice. Penetrating multisite linear electrodes potentially offer the ability to record from deep within tissue where neural networks are intact and active, while maintaining some of the same recording advantages as MEAs (Buzsáki, 2004). However, existing *in vitro* recording chambers lack access features that permit the realization of this recording configuration (Passeraub et al., 2003; Mohammed et al., 2008).

We sought to design an *in vitro* brain slice perfusion chamber that would enable extracellular recordings of network activity using a penetrating multisite

electrode inserted parallel to the surface of the tissue slice, at any tissue depth, and that would incorporate laminar solution flow across both surfaces of the slice to enhance tissue viability (Passeraub et al., 2003; Rambani et al., 2009; Hájos et al., 2009). The perfusion chamber that we designed, built, and tested utilizes arrays of microposts that immobilize the tissue slice while providing fluid flow to both surfaces for delivery of oxygen and nutrients. In addition, it incorporates a lateral opening that permits the insertion of a penetrating multisite linear-array recording electrode into the edge of the slice, and an opening in the top for insertion of stimulating or conventional recording electrodes. We illustrate the utility of this recording configuration by measuring evoked activity in the CA1 area of a hippocampal brain slice undergoing long-term potentiation of excitatory synaptic strength by theta-burst stimulation, and apply current source density analysis to reveal patterns of current flow during the potentiating stimulus.

Materials and methods

Chamber Design

The microfluidic perfusion device used in this study is fabricated from poly-dimethyl-siloxane (PDMS, Sylgard 184, Dow Corning, Midland, MI). The process involves pouring a liquid pre-polymer onto a microfabricated mold, curing the polymer, and then releasing the resulting solidified material from the mold (Duffy

et al., 1998). The final step requires that structural features of the mold do not mechanically impede the removal of the cured PDMS. Given this limitation, forming an enclosed 3- dimensional structure such as a microfluidic channel requires bonding the cured PDMS to another surface (Jo et al., 2000).

Perfusing both surfaces of a brain slice preparation enhances tissue viability for *in vitro* electrophysiology experiments (Rambani et al., 2009; Hájos et al., 2009). To accomplish this, we use a multi-stage process in which three layers of PDMS are individually molded, then bonded together via an oxygen-plasma surface treatment (Fig. 1). The first layer consists of a micropost array within a microfluidic channel. The brain slice is supported by the micropost array while the bottom surface of the tissue is perfused via the fluid channel. The second PDMS layer encloses the lower channel except for an opening located above the micropost array, which houses the slice. The shape of this opening closely fits the size and shape of the slice, and the thickness of the PDMS is matched to that of the tissue. The third layer of the chamber closely resembles the first, with a micropost array to hold the slice in place and a microfluidic channel to perfuse the upper surface.

An important, and novel, feature of our chamber is the inclusion of electrode access ports into the otherwise enclosed microfluidic environment surrounding the brain slice. Each port is an opening in the channel wall that connects the interior of the device with the exterior. The hydrophobic properties of the PDMS,

combined with the small dimensions of the electrode access ports, create surface-tension “virtual walls” at these openings. Through these virtual-wall access ports, electrodes can be inserted into the slice and the perfusion bath without causing fluid to spill out of the microfluidic channels, maintaining laminar flow over both surfaces of the slice. It is important to note that this principle is not limited to the top surface of the chamber – in our device, an opening in the lateral wall of the second PDMS layer allows a multisite linear-array recording electrode to horizontally penetrate the edge of the slice, parallel to the surface. This reproduces the electrode placement used in in vivo experiments (Buzsáki, 2004; Ward et al., 2009), and would be difficult to accomplish using conventional perfusion chambers.

Fabrication Procedure

The process for forming each PDMS layer is based on standard photolithography and microfabrication techniques utilizing silicon master molds (Jo et al., 2000). For this device, we use a monomer:crosslinker ratio of 10:1. The monomer and crosslinker are mixed by hand until the mixture becomes opaque with bubbles, and then degassed in a vacuum chamber to remove bubbles before being pouring onto the mold. The PDMS is cured at 95°C for 2 hours and slowly cooled to 40°C before removing the solidified polymer from the mold.

Master molds for each layer are photo-patterned with ultraviolet light. First, a silicon wafer is spin-coated with a photoresist (SU8 2100, MicroChem Corp., Newton, MA) according to the manufacturer's specifications, and heated to 65°C for 7 minutes and 95°C for 1 hour in a pre-exposure baking step. Next, the wafer with photoresist is exposed to ultraviolet light (l= 365nm) through a printed mask containing the design for the layer. Typically, a silicon master is a negative of the desired structure, and the final PDMS features are molded directly from this master. The middle PDMS layer is formed from this type of conventional negative master mold. In contrast, the top and bottom layers make use of a double casting process that serves to increase the fabrication yield of the high-aspect-ratio micropost arrays (Blake et al., 2007; Sniadecki and Chen, 2007). The features of the bottom and middle layers are of a uniform thickness, so a single coating of photoresist is sufficient. For the top layer, a second photoresist spin and UV exposure is used to create the electrode access ports on the top surface of the device (Fig. 2D). Following UV exposure, the wafers are post-exposure baked at 65°C for 5 minutes and 95°C for 20 minutes. Finally, the unexposed photoresist is removed with a developer solvent to form the master mold. A schematic of the procedure is shown in Fig. 2.

Next, PDMS is poured onto the silicon master molds and cured. Since the silicon wafers for the top and bottom layers were exposed to positive images of

the desired structure, curing polymer on these masters yields a flexible negative PDMS master mold (Fig. 2D). A silane gas treatment of the PDMS master prevented uncured PDMS from adhering to the surface (Sniadecki and Chen, 2007). Afterwards, these masters can be used to form the final top and bottom PDMS layers (Fig. 2B). For these layers, the channel depth and micropost height are 250 μm, which is defined by the thickness of the photoresist layer on the original silicon master. The double casting process, which utilizes a flexible PDMS master, is useful because the microposts (250 μm diameter) are difficult to release from a conventional rigid silicon master mold (Sniadecki and Chen, 2007). The middle layer, which houses the brain slice, requires a thickness matched to that of the tissue (in our case 500 μm) (Wu et al., 2004), which is also defined by the depth of the photoresist spin-coated onto the silicon wafer. To create a PDMS layer of uniform depth with a fully-penetrating space for the slice, we forced excess pre-polymer out of the master by applying pressure onto the photoresist features from above (Fig. 2C). Finally, the three PDMS layers are aligned and bonded together via oxygen-plasma surface treatment (Jo et al., 2000), leaving the outflow end of the top layer unbonded so slices can be easily inserted into the chamber.

Hippocampal slice preparation

All procedures were conducted according to the guidelines laid out in the *Guide for the Care and Use of Laboratory Animals* and approved by the University of Wisconsin Animal Care and Use Committee, Madison, Wisconsin. Mice were housed in an animal care facility under 12-hr cycles of light and dark. They had continuous access to food and water.

Brain slices were made from 5-7 week old male offspring of 129x1/SvJ (RCC, Fullinsdorf, Switzerland) breeding pairs. Mice were anesthetized with 2.5% isoflurane and decapitated. Heads were immediately submerged in ice-cold "dissection solution" that contained (in mM): NaCl 127, KCl 1.9, K2HPO4 0.8, NaHCO3 26, MgSO4 2.7, CaCl2 0.9, glucose 15, ascorbic acid 1, kynurenic acid 1 (Sigma) and saturated with 95% O2 / 5% CO2. After opening the skull, the brain was extracted and blocked by cutting off the cerebellum and prefrontal cortex. The brain was glued to a microtome slice tray with cyanoacrylate glue and 500 µm-thick coronal slices were cut using a vibrating microtome (Leica VT 1000S, Leica Microsystems, Nussloch GmbH, Nusslock, Germany). A portion of the slice that included the hippocampus was trimmed with a scalpel to provide for proper fit within the recording chamber. Brain slices recovered in a holding chamber filled with carbogenated artificial cerebrospinal fluid (ACSF) that contained (in mM): NaCl 127, KCl 1.9, K2HPO4 0.8, NaHCO3 26, MgSO4 1.44, CaCl2 2.17, glucose 15, for at least 1h at room temperature (20-22°C). Then slices were transferred to the recording chamber using a wide-open Pasteur

pipette. The chamber was perfused with ACSF at a flow rate of 2.5 ml/min, although laminar flow rates up to 6 ml/min have been shown to maintain network oscillations in hippocampal slices (Hájos et al., 2009). Experiments were performed at 30 ± 1°C. The recording solution temperature was controlled with an in-line temperature controller (Warner Instruments Corp., Hamden, CT). To prevent air/gas bubble formation, the solution reservoir containing ACSF was bubbled with carbogen at 38°C, and the temperature of the air surrounding the recording chamber was maintained at ~30°C using a forced-air patient warming system (Bair Hugger, Augustine Medical Inc., Eden Prairie, MN).

Electrode insertion and electrophysiological recordings

Extracellular potentials were recorded using a 16-channel linear-array recording electrode with iridium metal sites spaced 50 µm apart on a single shank 3 mm in length and 15 µm thick (NeuroNexus Technologies, Ann Arbor, MI) (Fig. 3). The linear-array recording electrode has a relatively small cross-sectional area (15x150 µm) and a sharp tip design that allowed it to effectively penetrate and cut through tissue with minimal damage (Bjornsson et al., 2006). Output pins from the linear-array recording electrode plugged directly into a 16-pin DIP socket custom interface that was mounted on a digital micromanipulator (Siskiyou Corporation, Grants Pass, OR) and attached to a buffer/preamp head

stage (Neuralynx Inc., Tucson, AZ). Under visual control, the manipulator was used to maneuver the linear-array recording electrode into the brain slice, by inserting it through the “virtual wall” opening in the brain slice chamber and into the edge of the brain slice, 100-200 μm below its top surface. The electrode was advanced until the tip reached the hippocampal fissure. We did not take any measures to optimize the recording depth that we used; we selected 100-200 mm based on our previous experience using sharp electrodes for extracellular recordings (Pearce, 1993, 1996), and it is possible that larger signals would have been obtained had the depth been optimized. Using the stereomicroscope, we were able to consistently insert the electrode in tissue slices at a speed of ~100 μm/s without encountering any compression that could result in lifting, warping or tearing of the tissue slice (Bjornsson et al., 2006). Viability of cells adjacent to the recording electrode sites was confirmed by recording spontaneous single-unit activity (Drake et al., 1988; Vetter et al., 2004, our data not shown).

Platinum/iridium concentric bipolar stimulating electrodes (FHC, Bowdoin, ME) inserted into *stratum radiatum* (SR) were used to activate the Schaffer collateral excitatory afferent pathway in the CA1 region (Fig. 3). Stimuli were delivered using a constant current stimulus isolator (model A365D, World Precision Instruments, Sarasota FL). Signals were amplified, low pass filtered at 3 kHz (LYNX-8 amplifiers, Neuralynx, Inc, Tucson, AZ), digitized at 10 kHz using an analog-to-digital converter (Digidata 1440A, Molecular Devices, Sunnyvale,

CA), and acquired using pClamp software (Version 10.2, Molecular Devices, Sunnyvale, CA).

Long-term potentiation (LTP) was evoked using a “triple theta burst stimulation” (TBSx3) protocol (Larson et al., 1986). TBSx3 consisted of three TBS trains at one- minute intervals. A single TBS train consisted of bursts of 5 stimuli delivered at 100 Hz, repeated 10 times at an interval of 200 ms, using a stimulus intensity (70-270 μA x 0.1 ms) that evoked a half-maximal population spike (PS). Test stimuli using lower stimulus intensities (38-70 μA x 0.1 ms) that evoked field excitatory postsynaptic potentials (fEPSPs) below PS threshold were applied at one-minute intervals (0.016 Hz). Baseline responses were considered stable if fEPSPs varied by less than 10% over the 10 minutes preceding TBS.

Electrophysiological data analysis

To assess LTP of the fEPSP, we used the channel in *stratum radiatum* (SR) that had the greatest slope prior to LTP induction. This channel was typically located 100-150 mm from the fEPSP “null point”, which corresponds to the border between SR and *stratum pyramidale* (SP) (Richardson et al., 1987). Data were analyzed using Clampfit (Version 10.2, Molecular Devices, Sunnyvale, CA). The slope of each fEPSP was normalized to the average of the 10 responses just preceding TBS. Potentiation of the fEPSP was expressed as the fractional

increase in the average of the normalized values between 50 to 60 min following TBSx3. PS amplitudes were measured from the channel at the “null point” for evoked fEPSPs, using AxoGraphX (Version 1.2.1, Molecular Devices, Sunnyvale, CA).

Current source density (CSD) analysis was used to derive the magnitudes of the current sources and sinks along the axis of the CA1 cells during TBSx3. We used an implementation of the CSD analysis based on the spline iCSD method developed by Pettersen and colleagues (Pettersen et al., 2006). We chose the spline method because it assumes a more realistic current distribution based on a columnar geometry of the underlying current source. Although there may be layer-specific differences in conductivity across laminated cortical structures, this has only a minor effect on the spatial profile of derived current sinks and sources (Holsheimer, 1987). Therefore, we assumed the conductivity to be uniform throughout the slice. CSD is expressed in units of $\mu A/mm^3$. We arbitrarily used warm colors (red and yellow) to represent current sinks and cold colors (blue) to represent current sources (Fig. 5).

Design considerations and troubleshooting

PDMS was chosen to construct the perfusion chamber because it offers many attractive physical and chemical properties in comparison to conventional

perfusion chamber materials, such as short construction time, fabrication repeatability, optical transparency, low cost, and low toxicity (Beebe et al., 2002). In particular, PDMS allows the fabrication of prototype devices having microscale features within a matter of hours (Beebe et al., 2000). Rapid prototyping can be vital in minimizing the time to arrive at an optimal design configuration, after which devices can be batch-processed with relatively short turnover times. PDMS is optically transparent to wavelengths of 230-700 nm, thus enabling standard microscope objectives for viewing samples through PDMS layers. The material is well suited for making numerous perfusion devices since it is a fairly inexpensive, elastic polymer with a low permeability to water. PDMS is not toxic to cellular environments and can be easily integrated for a number of biological applications (Beebe et al., 2002; Berdichevsky et al., 2009). Hence, we developed a microfluidic perfusion device that uses inexpensive, easily modified materials providing maximum experimental flexibility. The material properties of this device meet the standards of existing perfusion chambers (*e.g.* sterility, optical compatibility, *etc.*), while offering additional flexibility to quickly change experimental parameters (*e.g.* adding more inputs, modifying center layer to fit different slice shapes or thicknesses, *etc.*).

Although PDMS does possess many useful characteristics, its porous nature can lead to the collection of potentially harmful gas bubbles in the enclosed chamber. In our initial tests we found that the appearance of gas

bubbles along the walls of the fluid path was invariably detrimental to electrophysiological recordings, presumably because it led to poorly perfused areas of the slice. The formation of the gas bubbles depended on two factors: off-gassing from the PDMS, and out-gassing from the perfusate solution.

To address the off-gassing issue, we submerged the device in deionized water under vacuum for at least 2 hours before each experiment. After removing the device from the vacuum chamber, we dried the exterior portions of the device to ensure proper adhesion of the PDMS layers. In particular, it was critical to dry the area between the hinged area of the third PDMS layer and the second PDMS layer to prevent leaks from occurring. When dry, PDMS is notable for its ability to spontaneously adhere to itself. Keeping the hinged region dry allowed us to reposition the brain tissue slice between the microposts of the first and third layers, even repeatedly, to achieve an optimal orientation of the recording electrode along the axis of CA1 pyramidal cells.

Out-gassing of bubbles from the perfusate was addressed by controlling the perfusate and external temperature, a step that is necessary even with conventional recording chambers. To prevent the formation of microbubbles as the solution was re- warmed by an in-line heater just prior to its entry into the recording chamber, the temperature of the ACSF reservoir was set at 38 °C. This greatly reduced bubble formation within the recording chamber. However, it did not completely prevent bubble formation during experiments lasting several hours.

We found that warming the exterior air surrounding the chamber to within ~8 °C of the perfusate temperature was successful in preventing the formation of gas bubbles for experiments lasting up to 8 hours.

The perfusion recording chambers typically lasted for at least 20 experiments before failure. Chamber failure was due to physical damage of the PDMS from repeated folding of the top layer when inserting and removing brain slices. Additionally, with extended use, salt deposits decreased the hydrophobicity of the PDMS surface, and this could result in fluid leaking out of the chamber. However, when properly washed and maintained, the recording devices were functional for as long as a year with intermittent use, 40-50 experiments. After each experiment we carefully rinsed the chamber using ultrapure water to remove any salts remaining from the recording solution. Next we used isopropyl alcohol to remove tissue lipid residues and to dry the chamber. Chambers were stored in a dust free container to maintain surface characteristics. This maintenance protocol allowed us to reuse PDMS chambers until physical damage of the device occurred. The cleaning process was critical to maintaining a leak-free system.

Stimulating and recording electrodes were cleaned after each experiment by simply dipping in a beaker filled with ultrapure water and drying in air. Electrodes maintained in the fashion could be used daily for several months with little change in impedance.

Results

To demonstrate the ability of the brain slice chamber to maintain healthy tissue, we measured population responses in the hippocampal CA1 region following Schaffer collateral fiber stimulation. Electrical stimuli were applied to *stratum radiatum* (SR) using a bipolar stimulating electrode inserted perpendicular to the slice surface through an opening in layer 3 (Fig. 1B). Extracellular recordings of evoked activity were obtained using a 16-channel linear-array electrode inserted through an opening in layer 2. The electrode was inserted parallel to the surface of the slice, 100-200 mm below the upper surface, and with the tip positioned at the hippocampal fissure so that the recording sites spanned the layers of CA1 from the alveus to *stratum lacunosum-moleculare*.

Electrical stimuli induced population EPSPs in the dendritic layers, and action potentials that were evident as single "population spikes" (PS) at the *stratum pyramidale* (SP). In a total of 38 brain slices, the PS amplitude following supramaximal stimulation was 3.80 ± 1.39 mV (mean ± SD; range 2.10 - 7.10 mV). Responses were stable for up to 8 hours.

To illustrate the utility of this novel recording configuration, we induced LTP in a subset of slices, and used CSD analysis to derive spatiotemporal patterns of current sources and sinks during its induction. An example of the response induced by electrical stimulation subthreshold for an action potential generation

prior to LTP induction is shown in Fig. 4A. It is apparent that the evoked fEPSP spanned several recording sites. We used the site with the greatest slope before LTP induction to assess synaptic strength (Fig. 4A, bold trace).

LTP induced by a triple theta burst stimulation (TBSx3) protocol (see Materials and Methods for stimulation details) resulted in an increase in the mean fEPSP slope of 30 ± 7% (mean ± SD) in this single experiment (Fig. 4B), and the appearance of a PS (most evident at the SP recording site). On average, TBSx3 led to an increase in fEPSP slope of 35 ± 10% ($p<0.05$, $n=4$) (Fig. 4C).

To assess the spatiotemporal pattern of evoked activity during the LTP-inducing TBS, we applied CSD analysis. Figure 5 illustrates the CSD profiles obtained during the 1st (Fig. 5A) and 21st (Fig. 5B) bursts in a 30-burst TBSx3 protocol. In response to the first stimulus, the afferent volley (*), which itself extends over several channels in the middle of SR, is followed by a forward-propagating PS (**) that initiates in the apical dendrite and propagates to the SP, and slightly into *stratum oriens* (SO). Subsequent stimuli in the burst lead to synaptic responses (# - sinks in SR aligned with the afferent volley) that are progressively longer-lasting with each stimulus, but these do not lead to action potentials in the pyramidal cells. The activity pattern elicited during the 21st burst is similar, except that the second stimulus in the burst now also produces a forward- propagating PS. Qualitatively similar results were obtained in each of the slices to which the TBSx3 protocol was applied.

Discussion

The goal of the presented study was to design, build, and test an *in vitro* microfluidic perfusion chamber for performing extracellular recordings, using linear- array multisite recording electrodes that were originally developed for use *in vivo*. This new *in vitro* configuration afforded us the advantages inherent to brain slice preparations, such as the ability to study isolated circuits in a controlled microenvironment, and at the same time allowed us to measure the spatial and temporal characteristics of neuronal network activity using high fidelity linear-array recording electrodes.

A number of different approaches have been taken previously to enable multisite recordings from acute and cultured brain slice preparations. MEAs that are constructed from various materials (e.g., metal, silicon), and organized in diverse geometries, have been reported in the literature (Rutten et al., 2001), and are even available commercially (Ayanda Biosystems, Lausanne, Switzerland). They allow users to record brain slice surface potentials from multiple sites simultaneously. However, signal amplitudes (10s to 100s of mV) are substantially smaller than those obtained using conventional glass electrodes (several mV), due to two factors: damage to surface cells during the slicing process, and recording from the non-perfused surface of the slice.

To record from sites deeper within the tissue, and thus nearer to the cells

that generate the electrical signals, three-dimensional MEAs with protruding contacts have been developed (Heuschkel et al., 2002; Nam et al., 2006). This has led to an improved signal-to-noise ratio. But, even here, signals typically remain in the sub-millivolt range (Steidl et al., 2006). Presumably this reflects the limited height (60 mm) as well as geometry (conical protrusions that displace tissue) of the recording sites. To permit oxygen and nutrients to reach the tissue surface from which recordings are obtained, a perforated microelectrode array has also been developed (Boppart et al., 1992). Although the openings constituted only 6% of the recording surface, this did improve tissue longevity. Nevertheless, signals of only several hundred microvolts were obtained (Boppart et al., 1992). This may have been due in part to the use of surface electrodes, but it is likely that limited exchange through these openings also played a factor. Indeed, recent studies have highlighted the importance of maintaining high oxygen supply (Huchzermeyer et al., 2008), the need for high solution flow rates (Hájos et al., 2004), and the benefits of directing solution flow across both surfaces of brain slices (Hájos et al., 2009), for maintaining network activity *in vitro*. The amplitudes of the evoked responses that we recorded are similar to those typically obtained using conventional electrodes (Lipton et al., 1995), and substantially greater in amplitude than previously reported multisite recordings from brain slices. It is likely that both factors – recording from deep within the slice, and providing laminar flow of oxygenated ASCF to both slice surfaces to

enhance viability (Blake et al., 2007) – played roles in bringing about this improvement. Another potential benefit of this approach is the small volume of the recording chamber and the minimally exposed surface area through which oxygen can be lost. Recent studies have highlighted the importance of these two factors in maintaining healthy tissue slices with low solution flow rates (Hajos and Mody, 2009). In those experiments, a reduction in chamber volume from 2 mL to 0.5 mL permitted the solution flow rate to be reduced from 12-20 mL/min to 6 mL/min while still maintaining network activity requiring high levels of tissue oxygenation. Although we did not test the influence of changing solution flow rate in our experiments, the low chamber volume (0.062 mL) and the enclosed nature of the chamber design suggest that solution flow rates might be able to be reduced substantially from the 2.5 mL/min flow rate that we used here, while still maintaining adequate oxygenation.

By recording from multiple sites, the spatiotemporal pattern of current sinks and sources that give rise to the observed voltage deflections may be derived by CSD analysis (Wheeler and Novak, 1986). The spatial sampling rate should be at least twice that of the highest spatial frequency component in the distribution of extracellular current sinks and sources. For hippocampal slices, this is thought to require an electrode spacing of 100 mm (Bragin et al., 2000; Csicsvari et al., 2003A). The laminar profiles of field potentials that we obtained with 50 mm spaced electrodes were thus suitable for CSD analysis. The responses that we

observed resembled in many respects those reported previously using extracellular single point electrodes moved between recording sites (Richardson et al., 1987), including an early sink in the dendrites associated with a passive source at the soma, and a superimposed strong sink at the soma that corresponds to the action potential (Fig. 5). However, the direction of population spike propagation in the apical dendrite differed in our studies; we found that the spike invariably moved from the dendrite toward the soma (Fig. 5, 1st stimulus *), whereas it was reported previously that the population spike propagated from the somatic region into apical and basal dendrites. The reason for this difference is not entirely clear, but possible factors to be considered include stimulus strength and location, temperature, and details of slice preparation. In particular, the angle at which slices were cut could influence local circuitry activated by the stimulus, such as feedforward inhibition that impinges on the soma and can thus impact the ability to generate a somatic spike (Pouille and Scanziani, 2001).

In addition to the convenience that multisite recordings offer for deriving CSD profiles from single responses, this multisite approach enables the application of CSD analysis for individual events that either can not be repeated, such as irregularly occurring spontaneous bursts or interictal spikes, or for stimuli that lead to irreversible changes, such as LTP (Mitzdorf, 1985; Richardson et al., 1986; Wheeler and Novak, 1986). In this regard, the CSD that we present of theta bursts (Fig. 5) represents a unique application of the recording

configuration. We speculate that the enhancement and prolongation of the dendritic sinks during the later stimuli in a burst (Fig. 5, #) represents the recruitment of NMDA receptors that are initially blocked at hyperpolarized potentials. It will be useful to combine CSD analysis with complementary recording modalities and pharmacological tests to confirm this interpretation (Mann et al., 2005; Blake et al., 2007). It will also be useful to couple CSD analysis with imaging techniques to provide additional framework to study functional network activity.

The physical properties of PDMS, such as its hydrophobicity, and the use of low volumes, allow the creation of multiple openings in the perfusion chamber to provide access for electrophysiological equipment. Electrodes can be inserted through these “virtual walls” without breaking the surface tension. Other benefits of using PDMS and the construction techniques described herein are versatility, durability, and low cost. By altering the thickness of layer 2, and modifying the size of the opening in this layer, the chamber can be made to accommodate a variety of brain slice geometries and thicknesses. The materials are inexpensive (though specialized equipment for making new masks is necessary), and both the chambers and the recording electrodes can be re- used may times, further reducing costs.

Just as recording chamber technology continues to improve, so too does electrode technology – particularly for performing multisite recordings *in vivo*. The

approach that we describe here should be easily adapted to take advantage of these advances. The use of multi-shank recording electrodes will permit two-dimensional, and even three- dimensional, CSD analysis (Wheeler and Novak, 1986; Buzsáki, 2004). The incorporation of “tetrodes” will make it possible to record single units as well as field potentials, to aid investigations of the genesis of network oscillations (Csicsvari et al., 2003B). Introduction of multisite stimulating electrodes with precisely timed and spaced inputs will facilitate studies of integrative function. This perfusion chamber design can also serve as an *in vitro* model for screening drugs acting on the network level (Weiss et al., 2003), and the delivery of pharmacological agents to restricted regions of the slice, as laminar flow chambers permit (Blake et al., 2007), should also aid in studies of the roles played by ion channels distributed along the somatodendritic axis in integrative neuronal function. It is likely that additional uses for microfluidics, multisite recordings, and brain slice recordings will emerge in the coming years. The chamber design that we report here can play a role in bringing together all of these advances.

References

Aitken PG, Breese GR, Dudek FF, Edwards F, Espanol MT, Larkman PM, Lipton P, Newman GC, Nowak TS, Panizzon Jr. KL, Raley-Susrnan KL, Reid KH, Rice ME, Sarvey JM, Schoepp DD, Segal M, Taylor CP, Teyler TJ, Voulalas PJ. Preparative methods for brain slices: a discussion. J. Neuro. Methods, 1995;59:139-49.

Beebe DJ, Moore JS, Yu Q, Liu RH, Kraft ML, Jo BH, Devadoss C. Microfluidic tectonics: A comprehensive construction platform for microfluidic systems. Proc. Natl. Acad. Sci. USA, 2000;97:13488-93.

Beebe DJ, Mensing GA, Walker GM. Physics and applications of microfluidics in biology. Annu. Rev. Biomed. Eng., 2002;4:261–86.

Berdichevsky Y, Sabolek H, Levine JB, Staley KJ, Yarmush ML. Microfluidics and multielectrode array-compatible organotypic slice culture method. J. Neurosci. Methods, 2009;178:59-64.

Bjornsson CS, Oh SJ, Al-Kofahi YA, Lim YJ, Smith KL, Turner JN, De S, Roysam B, Shain W, Kim SJ. Effects of insertion conditions on tissue strain and vascular damage during neuroprosthetic device insertion. J. Neural Eng., 2006;3:196–207.

Blake AJ, Pearce TM, Rao NS, Johnson SM, Williams JC. Multilayer PDMS microfluidic chamber for controlling brain slice microenvironment. Lab on a Chip, 2007;4:842-849.

Boppart SA, Wheeler BC, Wallace CS. A flexible perforated microelectrode array for extended neural recordings. IEEE Trans. Biomed. Eng., 1992;39:37-42.

Bragin A, Hetke J, Wilson CL, Anderson DJ, Engel J Jr., Buzsáki G. Multiple site silicon-based probes for chronic recordings in freely moving rats: implantation, recording and histological verification. J. Neurosci. Methods, 2000;98:77-82.

Buzsáki G, Czopf J, Kondákor I, Kellényi L. Laminar distribution of hippocampal rhythmic slow activity (RSA) in the behaving rat: current-source density analysis, effects of urethane and atropine. Brain Res., 1986;365:125-37.

Buzsáki G. Large-scale recording of neuronal ensembles. Nature Neuro., 2004;7:446-51.

Csicsvari J, Jamieson B, Wise KD, Buzsáki G. Mechanisms of gamma oscillations in the hippocampus of the behaving rat. Neuron, 2003A;37:311-22.

Csicsvari J, Henze DA, Jamieson B, Harris KD, Sirota A, Bartho P, Wise KD, Buzsáki G. Massively Parallel Recording of Unit and Local Field Potentials With Silicon- Based Electrodes. J. Neurophysiol., 2003B;90:1314-23.

Drake KL, Wise KD, Farraye J, Anderson DJ, Bement SL. Performance of planar multisite microprobes in recording extracellular single-unit intracortical

activity. IEEE Trans. Biomed. Eng., 1988;35:719-32.
Duffy DC, McDonald JC, Schueller O, Whitesides GM. Rapid prototyping of microfluidic systems in poly(dimethylsiloxane). Anal. Chem., 1998;70:4974–84.
Freeman JA, Nicholson C. Experimental optimization of current source-density technique for anuran cerebellum. J. Neurophysiol., 1975;38:369-82.
Gholmieh G, Soussou W, Han M, Ahuja A, Hsiao M, Song D, Tanguay Jr. AR, Berger TW. Custom-designed high-density conformal planar multielectrode arrays for brain slice electrophysiology. J. Neurosci. Methods, 2006;152:116-29.
Hájos N, Pálhalmi J, Mann EO, Németh B, Paulsen O, Freund TF. Spike Timing of distinct types of GABAergic interneuron during hippocampal gamma oscillations in vitro. J. Neurosci., 2004;24:9127-37.
Hájos N, Ellender TJ, Zemankovics R, Mann EO, Exley R. Maintaining network activity in submerged hippocampal slices: importance of oxygen supply. Eur. J. Neurosci., 2009;29:319-27.
Heuschkel MO, Fejtl M, Raggenbass M, Bertrand D, Renaud P. A three-dimensional multi-electrode array for multi-site stimulation and recording in acute brain slices. J. Neurosci. Methods, 2002;114:135-48.
Huchzermeyer C, Albus K, Gabriel H, Otáhal O, Taubenberger N, Heinemann U, Kovács R, Kann O. Gamma oscillations and spontaneous network activity in the hippocampus are highly sensitive to decreases in pO2 and concomitant changes in mitochondrial redox state. J. Neurosci., 2008;28:1153-62.
Jo B, Van Lerberghe LM, Motsegood KM, Beebe DJ. Three-dimensional micro-channel fabrication in polydimethylsiloxane (PDMS) elastomer. J. MEMS, 2000;9:76–81.
Larson J, Wong D, Lynch G. Patterned stimulation at the theta frequency is optimal for the induction of hippocampal long-term potentiation. Brain Res., 1986;368:347- 50.
Lipton P, Aitken PG, Dudek FE, Eskessen K, Espanol MT, Ferchmin PA, Kelly JB, Kreisman NR, Landfield PW, Larkman PM. Making the best of brain slices: comparing preparative methods. J. Neurosci. Methods, 1995;59:151-6.
Mann EO, Suckling JM, Hájos N, Greenfield SA. Perisomatic feedback inhibition underlies cholinergically induced fast network oscillations in the rat hippocampus in vitro. Neuron, 2005;45:105-17.
Mitzdorf U. Current source-density method and application in cat cerebral cortex: investigation of evoked potentials and EEG phenomena. Physiol. Rev., 1985;65:37-100.
Mohammed JS, Caicedo HH, Falla CP, Eddington DT. Microfluidic add-on for standard electrophysiology chambers. Lab on a Chip, 2008;8:1048-55.
Nam Y, Wheeler BC, Heuschkel MO. Neural recording and stimulation of dissociated hippocampal cultures using microfabricated three-dimensional

tip electrode array. J. Neurosci. Methods, 2006;178:296-99.
Passeraub PA, Almeida AC, Thakor NV. Design, micro-fabrication and analysis of a microfluidic chamber for the perfusion of brain tissue slices. Biomed. Microdev., 2003;5:147–55.
Pearce RA. Physiological evidence for two distinct GABA responses in rat hippocampus. Neuron, 1993;10:189-200.
Pearce RA. Volatile anaesthetic enhancement of paired-pulse depression investigated in the rat hippocampus in vitro. J. Phys., 1996;492:823-40.
Pettersen KH, Devor A, Ulbert I, Dale AM, Einevoll GT. Current-source density estimation based on inversion of electrostatic forward solution: effects of finite extent of neuronal activity and conductivity discontinuities. J. Neurosci. Methods, 2006;154:116-33.
Pouille F, Scanziani M. Enforcement of temporal fidelity in pyramidal cells by somatic feed-forward inhibition. Science, 2001;293:1159-63.
Rambani K, Vukasinovic J, Glezer A, Potter SM. Culturing thick brain slices: An interstitial 3D microperfusion system for enhanced viability. J. Neurosci. Methods, 2009;180:243-54
Richardson TL, Turner RW, Miller JJ. Action-potential discharge in hippocampal CA1 pyramidal neurons: current source-density analysis. J. Neurophys., 1987;58:981- 96.
Rutten W, Mouveroux J, Buitenweg J, Heida C, Ruardij T, Marani E, Lakke E. Neuroelectronic interfacing with cultured multielectrode arrays toward a cultured probe. Proc. IEEE, 2001; 89:1013-29.
Sarvey JM, Burgard EC, Decker G. Long-term potentiation: studies in the hippocampal slice. J. Neurosci. Methods, 1989;28:109-24.
Sniadecki NJ, Chen CS. Microfabricated silicone elastomeric post arrays for measuring traction forces of adherent cells. Methods in Cell Biology, 2007;83:313-328.
Steidl EM, Neveu E, Bertrand D, Buisson B. The adult rat hippocampal slice revisited with multi-electrode arrays. Brain Res., 2006;1096:70-84.
Taube JS, Schwartzkroin PA. Mechanisms of long-term potentiation: a current-source density analysis. J. Neurosci., 1988;8:1645-55.
Traub RD, Miles R, Wong RK. Model of the origin of rhythmic population oscillations in the hippocampal slice. Science, 1989;243:1319-25.
Vetter RJ, Williams JC, Hetke JF, Nunamaker EA, Kipke DR. Chronic neural recording using silicon-substrate microelectrode arrays implanted in cerebral cortex. IEEE Trans. Biomed. Eng., 2004;51:896-904.
Vida I, Czopf J, Czéh G. A current-source density analysis of the long-term potentiation in the hippocampus. Brain Res., 1995;671:1-11.
Weiss T, Veh RW, Heinemann U. Dopamine depresses cholinergic oscillatory network activity in rat hippocampus. Eur. J. Neurosci., 2003;18:2573-80.
Ward MP, Rajdev P, Ellison C, Irazoqui PP. Toward a comparison of

microelectrodes for acute and chronic recordings Brain Res., 2009;In Press:1-19.

Wheeler BC, Novak JL. Current source density estimation using microelectrode array data from the hippocampal slice preparation. IEEE Trans. Biomed. Eng., 1986;33:1204–12.

Wu C, Luk WP, Gillis J, Skinner F, Zhang L. Size does matter: generation of intrinsic network rhythms in thick mouse hippocampal slices. J. Neurophysiol., 2005;93:2302–17.

Figure legends

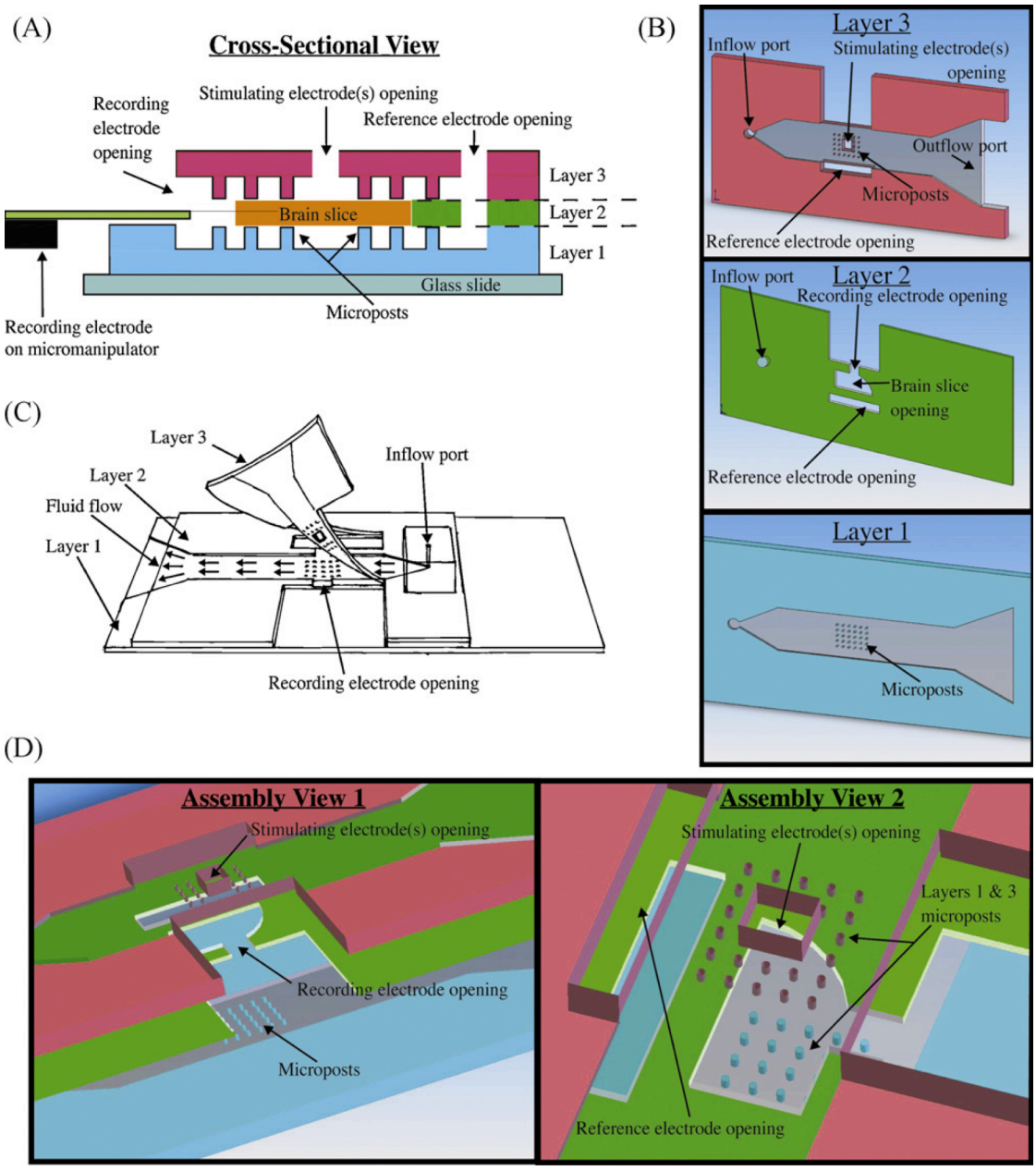

Fig. 1. Microfluidic perfusion chamber design. (A) A cross-section at the center of the microposts reveals the locations of the electrode openings relative to the brain slice and the different layer features. (B) A computer aided design (CAD) model displays the distinct features from a bottom surface view for each individual layer. (C) A free-hand drawing shows how the device appears after each layer is assembled and how the top layer is partially bonded only at the front. This allows a brain slice to be positioned properly at the electrode openings before the PDMS is temporarily sealed for perfusion to commence. (D) A CAD model shows an exploded three-dimensional view of layers and provides an idea of how alignment of the top and side openings is necessary for the integrity of the chamber.

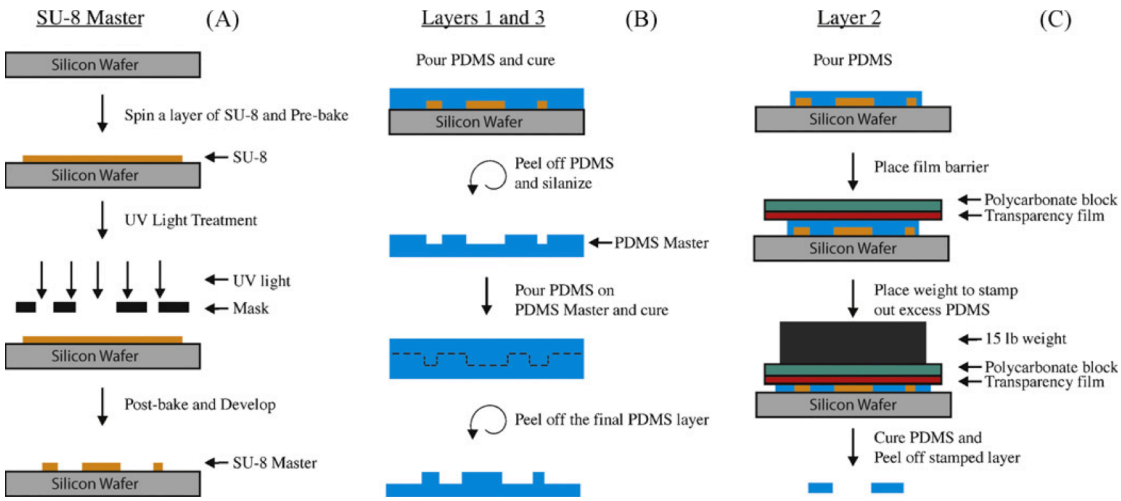

Fig. 2. Microfluidic perfusion chamber fabrication process. (A) A unique SU-8 master is constructed for each layer, layer 2 is depicted. The SU-8 is spun onto a silicon wafer at a set speed that correlates with a desired thickness. After spinning the SU-8, a mask design, distinct for each layer, is used in conjunction with a UV light to project the mask design onto the SU-8, where exposed SU-8 crosslinked. Each layer has a different SU-8 master that is used to make a PDMS mold for each layer. (B) Layers 1 and 3 use a double-negative PDMS molding process, as shown here for layer 1. This process involves creating a PDMS master from the SU-8 master that enables the reliable production of microposts since the PDMS master is more flexible. (C) A “cookie-cutter” method is used to cut out the PDMS for layer 2. (D) Layer 1 uses a single mask, whereas layer 3 uses two masks that define the electrode openings.

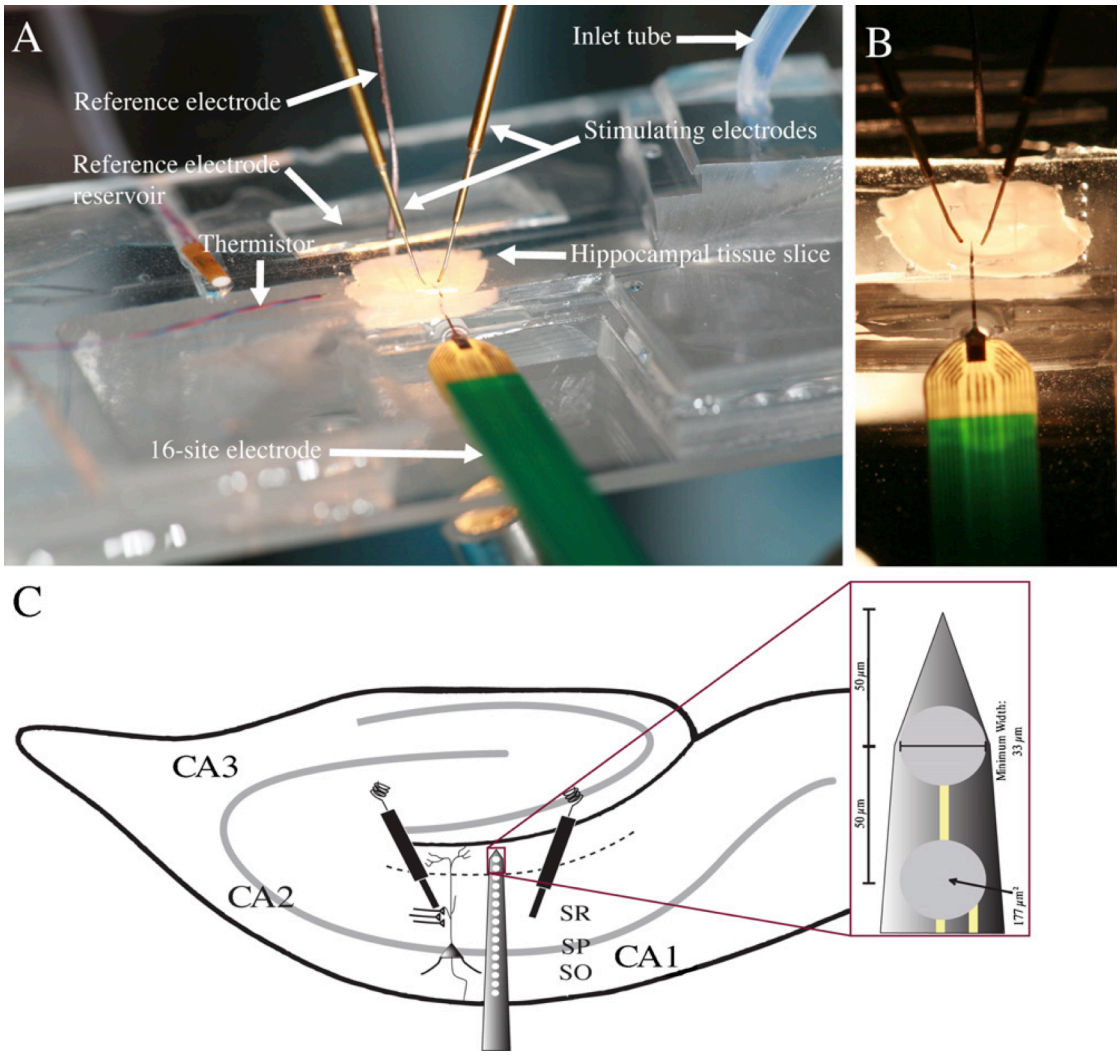

Fig. 3. Experimental setup. (A) Photograph of the experimental setup, showing the arrangement of electrodes used to stimulate and record from a hippocampal brain slice. (B) Higher magnification photograph. The recording electrode is inserted through the side opening into the edge of the hippocampal slice; stimulating electrodes are inserted through the top opening. (C) A schematic diagram of the hippocampus with a 16-channel recording electrode and two stimulating electrodes in place. The recording probe is inserted perpendicularly to the hippocampal layers, allowing for simultaneous data collection along the somatodendritic axis of pyramidal neurons. Stimulating electrodes are placed in stratum radiatum to stimulate axons of the Schaffer collateral pathway. Inset: expanded view of the tip of the NeuroNexus probe that describes recording site characteristics. SO: stratum oriens; SP: stratum pyramidale; SR: stratum radiatum.

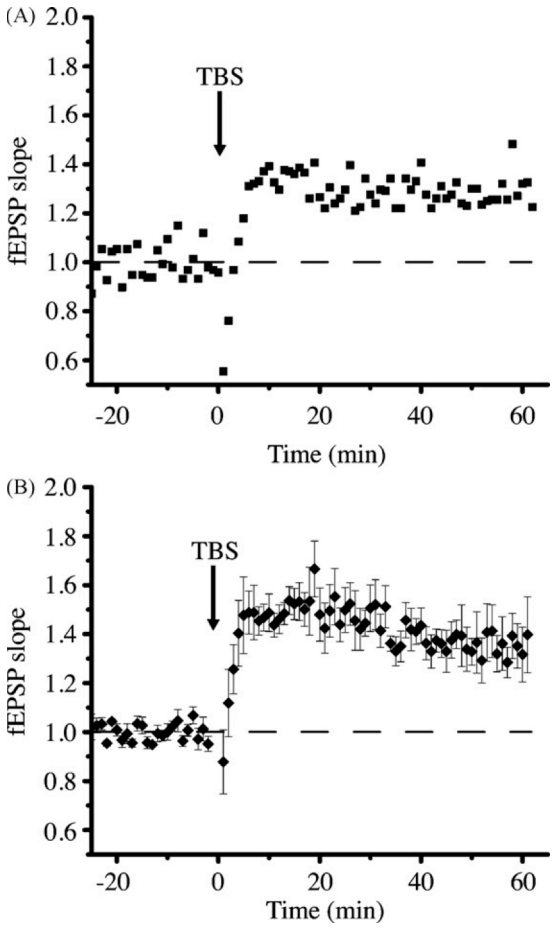

Fig. 4. Measurement of long-term potentiation using a 16-channel recording elec- trode. (A) Single field excitatory potentials (fEPSPs) at each of the 16 recording sites before (left) and after (right) theta burst stimulation (TBS). The channel with the greatest rising slope (thick line) was used for fEPSP slope measurements. Scale bar: 1 mV, 20 ms. Approximate locations of recording sites are designated by letter code: HF, hippocampal fissure; SLM, stratum lacunosum-moleculare; SR, stratum radiatum; SP, stratum pyramidale; SO, stratum oriens; ALV, alveus. (B) Effect of TBS on fEPSP slope in the experiment illustrated in panel A. Responses were normalized to the mean response during the 20-min baseline period. (C) Average effect of TBS on fEPSP slope in four different experiments. Error bars represent standard deviation.

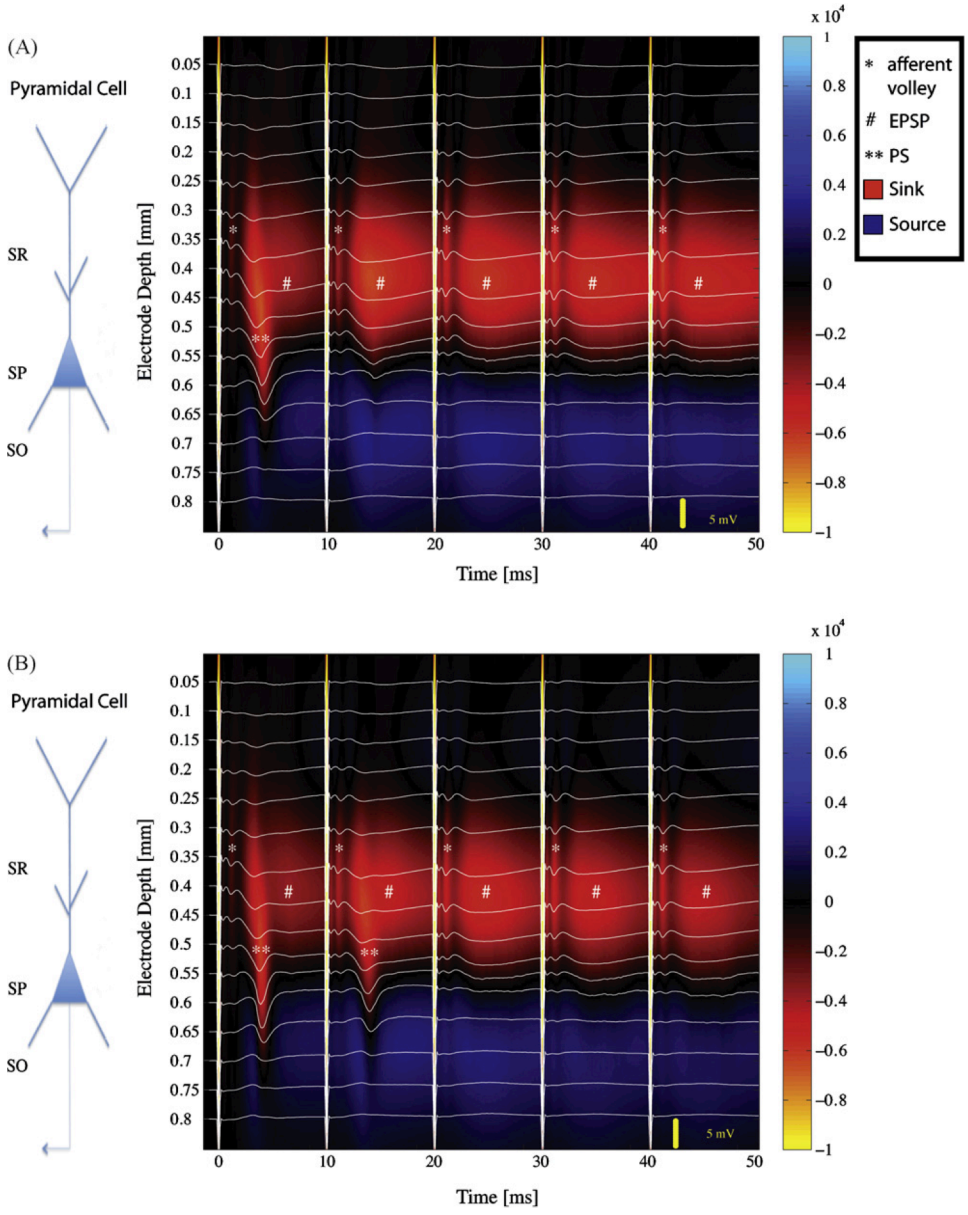

Fig. 5. Laminar profiles of the field potentials evoked during theta burst stimulation, and the corresponding current source density (CSD) analysis. Evoked potentials (white traces) are superimposed on pseudo-color images of CSD profiles. Warm colors represent current sinks, cool colors current sources. Thick vertical white lines are stimulus artifacts. A schematic diagram of a pyramidal cell is shown to the left, with corresponding hippocampal layers labeled: SR, stratum radiatum; SP, stratum pyramidale; SO, stratum oriens. (A) Response to the first burst of the first train. The first stimulus in the burst elicited a brief sink in SR corresponding to the fiber volley (*), followed by a field excitatory postsynaptic potential (fEPSP) that propagated to the somatic region and resulted in a population spike (**). Subsequent stimuli elicited only fEPSPs (#). (B) The first burst of the third train. Responses are similar to the first burst (panel A) except that a current sink that propagated from the dendrites to the soma was evident following both the first and second stimuli in the burst. (For interpretation of the references to color in the figure caption, the reader is referred to the web version of the article.)

CHAPTER 3

Etomidate blocks LTP and impairs learning but does not enhance tonic inhibition in mice carrying the N265M point mutation in the beta3 subunit of the $GABA_A$ receptor

Etomidate blocks LTP and impairs learning but does not enhance tonic inhibition in mice carrying the N265M point mutation in the beta3 subunit of the $GABA_A$ receptor

Zarnowska ED[1]*, Rodgers FC[1,2]*, Oh I[3], Rau V[3], Jurd R[4,6], Rudolph U[4,5], Eger EI 2[nd3] and Pearce RA[1]

[1]School of Medicine and Public Health, Department of Anesthesiology, [2]Neuroscience Training Program, University of Wisconsin-Madison, [3]Department of Anesthesia, University of California-San Francisco, [4]Institute of Pharmacology and Toxicology, University of Zurich, [5]Laboratory of Genetic Neuropharmacology, McLean Hospital, and Department of Psychiatry, Harvard Medical School University, Belmont

* These authors contributed equally to this work.

[6] Present address: Department of Neurology, NYU Langone Medical Center

Corresponding authors: Ewa D. Zarnowska at edzarnowska@wisc.edu or Robert A. Pearce at rapearce@wisc.edu, University of Wisconsin, 1111 Highland Ave, WIMR II, Madison, WI 53705, +1 608 263-4429

Acknowledgement: This research was supported by the NIH grants: GM047818, GM101497, GM086448. The authors thank Mark Perkins for expert technical assistance and Sijian Wang for statistical consultation.

Highlights

- Etomidate does not potentiate tonic inhibition in hippocampal CA1 pyramidal neurons from β3-N265M mice, indicating that tonic inhibition is mediated by β3-subunit containing $GABA_A$ receptors in these cells.
- Etomidate blocks synaptic plasticity *in vitro* and learning *in vivo* in β3-N265M mice, indicating that these effects are mediated by receptors that lack β3 subunits.
- The dissociation between enhancement of tonic current and suppression of LTP suggests that additional or alternative inhibitory processes underlie etomidate's amnestic effects.

Abstract

Enhancement of tonic inhibition mediated by extrasynaptic α5-subunit containing $GABA_A$ receptors has been proposed as the mechanism by which a variety of anesthetics, including the general anesthetic etomidate, impair learning and memory. Since α5 subunits preferentially partner with β3 subunits, we tested the hypothesis that etomidate acts through β3-subunit containing $GABA_A$ receptors to enhance tonic inhibition, block LTP, and impair memory. We measured the effects of etomidate in wild type mice and in mice carrying a point mutation in the β3-subunit of the $GABA_A$ receptor (β3-N265M) that renders the functional receptor insensitive to etomidate. We found that etomidate enhanced tonic inhibition in CA1 pyramidal cells of the hippocampus in wild type but not in mutant mice, demonstrating that tonic inhibition is mediated by β3-subunit containing $GABA_A$ receptors. However, despite its inability to enhance tonic inhibition, etomidate did block LTP in brain slices from mutant mice as well as in those from wild type mice. Etomidate also impaired fear conditioning to context, with no differences between genotypes. We conclude that etomidate enhances tonic inhibition in pyramidal cells through its action on α5β3-containing $GABA_A$ receptors, whereas etomidate blocks LTP and impairs learning by other means. The critical anesthetic targets underlying amnesia might include other forms of inhibition imposed on pyramidal neurons (e.g. slow phasic inhibition), or inhibitory processes on non-pyramidal cells (i.e. interneurons).

Keywords

Hippocampus; Tonic inhibition; Etomidate; LTP; Learning; GABA receptors

1. Introduction

The ability of general anesthetics to cause sedation, amnesia, and immobility has been a subject of interest and intense study for many years. There is now an emerging recognition that these different anesthetic end-points may reflect different anesthetic actions at the molecular, cellular and network levels (Rudolph and Antkowiak, 2004). The present study addresses the mechanism by which the general anesthetic etomidate impairs learning and memory.

$GABA_A$ receptors ($GABA_ARs$) are heteropentameric ligand-gated anion channels responsible for the majority of inhibitory synaptic transmission in the brain. Functional $GABA_A$ receptors most commonly incorporate two α-subunits, two β-subunits, and one γ-subunit (Olsen and Sieghart, 2008). $GABA_ARs$ are considered to be important targets of a variety of agents, including etomidate (Jones et al., 1992; Jones and Harrison, 1993; Uchida et al., 1995). Because of its favorable hemodynamic profile, etomidate is used in the clinical setting to induce anesthesia in patients at risk for cardiovascular compromise, and in other select circumstances such as electroconvulsive therapy (Forman, 2011). It has also become an important experimental drug because its receptor sensitivity can be controlled by genetic manipulation: the discovery that receptors that incorporate β1-subunits are markedly less sensitive to etomidate compared to those that incorporate β2- and β3-subunits (Sanna et al., 1997) led to the identification of a single amino acid residue in the pore-forming transmembrane

domain that controls etomidate sensitivity (Belelli et al., 1997). Mice carrying single point mutations in these subunits (β2-N265S or β3-N265M) were found to resist etomidate's action in studies of sedation and immobility (Jurd et al., 2003; Reynolds et al., 2003). The impact of these mutations on etomidate-induced amnesia was not tested.

It was shown previously that genetic and pharmacologic manipulations that reduce or eliminate inhibitory current carried by $GABA_AR$ α5-subunits (α5-KO) are resistant to etomidate's suppression of long term potentiation (LTP) *in vitro* and learning and memory *in vivo* (Cheng et al., 2006). Because the majority of α5-$GABA_ARs$ are located extrasynaptically on pyramidal cells, where they mediate a persistent conductance termed "tonic inhibition" (Caraiscos et al., 2004), and tonic inhibition is strongly enhanced by amnestic drugs, it was proposed that the effect of etomidate on synaptic plasticity is due to its enhancement of tonic inhibition (Cheng et al., 2006; Orser, 2007; Martin et al., 2009). Since α5-subunits preferentially partner with β3-subunits (Luddens et al., 1994; Sur et al., 1998), we hypothesized that mice carrying the N265M mutation in the β3-subunit would similarly resist etomidate's enhancement of tonic inhibition and suppression of LTP *in vitro* and learning *in vivo*.

We found that tonic inhibition in the β3-N265M mice was indeed insensitive to etomidate, showing that this form of inhibition is mediated by β3-

subunit containing $GABA_A$Rs. Surprisingly, although etomidate did not enhance tonic inhibition in these mice, it did suppress synaptic plasticity *in vitro* and learning *in vivo*. We conclude that tonic inhibition in CA1 pyramidal cells is mediated by $\alpha5\beta3$-subunit containing $GABA_A$Rs, but that this form of inhibition does not play a key role in anesthetic suppression of synaptic plasticity in these neurons. Rather, etomidate appears to control synaptic plasticity and learning through $\alpha5$-containing $GABA_A$Rs receptors that incorporate $\beta1$ or $\beta2$ subunits.

2. Materials and Methods

All experiments were performed in accordance with the National Institutes of Health guide the Guide *for the Care and use of Laboratory Animals* (NIH Publications No. 8023, revised 1978) and were approved by the University of Wisconsin Institutional Animal Care and Use Committee, Madison, Wisconsin, or by the University of California Institutional Animal Care and Use Committee, San Francisco, California. All efforts were made to minimize animals suffering and reduce the number of animals used.

2.1 Mice

The male offspring of heterozygous breeding pairs homozygous for an asparagine-to-methionine point mutation at position 265 of the $GABA_A$ receptor β3 subunit (β3-N265M), and homozygous wild-type controls, were used for this study. The strain background of the β3-N265M mice was 129X1/SvJ. Mice were genotyped using DNA template from tail tips, amplified by PCR using the specific primers: *RJM-8* (5′-GTT CAG CTT CCA TTC TCA CTG-3′) and *RJM-24* (5′-GCT ATG GCT TTC TGG TGG AG-3′). Animals were housed in the animal care facility under 12-h cycles of light and dark and had continuous access to standard mouse chow and water.

2.2 Slice preparation

LTP studies: Hippocampal brain slices were prepared from mice aged 42-77 days (57±9, n=31). Before decapitation mice were anesthetized with 2.5% isoflurane (Novaplus, Hospira, Inc., Lake Forest, IL), then the brain was removed, blocked by removing the cerebellum and olfactory cortex, glued to a microtome slice tray with cyanoacrylate glue (Krazy Glue Instant, Westerville, OH), and placed for slicing in ice-cold cutting artificial cerebrospinal fluid ("cutting aCSF") containing (in mM) 127 NaCl, 1.9 KCl, 2.7 $MgSO_4x7H_2O$, 0.9 $CaCl_2x2H_2O$, 26 $NaHCO_3$, 1.2 KH_2PO_4, 1 ascorbic acid, 15 glucose, bubbled with 95% O_2-5% CO_2 ("carbogen"). Coronal slices 500 μm thick were cut using a vibratome (Leica VT 100S, Leica Microsystems Nussloch GmbH, Nussloch, Germany). A portion of the slice including the hippocampus was trimmed with a scalpel to ensure proper fit within a custom-manufactured microfluidic recording chamber (Blake et al., 2010). Brain slices recovered in a holding chamber filled with carbogenated recording aCSF containing (in mM) 127 NaCl, 1.9 KCl, 26 $NaHCO_3$, 1.2 KH_2PO4, 1.4 $MgSO_4x7H_2O$, 2.2 $CaCl_2x2H_2O$, 15 glucose, 1 ascorbic acid for at least 60 min at room temperature (20 - 22 °C). This same solution was used for recording ("recording aCSF").

Patch clamp studies: Hippocampal brain slices were prepared from mice aged 40-50 days (44±1, n=7). Before decapitation mice were anesthetized with 2.5-3% isoflurane then the brain was removed and placed in ice-cold N-methyl-D-glucamine (NMDG)-based cutting solution containing (in mM): 2.5 KCl, 1.25

Na_2HPO_4, 25 $NaHCO_3$, 10 $MgSO_4x7H_2O$, 0.5 $CaCl_2x2H_2O$, 25 glucose, 110 NMDG, 2.5 sodium ascorbate, bubbled with carbogen (pH adjusted with 6N HCl to 7.3, 300-310 mOsm) (Ting and Feng, 2011). Horizontal slices 350 μm thick were cut with oscillating blade microtome 7000 smz2 vibratome (Campden Instruments, Loughborough, England). Thereafter slices recovered while submerged in warmed (35 °C), carbogenated cutting solution which was next slowly exchanged (at a rate of 5 ml/min) with warmed (35 °C), carbogenated recording aCSF containing (in mM): 130 NaCl, 2.5 KCl, 1.25 Na_2HPO_4, 25 $NaHCO_3$, 2 $MgSO_4x7H_2O$, 2 $CaCl_2x2H_2O$, 10 glucose, 2.5 sodium ascorbate (pH 7.3, 300-310 mOsm). The exchange process was completed in 30 minutes. The slices were maintained at room temperature until they were transferred to the recording chamber.

2.3 Data acquisition

LTP studies: Slices were transferred to a microfluidic recording chamber (Blake et al., 2010) perfused with recording aCSF at a flow rate of 2.5 ml/min. The bath temperature was maintained at 30 ± 0.5 °C using an in-line temperature controller (Warner Instruments Corp., Hamden, CT). A 16-channel linear recording electrode (50 μm separating recording sites; NeuroNexus Technologies, Ann Arbor, MI) was inserted orthogonal to the hippocampal layers, in the middle

of CA1, at a depth (along the rostral - caudal axis) of 200 μm beneath the surface of the tissue. Field excitatory postsynaptic potentials (fEPSPs) were electrically evoked by a tungsten stereotrode stimulating electrode (0.5 MΩ, World Precision Instruments, Sarasota, FL) placed in *stratum radiatum* for activation of the Schaffer collateral/commissural path (SC). Recorded signals were amplified 1000x, band-pass filtered between 1-3000 Hz (model LYNX-8 amplifiers, Neuralynx Inc., Tucson, AZ), digitized at 10 kHz using an analog-to-digital converter (Digidata 1440A, Molecular Devices, Sunnyvale, CA), and acquired using pClamp software (Version 10.2, Molecular Devices). Stimuli of 0.1 ms duration were delivered using a constant current stimulus isolator (model A365D, World Precision Instruments, Sarasota, FL). SC axons were stimulated at 0.03 Hz, using stimulus intensity ("baseline") adjusted to evoke responses below half-maximal fEPSP amplitude. Baseline stimulus amplitude was typically between 30 - 90 μA. LTP protocols consisted of a 30 min stable baseline recording period in which evoked fEPSP slope changed by less than 10%, followed by a theta burst stimulus (TBS), and then an additional 60 min recording period. The LTP-inducing TBS (“40x5Hz”) consisted of 10 bursts delivered every 200 ms (i.e. 5 Hz inter-burst interval) with each burst consisting of 4 pulses separated by 10 ms (i.e. 100 Hz inter-stimulus interval). The stimulus intensity during the burst was adjusted to evoke half-maximal population spike amplitude, judged by measuring

the amplitude of the downward-going negative voltage peak in the pyramidal channel (see below) online during recordings.

Patch-clamp studies: Slices were transferred to a submersion-style recording chamber perfused at a flow rate of 2.5-3 ml/min with recording aCSF containing kynurenic acid (KA, 3 mM). The bath temperature was maintained at 30 ± 0.5 °C using an in-line temperature controller (Warner Instruments Corp.). Pyramidal cells in the CA1 region were visualized with a 40 x water immersion objective and IR-DIC video camera installed on BX50WI microscope (Olympus America Inc., Center Valley, PA). Patch clamp recordings were obtained using a MultiClamp 700B amplifier (Molecular Devices), low pass filtered at 4 kHz, digitized at 10 kHz using an analog-to-digital converter (Digidata 1322A, Molecular Devices), and acquired using pClamp software (Version 10.3, Molecular Devices). Borosilicate glass pipettes (O.D. 1.5 mm x I.D. 0.86 mm, Sutter Instruments, Novato, CA) were pulled to tip diameters of ~1 μm using a horizontal puller (P-97, Sutter Instruments) then filled with an intracellular solution containing (in mM) 90 CsCl, 30 KCl, 5 NaCl, 10 NaHEPES, 5 EGTA, 4 Mg_2ATP 2, 0.4 Na_3GTP, 10 Na_2phosphocreatine, 4 QX-314, pH adjusted with 1M CsOH to 7.3 (290±5 mOsm). The resistances of filled pipettes were 5-7 MΩ. Whole-cell, voltage-clamp recordings were performed at a -60 mV holding potential. Cell capacitances and membrane resistances were measured using the software membrane test algorithm. Series resistances were not compensated but were

monitored, and recordings were discontinued if resistance increased more than 25%. Uncompensated series resistances were 10-20 MΩ.

2.4 Behavioral testing

Behavioral testing was conducted at the University of California, San Francisco. Three to 10 male mice, between 60 to 80 days old, of each genotype (7 on average per group) were assessed at 0, 7.5, 9.38, 10.3, 11.25 and 15 mg/kg etomidate. These doses were chosen based on a previous study indicating that etomidate's ED_{50} for conditional freezing for a similar fear conditioning protocol in 129/SvJ x C57BL/6J mice was 11 mg/kg (Benkwitz et al., 2007). A 35% propylene glycol solution (Sigma, St. Louis, MO) was used for all vehicle injections. The intraperitoneal injection of etomidate was given 30 minutes before training, and all mice were injected at 7.7 ml/kg body weight.

Thirty minutes after the injection, groups of four mice at a time were transported from their home cage and transferred to fear conditioning chambers (27 cm L×24.5 cm W×20 cm H) constructed of clear acrylic. The chamber floor was made of 31 stainless steel bars (3 mm in diameter, spaced 7 mm center to center) and was connected to a shock delivery system (San Diego Instruments, San Diego, CA). Before and after each session, the chambers walls were cleaned with 5% Pine Scented Disinfectant (Midland, Inc., Sweetwater, TN). Pine solution was placed in a dish underneath each chamber as well. Room lights

were left on and white noise (65 db) was played in the background. The odor, tactile, auditory and visual stimuli of the chamber comprised the training "context".

After a 3-min baseline period, mice received 6 shocks (1 mA, 2 s), separated by 1 min. They were removed from the chamber 30 s after the last shock. Mice were tested for fear to the training context the following day by placement back in their training chamber in the absence of shock for a period of 8 min. The context tested was identical to the training context.

Freezing, the absence of all movement except that necessary for respiration, is an innate defensive response in rodents and is a reliable measure of learned fear (Fanselow, 1980). A camera installed in an experimental room transmitted a video to the monitor placed in adjoining room where animals were scored online by the observer. The observer scoring the behavior was blinded to the genotypes of the mice. Each animal's behavior was scored every 8 s during the test. If the animal showed freezing, it was given a score of "1" for that observation; if the animal showed movement, it was given a score of "0" for that observation. A percentage was calculated by dividing the number of freezing observations a mouse had by the total number possible during the observation period. This number represented the animal's freezing score.

To derive ED_{50} values for etomidate suppression of fear conditioning, data were fit by a logistic dose response curve: y = A2 + (A1-A2)/(1 + (x/x0)^p), where A1 (max value) was fixed at 1 and A2 (min value) was fixed at 0, and ED_{50}=x0.

2.5 Data analysis

Electrophysiological data were analyzed using Clampfit 10.2 and 10.3 (Molecular Devices), Origin 9.0 (Microcal Software Inc., Northampton, MA), GraphPad Prism 6.05 (GraphPad Software Inc., La Jolla, CA), custom-written R programming language scripts (R Foundation for Statistical Computing, Vienna, Austria), and Mini Analysis Program 6 (Synaptosoft Inc., Decatur, GA).

2.6 Measurement of LTP

The recording electrode site used for LTP analysis was the site with the largest amplitude fEPSP in response to the baseline stimulus ("dendritic channel"). Field EPSP slopes were analyzed using Clampfit (10.2, Molecular Devices) to determine the maximum rate of rise at the dendritic channel. The electrode site closest to the pyramidal cell layer ("pyramidal channel"), used for population spike analysis, was chosen by examining the evoked waveform in response to a stimulus that was suprathreshold for population spike generation. Slices without population spikes of at least 0.5 mV prior to TBS, or that showed unstable responses before or after TBS, were excluded from

analysis. The coefficient of variation of the pre-tetanus baseline for the slices that met these inclusion criteria was 0.09. LTP was calculated as the percentage change of the fEPSP slope collected 10 min pre-TBS and the last 10 min (51-60 min) post-TBS of the LTP experiment.

2.7 Detection and measurement of tonic inhibition

Tonic inhibition was measured by adding the non-competitive $GABA_A$ receptor antagonist picrotoxin (PTX, 200 μM) to the aCSF superfusate. The amount of tonic current was calculated as the difference in baseline current before and after the addition of PTX. The mean current values were obtained from Gaussian fits to all point amplitude histograms. Histograms (1 pA bin-width) were constructed using 1 min of data before and 20 sec of data after the PTX effect had stabilized, which required ~2 min. The histogram generated from data before PTX application had skewed distribution towards larger negative value. To ensure that sIPSCs were not included into the measurement of tonic inhibition, the Gaussian fit was applied to the unskewed (outward current) portion of the distribution. The resulting parameters were used to simulate a symmetric Gaussian curve. The difference between peak values of two simulated Gaussians was used as the measure of the baseline tonic current.

2.8 Detection and measurement of sIPSCs

To detect sIPSCs, the search protocol threshold was set at 3 times the root mean square (RMS) noise level, which typically was 3-6 pA. For each cell, at least 40 sIPSCs were averaged, normalized, and characterized by their 10-90% rise and weighted decay times. The sIPSCs used for averaging were selected based on the presence of a stable baseline level and the lack of spontaneous events during the deactivation phase. These events were aligned at the time of half-maximal amplitude of the rising phase. The decay phases of averaged fast sIPSCs were fitted to bi-exponential functions using a Simplex fitting algorithm Mini Analysis Program 6 (Synaptosoft Inc.).

2.9 Statistics

Data are presented as mean ± SEM unless indicated otherwise, with *n* specifying the number of mice, slices or recorded cells. Means were compared using two-way ANOVA or two-tailed t-tests, or when appropriate based on prior information, on one-tailed t-tests (unpaired, unless indicated otherwise). The critical value for statistical significance was set at $p < 0.05$. The Benjamini-Hochberg procedure to correct for multiple comparisons (Benjamini and Hochberg, 1995). Variance in the ratio between independent estimates was calculated by the formula $\sigma_{A/B} \approx \left|\frac{A}{B}\right| \sqrt{\left(\frac{\sigma_A}{A}\right)^2 + \left(\frac{\sigma_B}{B}\right)^2}$ where $\sigma_{A/B}$ is the standard deviation of the ratio, A is the mean of A, B is the mean of B, σ_A is the standard deviation of B, and σ_B is the standard deviation of B.

2.10 Chemicals

For electrophysiological experiments *in vitro*, etomidate ((*R*)-1-(1-phenylethyl)-1*H*-imidazole-5-carboxylic acid ethyl ester) was purchased from Tocris as a powder that was dissolved in DMSO and kept in aliquots at 50 mM concentration. For each experiment, an aliquot was thawed and diluted appropriately in recording aCSF. The final concentration of DMSO did not exceed 0.1%, which in previous studies was found to have no effect on $GABA_A$Rs (Harney et al., 2003). Effects of etomidate were quantified in slices that had been pre-incubated in etomidate for at least 1 hour (Benkwitz et al., 2007). For behavioral experiments *in vivo*, etomidate was purchased pre-dissolved in a 35% propylene glycol solution at a concentration of 2 mg etomidate/ml solution (Hospira, Inc; Lake Forest, IL). All salts were obtained from Sigma-Aldrich, and kynurenic acid from Abcam Biochemicals®, NaHEPES from ChemCruz™ Biochemicals, and $CaCl_2x2H_2O$ from Fisher Scientific.

3. Results

3.1 Etomidate does not enhance tonic inhibition in β3-N265M mice

To test the hypothesis that tonic inhibition is mediated by $GABA_A$ receptors that contain β3-subunits, we measured and compared the amplitudes of tonic currents in wild type and β3-N265M mice, under control conditions and in the presence of 1 μM etomidate (Fig.1). Under control conditions, the level of tonic

current approached, but did not reach, statistical significance (WT 4.7±2.3 pA, n=7, p=0.08; β3-N265M 4.7±2.5 pA, n=7, p=0.1, one-tailed t-test). These values did not differ between genotypes (p=0.99, two-tailed t-test). Etomidate increased the amplitude of tonic current in WT mice (22.45±2.8 pA; p=0.001 *vs*. WT control, one-tailed t-test) but not in β3-N265M mice (6.05±2.8 pA; p=0.4 *vs.* mutant control, one-tailed t-test).

We conclude from these results that tonic inhibition in CA1 pyramidal neurons arises mostly or entirely from receptors that incorporate β3-subunits.

3.2. *Etomidate effect on deactivation of $GABA_{A,fast}$ is reduced in β3-N265M mice*

Spontaneous fast inhibitory postsynaptic currents (sIPSCs) were evident in our whole cell recordings before PTX was applied. We characterized and compared the properties of these "$GABA_{A,fast}$" sIPSCs in WT and β3-N265M mice, in the absence and presence of 1 μM etomidate (Table 1).

We found that the frequency, amplitude, and kinetic properties of $GABA_{A,fast}$ did not differ between genotypes under control conditions (p=0.3-0.9, two-tailed t-test). Etomidate increased the weighted decay time constant (τ_w) by 175±26% in WT mice (p=0.006, one-tailed t-test), and by 127±8% in β3-N265M mice (p=0.001, one-tailed t-test) (Table 1). These effects of etomidate on τ_w were significantly different between genotypes (p=0.03, two-tailed t-test).

We conclude from these results that β3-subunit containing $GABA_A$Rs contribute in part to fast phasic inhibition in CA1 pyramidal cells.

3.3 Etomidate blocks LTP in brain slices from β3-N265M knock-in mice

It has been proposed that enhancement of tonic inhibition in CA1 pyramidal cells by etomidate accounts for its ability to block synaptic plasticity *in vitro* and learning and memory *in vivo* (Cheng et al., 2006). Thus, we hypothesized that etomidate would fail to block LTP or impair memory in β3-N265M mice, since it did not potentiate tonic inhibition. To test this hypothesis, we induced LTP of the fEPSP using TBS in slices from WT and β3-N265M mice under control conditions and in the presence of 0.25 μM etomidate (Fig.2).

Theta burst stimulation induced LTP under drug-free conditions in both genotypes (WT 165±17%, n=7; β3-N265M 160±10%, n=7), and etomidate reduced the amplitude of LTP (WT 129±11%, n=8; β3-N265M 122±7%, n=7), by an amount that did not differ between genotypes (genotype $F(1,25)=0.4$, $p=0.5$; drug $F(1,25)=10.24$, $p<0.01$; interaction $F(1,25)=0.01$, $p=0.9$; two-way ANOVA).

From these results we conclude that, contrary to our expectation, etomidate is able to block synaptic plasticity *in vitro* in β3-N265M mice as well as in WT mice. The discrepancy between the effect of etomidate on tonic inhibition and on LTP suggests that enhanced tonic inhibition is not the mechanism by which etomidate blocks TBS-induced synaptic plasticity.

3.4 Etomidate impairs fear conditioning to context in β3-N265M mice

To test whether etomidate impairs learning and memory *in vivo* by modulating $GABA_A$ receptors that incorporate β3-subunits, we compared effects of different doses of etomidate on contextual fear conditioning in WT and β3-N265M mice (Fig.3).

Under drug-free conditions, freezing scores did not differ in WT *vs.* β3-N265M mice (55.7±9.5%, n=10 *vs.* 35±11.5%, n=8; p=0.86, two-tailed t-test). Increasing doses of etomidate (7.5-15 mg/kg) reduced freezing scores in both genotypes (Fig. 3), with an ED_{50} dose of 8.2±1.1 mg/kg, 95% confidence interval [CI] 4.5-9.6 mg/kg for WT, and 8.8±0.8 mg/kg, 95% confidence interval [CI] 6.6-10.7 mg/kg, for β3-N265M mice.

From these results we conclude that etomidate is able to block learning and memory *in vivo* in β3-N265M mice as in WT mice, thus mirroring our findings above for TBS-induced LTP. Taken together, our findings indicate that neither tonic inhibition nor β3-$GABA_A$Rs contribute critically to the amnestic effect of etomidate.

4. Discussion

The data presented here support the hypothesis that $\alpha5\beta3$-$GABA_A$Rs underlie tonic inhibition in pyramidal cells in the hippocampal CA1 region. However, they also show that impairment of learning *in vivo* and LTP *in vitro* by etomidate is independent of $\beta3$-subunit containing $GABA_A$Rs. This dissociation between enhanced tonic inhibition and impaired plasticity and memory challenges the notion that tonic inhibition mediates the amnestic effect of etomidate, as derived from studies of $\alpha5$-KO mice (Cheng et al., 2006; Martin et al., 2009).

To arrive at these conclusions we used mice carrying a point mutation in the $\beta3$-subunit of the $GABA_A$R that renders these receptors insensitive to etomidate (Jurd et al., 2003). This model allowed us to dissect the roles of different β-subunits in etomidate enhancement of tonic inhibition and suppression of learning and memory. Our results are consistent with previous reports that $\alpha5$-$GABA_A$Rs mediate tonic inhibition in CA1 pyramidal neurons (Caraiscos et al., 2004), and that $\alpha5$-$GABA_A$Rs are important for learning and memory (Collinson et al., 2002; Crestani et al., 2002). However our data indicate that $\alpha5$-subunits do so in partnership with either $\beta1$- or $\beta2$-subunits, both of which are sensitive to modulation by etomidate (Sanna et al., 1997; Janssen et al., 2009). One caveat that should be noted is that we have not measured $\alpha5$-subunit expression directly, so it is possible that associated changes in these subunits may have occurred in

these mice. However, substantial changes in α5 subunit expression seems unlikely, since the knock-in mutation does not alter expression of the β3 subunit itself, nor of any of the other subunits that have been measured (α1, α2, α3, β2/3, γ2) (Jurd et al., 2003).

The finding that etomidate achieves its amnestic effects through selective modulation of α5β1- or α5β2-containing $GABA_ARs$ is unexpected. Previous investigators showed that α5 subunits are essential for etomidate-induced amnesia (Cheng et al., 2006), that α5 subunits preferentially co-assemble with β3 subunits (Luddens et al., 1994; Sur et al., 1998), that properties of recombinant $\alpha5\beta3\gamma2$ receptors are similar to those of native receptors in CA1 pyramidal cells, which are enriched in α5 and β3 subunits (Burgard et al., 1996; Sur et al., 1998; Caraiscos et al., 2004), and that α5 and β3 subunits are co-depleted in mice lacking either the β3 or α5 subunits (Olsen and Homanics, 2000). However, there is also evidence that native $\alpha5\beta1$ and $\alpha5\beta2$ receptors do exist, although they constitute a minority of α5-containing receptors (Ju et al., 2009).

Our findings do support behavioral results obtained in forebrain specific β3-KO mice showing that β3-$GABA_ARs$ do not mediate etomidate-induced amnesia (Rau et al., 2011). Previous experiments in β3-N265M mice similarly showed that propofol-induced amnesia is independent of β3-$GABA_ARs$ (Zeller et al., 2007). Experiments with isoflurane produced conflicting results: studies in β3-N265M

knock-in mice indicated no contribution of β3 subunits (Liao et al., 2005) but studies in forebrain-specific knockout suggested a partial contribution (Rau et al., 2011). Because of the lower likelihood for compensatory changes in receptor expression in knock-in *vs.* knock-out mice, the present results strengthen the evidence that etomidate acts through receptors that lack β3-subunits.

Since β3-$GABA_A$R-mediated tonic inhibition appears not to be the means by which etomidate impairs synaptic plasticity and learning, what inhibitory processes might be involved? Our analysis of spontaneous $GABA_{A,fast}$ IPSCs showed that non-β3-subunit containing $GABA_A$Rs participate in fast phasic inhibition in CA1 pyramidal cells (Table 1). However, fast inhibitory currents are relatively insensitive to amnestic concentrations of etomidate (Dai et al., 2009), suggesting that $GABA_{A,fast}$ inhibition is unlikely to contribute substantially. By contrast, $GABA_{A,slow}$, an inhibitory current that overlaps anatomically with excitatory receptors on the dendrites (Pearce, 1993), was shown previously to engage α5-$GABA_A$Rs (Zarnowska et al., 2009), and to be particularly sensitive to amnestic concentrations of etomidate (Dai et al., 2009). This form of inhibition thus appears to be well suited to anesthetic control of synaptic plasticity and memory.

It is also possible that etomidate targets α5 subunits on interneurons to control synaptic plasticity and memory. $GABA_{A,slow}$ synapses have been

observed in interneurons (Banks et al., 2000), and activation of synaptic α5-$GABA_A$Rs significantly reduces the excitability of *oriens lacunosum-moleculare* (OLM) interneurons (Salesse et al., 2011). In addition, OLM interneurons have been shown to impact mnemonic processes in the hippocampus by inhibiting other interneurons located in *stratum radiatum* of the hippocampus (Leao et al., 2012). Thus, etomidate may target non-β3-subunit containing $GABA_A$Rs on interneurons to impair learning and memory and synaptic plasticity through "disinhibition" (Freund and Gulyas, 1997; Pi et al., 2013; Wolff et al., 2014). Experiments that restrict changes in receptor expression or anesthetic sensitivity to specific classes of neurons, such as O-LM interneurons (Lee and Maguire, 2013) will be useful for testing these possibilities.

Figure legends

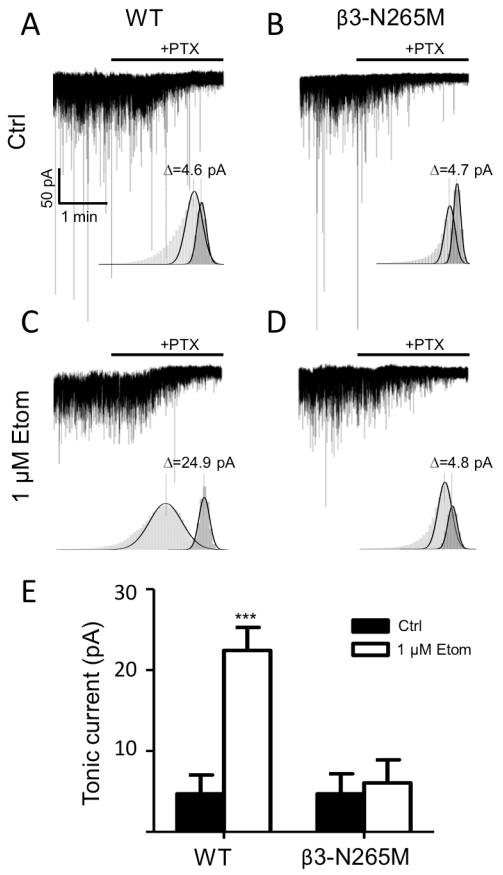

Fig.1. Tonic inhibition is mediated by β3-subunit containing $GABA_A$ receptors. (A and C) Representative traces containing spontaneous inhibitory currents recorded in WT mice in the absence (Ctrl) and presence of etomidate (1 μM Etom). (B and D) Representative traces containing spontaneous inhibitory currents recorded in β3N265M mice in the absence (Ctrl) and presence of etomidate (1 μM Etom). Insets show frequency histograms (light and dark grey) with overlaid Gaussian fits (black). The peaks of the fits were used as a measure of the amplitude of tonic currents before and after application of the non-competitive $GABA_A$Rs channel-blocker, picrotoxin (PTX, 200 μM). (E) Summary bar plot of average amplitudes of tonic inhibition measured in the two genotypes under different conditions.

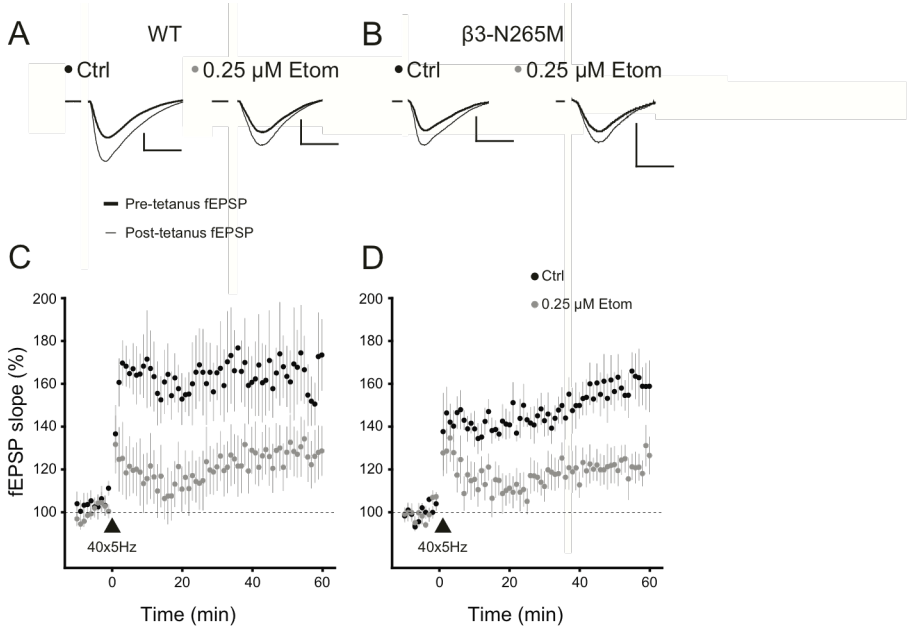

Fig.2. Effect of etomidate on long-term potentiation does not depend on β3-subunit containing $GABA_A$ receptors. (A and B) Representative traces showing field excitatory post-synaptic potentials (fEPSPs) recorded from *stratum radiatum* of the CA1 region in slices from WT (A) and β3-N265M mice (B) in the absence (Ctrl) and presence of etomidate (0.25 μM Etom). Traces are the averages of fEPSPs acquired 10 min pre-TBS (thick line) and the last 10 min (51-60 min) post-TBS (thin line). Scale bars indicate 0.5 mV and 10 ms. (C and D) Summary time series of the fEPSPs slope changes following 40x5Hz TBS (triangle) in WT (C) and β3-N265M mice (D) in the absence (black circles, Ctrl) and presence of etomidate (grey circles, 0.25 μM Etom). *N*=7-8 slices per group.

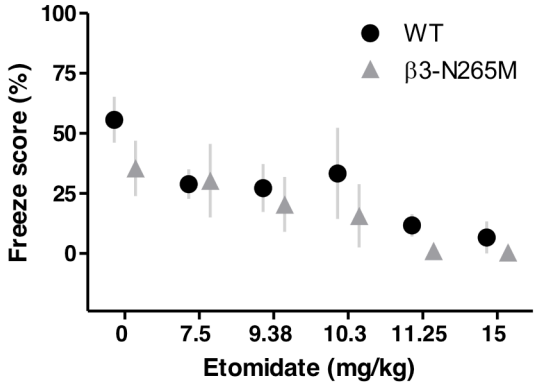

Fig.3. Effect of etomidate on contextual fear conditioning does not depend on β3-subunit containing $GABA_A$ receptors. Learning was assessed as % time spent freezing when re-exposed to context in WT (black circles) and β3-N265M (grey triangles) mice. Increasing doses of etomidate reduced freezing scores equally in both genotypes.

	$GABA_{A,fast}$	Frequency (s^{-1})	10-90% RT (ms)	Amplitude (pA)	τ1 (ms)	τ2 (ms)	A1 (%)	τw (ms)
WT	Ctrl	21.1±2.7	0.61±0.03	-37.8±2.4	7.0±0.6	13.7±2.3	73±6	8.5±0.6
	Etom	14.9±2.0	0.59±0.04	-34.1±3.6	4.1±0.4**	21.7±3.1	38±3***	14.9±2.0*
β3-N265M	Ctrl	19.3±1.7	0.60±0.04	-39.6±3.6	4.9±0.4	15.2±2.7	67±7	7.7±0.5
	Etom	17.2±1.5	0.60±0.04	-34.6±2.5	4.3±0.6	17.6±2.0	55±5	9.8±0.2**

Table 1. Average measures of $GABA_{A,fast}$ IPSCs recorded from CA1 pyramidal cells in WT and β3-N265M mice, in the absence (Ctrl) and presence of 1 μM of etomidate (Etom). Statistical significance *P<0.05, **P<0.01, ***P<0.001, *n*=7 cells for each condition.

References

Banks MI, White JA, Pearce RA (2000) Interactions between distinct GABA(A) circuits in hippocampus. Neuron 25:449-457.

Belelli D, Lambert JJ, Peters JA, Wafford K, Whiting PJ (1997) The interaction of the general anesthetic etomidate with the gamma-aminobutyric acid type A receptor is influenced by a single amino acid. Proc Natl Acad Sci U S A 94:11031-11036.

Benjamini Y, Hochberg Y (1995) Controlling the False Discovery Rate: A Practical and Powerful Approach to Multiple Testing. Journal of the Royal Statistcal Society 57:289-300.

Benkwitz C, Liao M, Laster MJ, Sonner JM, Eger EI, 2nd, Pearce RA (2007) Determination of the EC50 amnesic concentration of etomidate and its diffusion profile in brain tissue: implications for in vitro studies. Anesthesiology 106:114-123.

Blake AJ, Rodgers FC, Bassuener A, Hippensteel JA, Pearce TM, Pearce TR, Zarnowska ED, Pearce RA, Williams JC (2010) A microfluidic brain slice perfusion chamber for multisite recording using penetrating electrodes. Journal of Neuroscience Methods 189:5-13.

Burgard EC, Tietz EI, Neelands TR, Macdonald RL (1996) Properties of recombinant gamma-aminobutyric acid A receptor isoforms containing the alpha 5 subunit subtype. Molecular Pharmacology 50:119-127.

Caraiscos VB, Elliott EM, You-Ten KE, Cheng VY, Belelli D, Newell JG, Jackson MF, Lambert JJ, Rosahl TW, Wafford KA, MacDonald JF, Orser BA (2004) Tonic inhibition in mouse hippocampal CA1 pyramidal neurons is mediated by α5 subunit-containing γ-aminobutyric acid type A receptors. Proceedings of the National Academy of Sciences of the United States of America 101:3662-3667.

Cheng VY, Martin LJ, Elliott EM, Kim JH, Mount HTJ, Taverna FA, Roder JC, MacDonald JF, Bhambri A, Collinson N, Wafford KA, Orser BA (2006) α5GABAA Receptors Mediate the Amnestic But Not Sedative-Hypnotic Effects of the General Anesthetic Etomidate. The Journal of Neuroscience 26:3713-3720.

Collinson N, Kuenzi FM, Jarolimek W, Maubach KA, Cothliff R, Sur C, Smith A, Otu FM, Howell O, Atack JR, McKernan RM, Seabrook GR, Dawson GR, Whiting PJ, Rosahl TW (2002) Enhanced learning and memory and altered GABAergic synaptic transmission in mice lacking the alpha 5 subunit of the GABAA receptor. J Neurosci 22:5572-5580.

Crestani F, Keist R, Fritschy JM, Benke D, Vogt K, Prut L, Bluthmann H, Mohler H, Rudolph U (2002) Trace fear conditioning involves hippocampal alpha5 GABA(A) receptors. Proc Natl Acad Sci U S A 99:8980-8985.

Dai S, Perouansky M, Pearce RA (2009) Amnestic concentrations of etomidate modulate GABAA,slow synaptic inhibition in hippocampus. Anesthesiology 111:766-773.

Fanselow MS (1980) Conditioned and unconditional components of post-shock freezing. Pavlov J Biol Sci 15:177-182.

Forman SA (2011) Clinical and molecular pharmacology of etomidate. Anesthesiology 114:695-707.

Freund TF, Gulyas AI (1997) Inhibitory control of GABAergic interneurons in the hippocampus. Can J Physiol Pharmacol 75:479-487.

Harney SC, Frenguelli BG, Lambert JJ (2003) Phosphorylation influences neurosteroid modulation of synaptic GABAA receptors in rat CA1 and dentate gyrus neurones. Neuropharmacology 45:873-883.

Janssen MJ, Ade KK, Fu Z, Vicini S (2009) Dopamine modulation of GABA tonic conductance in striatal output neurons. J Neurosci 29:5116-5126.

Jones MV, Harrison NL (1993) Effects of volatile anesthetics on the kinetics of inhibitory postsynaptic currents in cultured rat hippocampal neurons. J Neurophysiol 70:1339-1349.

Jones MV, Brooks PA, Harrison NL (1992) Enhancement of gamma-aminobutyric acid-activated Cl- currents in cultured rat hippocampal neurones by three volatile anaesthetics. J Physiol 449:279-293.

Ju YH, Guzzo A, Chiu MW, Taylor P, Moran MF, Gurd JW, MacDonald JF, Orser BA (2009) Distinct properties of murine alpha 5 gamma-aminobutyric acid type a receptors revealed by biochemical fractionation and mass spectroscopy. J Neurosci Res 87:1737-1747.

Jurd R, Arras M, Lambert S, Drexler B, Siegwart R, Crestani F, Zaugg M, Vogt K, Ledermann B, Antkowiak B (2003) General anesthetic actions in vivo strongly attenuated by a point mutation in the GABAA receptor beta3 subunit. FASEB J 17:250 - 252.

Leao RN, Mikulovic S, Leao KE, Munguba H, Gezelius H, Enjin A, Patra K, Eriksson A, Loew LM, Tort ABL, Kullander K (2012) OLM interneurons differentially modulate CA3 and entorhinal inputs to hippocampal CA1 neurons. Nat Neurosci 15:1524-1530.

Lee V, Maguire J (2013) Impact of inhibitory constraint of interneurons on neuronal excitability. J Neurophysiol 110:2520-2535.

Liao M, Sonner JM, Jurd R, Rudolph U, Borghese CM, Harris RA, Laster MJ, Eger EI, 2nd (2005) Beta3-containing gamma-aminobutyric acidA receptors are not major targets for the amnesic and immobilizing actions of isoflurane. Anesth Analg 101:412-418, table of contents.

Luddens H, Seeburg PH, Korpi ER (1994) Impact of beta and gamma variants on ligand-binding properties of gamma-aminobutyric acid type A receptors. Mol Pharmacol 45:810-814.

Martin LJ, Oh GH, Orser BA (2009) Etomidate targets alpha5 gamma-aminobutyric acid subtype A receptors to regulate synaptic plasticity and memory blockade. Anesthesiology 111:1025-1035.

Olsen RW, Homanics GE (2000) Function of $GABA_A$ receptors:insights from mutant and knockout mice. Philadelphia: Lippincot, Williams & Willkins.

Olsen RW, Sieghart W (2008) International Union of Pharmacology. LXX. Subtypes of gamma-aminobutyric acid(A) receptors: classification on the basis of subunit composition, pharmacology, and function. Update. Pharmacol Rev 60:243-260.

Orser BA (2007) Lifting the fog around anesthesia. Sci Am 296:54-61.

Pearce RA (1993) Physiological evidence for two distinct GABAA responses in rat hippocampus. Neuron 10:189-200.

Pi HJ, Hangya B, Kvitsiani D, Sanders JI, Huang ZJ, Kepecs A (2013) Cortical interneurons that specialize in disinhibitory control. Nature 503:521-524.

Rau V, Oh I, Liao M, Bodarky C, Fanselow MS, Homanics GE, Sonner JM, Eger EI, 2nd (2011) Gamma-aminobutyric acid type A receptor beta3 subunit forebrain-specific knockout mice are resistant to the amnestic effect of isoflurane. Anesth Analg 113:500-504.

Reynolds DS, Rosahl TW, Cirone J, O'Meara GF, Haythornthwaite A, Newman RJ, Myers J, Sur C, Howell O, Rutter AR, Atack J, Macaulay AJ, Hadingham KL, Hutson PH, Belelli D, Lambert JJ, Dawson GR, McKernan R, Whiting PJ, Wafford KA (2003) Sedation and Anesthesia Mediated by Distinct GABAA Receptor Isoforms. The Journal of Neuroscience 23:8608-8617.

Rudolph U, Antkowiak B (2004) Molecular and neuronal substrates for general anaesthetics. Nat Rev Neurosci 5:709-720.

Salesse C, Mueller CL, Chamberland S, Topolnik L (2011) Age-dependent remodelling of inhibitory synapses onto hippocampal CA1 oriens-lacunosum moleculare interneurons. The Journal of Physiology 589:4885-4901.

Sanna E, Murgia A, Casula A, Biggio G (1997) Differential subunit dependence of the actions of the general anesthetics alphaxalone and etomidate at gamma-aminobutyric acid type A receptors expressed in Xenopus laevis oocytes. Mol Pharmacol 51:484-490.

Sur C, Quirk K, Dewar D, Atack J, McKernan R (1998) Rat and Human Hippocampal α5 Subunit-Containing γ-Aminobutyric AcidA Receptors Have α5β3γ2 Pharmacological Characteristics. Molecular Pharmacology 54:928-933.

Ting JT, Feng G (2011) Improved methods for acute brain slice preparation from adult and aging brain. Society for Neuroscience Annual Meeting Abstracts Book 520.29.

Uchida I, Kamatchi G, Burt D, Yang J (1995) Etomidate potentiation of GABAA receptor gated current depends on the subunit composition. Neurosci Lett 185:203-206.

Wolff SB, Grundemann J, Tovote P, Krabbe S, Jacobson GA, Muller C, Herry C, Ehrlich I, Friedrich RW, Letzkus JJ, Luthi A (2014) Amygdala interneuron subtypes control fear learning through disinhibition. Nature 509:453-458.

Zarnowska ED, Keist R, Rudolph U, Pearce RA (2009) GABAA receptor α5 subunits contribute to GABAA, slow synaptic inhibition in mouse hippocampus. Journal of Neurophysiology 101:1179-1191.

Zeller A, Arras M, Jurd R, Rudolph U (2007) Mapping the contribution of beta3-containing GABAA receptors to volatile and intravenous general anesthetic actions. BMC Pharmacol 7:2.

CHAPTER 4

Etomidate blocks long-term potentiation *in vitro* by targeting α5-$GABA_A$Rs on non-pyramidal cells

Etomidate blocks long-term potentiation *in vitro* by targeting α5-GABA$_A$Rs on non-pyramidal cells.

F. Clifford Rodgers[1,2*], Ewa D. Zarnowska[2*], Elif Engin[3], Ruth Keist[4], Uwe Rudolph[3], and Robert A. Pearce[2]

1. Neuroscience Training Program, University of Wisconsin, Madison, WI

2. Department of Anesthesiology, University of Wisconsin, Madison, WI

3. Department of Psychiatry, McLean Hospital, Harvard Medical School, Belmont, MA

4. Institute of Pharmacology and Toxicology, University of Zurich, Zurich, Switzerland

* These authors contributed equally to this work.

Abstract

Previous experiments using genetic and pharmacological manipulations have provided strong evidence that etomidate impairs synaptic plasticity and memory by modulating a5-subunit containing $GABA_ARs$ (a5-$GABA_ARs$). Since a5-$GABA_ARs$ mediate tonic inhibition (TI) in hippocampal CA1 pyramidal cells, and etomidate enhances TI, etomidate enhancement of TI in pyramidal cells has been proposed as the underlying mechanism (Martin et al., 2009). Here we tested this hypothesis by selectively removing a5-$GABA_ARs$ from pyramidal neurons (CA1-pyr-α5-KO) and comparing the ability of etomidate to enhance TI and block LTP in *fl*-a5 (WT), global-a5-KO (gl-α5-KO), and CA1-pyr-α5-KO mice. Etomidate suppressed LTP in slices from WT and CA1-pyr-α5-KO but not gl-α5-KO mice. There was a trend toward reduced TI in both gl-α5-KO and CA1-pyr-α5-KO mice, but etomidate enhanced TI to similar levels in all genotypes. The dissociation between effects of etomidate on TI and LTP in global-a5KO mice does not support increased TI as the mechanism by which etomidate impairs LTP and memory. Rather, the ability of etomidate to block LTP in WT and CA1-pyr-α5-KO mice, but not in gl-α5-KO mice, points toward a5-$GABA_ARs$ on non-pyramidal neurons as the essential effectors controlling plasticity in this *in vitro* model of learning and memory.

Introduction

The mechanism by which general anesthetics produce their assorted effects, such as sedation, hypnosis, immobility, and amnesia, remains a topic of intense interest and investigation. Recognizing that a single unitary mechanism is unlikely, a major goal of current research in this area is to relate specific molecular- and cellular-level targets to their network- and behavioral-level consequences.

Of the many candidate targets that have been considered, $GABA_A$ receptors ($GABA_ARs$) are perhaps the most universally recognized and extensively studied. They comprise a family of heteropentameric ligand-gated anion channels that are composed of five subunits, selected from a number of subfamilies (α1-6, β1-3, γ1-3, δ, π and ρ) – most commonly two a, two b, and one g subunit (Olsen and Sieghart, 2008). These receptors are modulated by a wide range of anesthetic agents, some of which act on additional molecular targets, and others of which are relatively specific (Jones et al., 1992; Jones and Harrison, 1993; Uchida et al., 1995). This latter group includes etomidate, an imidazole derivative that is used clinically as an induction agent and sedative, and that has become an important experimental compound in mechanistic studies of general anesthesia because of its target specificity (Jones et al., 1992; Uchida et al., 1995; Forman, 2011).

Like many other general anesthetics, etomidate produces amnesia at a fraction of the concentration that produces the other end points of anesthesia (Rudolph and Antkowiak, 2004). Substantial evidence indicates that it does so by enhancing the activity of a5-subunit containing $GABA_A$Rs (Cheng et al., 2006; Orser, 2007; Martin et al., 2009). Although they are sparsely expressed elsewhere in the brain, a5-$GABA_A$Rs are enriched in the hippocampus, where they are found at extrasynaptic sites and give rise to a persistent conductance termed "tonic inhibition" (McKernan et al., 1991; Sieghart and Sperk, 2002; Caraiscos et al., 2004b). Since etomidate can enhance tonic inhibition (Cheng et al., 2006), and changes in tonic inhibition can alter dendritic integration and long term potentiation (LTP) (Martin et al., 2009), a causal link has been proposed between the two.

Our recent finding that the effects of etomidate on tonic inhibition in pyramidal cells can be dissociated from its effects on memory *in vivo* and synaptic plasticity *in vitro* challenges this notion (Zarnowska et al., 2014). Studying mice that carry a mutation in β3-$GABA_A$Rs that renders them insensitive to etomidate, we found that the drug no longer enhanced tonic inhibition, but it did still impair fear conditioning to context (a hippocampus-dependent memory task) and it blocked LTP (Zarnowska et al., 2014). One possible explanation for this dissociation is that etomidate might act primarily by modulating α5-$GABA_A$Rs found elsewhere on pyramidal neurons, such as $GABA_{A,slow}$ synapses, a subset

of which utilize α5-GABA$_A$Rs (Zarnowska et al., 2009; Capogna and Pearce, 2011). Alternatively, etomidate might impair memory by targeting α5-GABA$_A$Rs found on non-pyramidal cells, as described recently for O-LM interneurons (Salesse et al., 2011) and glia (Velez-Fort et al., 2012). We report here the results of experiments designed to distinguish between these two possibilities.

Methods

Materials and Methods

All experiments were performed in accordance with the National Institutes of Health *Guide for the Care and Use of Laboratory Animals* (Eighth Edition 2011, National Academic Press) and were approved by the University of Wisconsin-Madison (UW-Madison) Institutional Animal Care and Use Committee, Madison, Wisconsin and McLean Hospital Institutional Animal Care and Use Committee, Belmont, Massachusetts. All efforts were made to minimize the suffering of animals and to reduce the number of animals used.

Generation of genetically modified mice

Generation of the α5 floxed and knockout alleles: An α5 floxed allele ($Gabra5^{tm2.1Uru}$) was generated by flanking exon 5 of the *Gabra*5 gene with two *lox*P sites (*fl*-α5). These *fl*-α5 mice were used as a pseudo-wild type for the experiments. Excision of the *lox*P-flanked exon5 by cre-*lox*P-mediated recombination resulted in the α5 knockout allele ($Gabra5^{tm2.2Uru}$).

Generation of global α5 knockout animals: Global *Gabra*5 knockout animals (gl-α5-KO) were generated by crossing α5-/- mice (Collinson et al., 2002) with *fl*-α5 mice. Mice used for patch clamp experiments were derived from homozygous breeding of *promoter-cre-fl-α5* mice at McLean Hospital. These

animals were transferred to UW-Madison at 22-25 days of age and used for experiments at 8-16 weeks of age. Mice used for LTP experiments were generated by heterozygous breeding of *CAMKIIα-cre-fl-α5* x *fl-α5* mice at UW-Madison and used at 8-10 or 16 weeks of age.

Generation of conditional α5 knockout animals: Conditional *Gabra*5 knockout animals, in which knockout was restricted to pyramidal neurons, primarily in the CA1 area of the hippocampus (CA1-pyr-α5-KO), were generated by crossing CaMKIIa-Cre (T29-1) mice (Tsien et al., 1996) and Gabra5 floxed mice (*fl*-α5). Essentially, female CaMKIIa-Cre / *fl*-α5 mice were bred with male *fl*-α5 mice to obtain experimental animals. The distribution of genotypes in offspring was approximately 50% KO and 50% WT littermates. All offspring were genotyped to detect the existence of two floxed alleles to exclude germline recombination and the presence or absence of cre. The CA1-pyr-α5-KO mice originated from McLean Hospital and were bred continuously in the animal facilities of the UW-Madison.

All mice used for these studies were on the C57BL/6J background.

Immunocytochemistry

Expression of the α5 subunit was analyzed in mice at 1, 2, and 6 months of age. Mice were deeply anesthetized with pentobarbital (50 mg/kg, i.p.) and transcardially perfused with 4% paraformaldehyde in 0.15 M phosphate buffer

(pH 7.4). Brains were postfixed for 3 hours, cryoprotected in sucrose, frozen and cut parasaggitally at 40 μm with a sliding microtome. Sections were collected in PBS and stored in an antifreeze solution prior to staining. Free-floating sections were incubated overnight at 4°C with primary antibodies for GABAA receptor α1-, α2-, α3-, and α5 subunits as well as the β2/3 subunits and the γ2 subunit diluted in Tris buffer containing 2% normal goat serum and 0.2% Triton X-100. Sections were washed and incubated for 30 minutes at room temperature in biotinylated secondary antibodies (1:300, Jackson Immunoresearch, West Grove, PA) in the same buffer as the primary antibodies. After washing, sections were incubated in ABC complex (1:100 in Tris buffer, Vectastain Elite Kit, Vector Laboratories, Burlingame, CA) and after another wash finally incubated with diaminobenzidine tetrahydrochloride (DAB; Sigma, St. Louis, MO) in Tris buffer (pH 7.7) containing 0.015% hydrogen peroxide. The color reaction was stopped after 5-20 minutes with ice-cold PBS. Sections were mounted on gelatin-coated slides, air dried, and dehydrated in an ascending series of ethanol, cleared in xylene, and coverslipped with Eukitt (Erne Chemie, Dällikon, Switzerland). Sections from wild type and mutant mice were processed in parallel under identical conditions to minimize variability in staining intensity.

Electrophysiology

Slice preparation

LTP studies: Tranverse (500 μm-thick) hippocampal slices were prepared from male mice 8 weeks (45-80 days old, 62±8 days, mean ± SD, 41 mice) or 16 weeks (110-121 days old, 115±6 days, mean ± SD, 3 mice) of age. The preparation procedure was detailed previously (Zarnowska et al., 2014). Slices were recovered in carbogenated (95% O_2/5% CO_2), artificial cerebrospinal fluid (aCSF) containing (in mM) 127 NaCl, 1.9 KCl, 1.2 KH_2PO_4, 26 $NaHCO_3$, 1.4 $MgSO_4x7H_2O$, 2.2 $CaCl_2x2H_2O$, 2.5 ascorbic acid, 15 glucose and maintained at room temperature (21-23 °C) until transfer to the experimental chamber.

Patch-clamp studies: Horizontal (350 μm-thick) hippocampal slices were prepared from male mice aged between 7-9 weeks (64±1.5 days, mean ± SD, 19 mice) or 3-5 weeks (32.5±1.5 days, mean ± SD, 11 mice). The preparation procedure was detailed elsewhere (Zarnowska et al., 2014). In short, an ice-cold and oxygenated NMDG-based cutting solution was used for transcardiac perfusion and slicing of the brain. Slices recovered while submerged in warmed (35 °C) carbogenated cutting solution, which was slowly exchanged (at rate 5 ml/min) with warmed (35 °C) carbogenated aCSF containing (in mM): 130 NaCl, 2.5 KCl, 1.25 Na2HPO4, 25 NaHCO3, 2 MgSO4x7H2O, 2 CaCl2x2H2O, 10 glucose, 2.5 sodium ascorbate (pH 7.3, 300-310 mOsm). Thereafter the slices were maintained at room temperature (21-23 °C) until transfer to the experimental chamber.

Data acquisition

LTP studies: Extracellular recordings were obtained using a 16-channel linear array recording electrode (50 μm separating recording sites; NeuroNexus Technologies, Ann Arbor, MI) inserted orthogonal to the hippocampal layers in the middle of the hippocampal CA1 region. Slices were bathed in ACSF at a flow rate of 2.5 – 3.0 mL/min at a temperature of 30 ± 0.5 °C. Field excitatory postsynaptic potentials (fEPSPs) were electrically evoked by a tungsten stereotrode stimulating electrode (0.5 MΩ, World Precision Instruments, Sarasota, FL) placed in *stratum radiatum*, activating Schaffer collateral/commissural fibers. Recorded signals were digitized at 10 kHz using an analog-to-digital converter (Digidata 1440A, Molecular Devices, Sunnyvale, CA), amplified 1000x, band-pass filtered between 1-3000 Hz (Model Lynx-8 amplifiers, Neuralynx Inc., Tucson, AZ) and acquired using pClamp software (Version 10.2, Molecular Devices, Sunnyvale, CA). Stimuli of 0.1 ms duration were delivered using a constant current stimulus isolator (Model A365D, World Precision Instruments, Sarasota, FL) at 0.03 Hz using a stimulus intensity ("baseline") adjusted to evoke responses below half-maximal fEPSP amplitude. Baseline stimulus amplitude ranged from 30-150 mA and was typically between 30-90 mA. The recording electrode site used for LTP analysis was selected by choosing the site with the largest amplitude of fEPSP in response to a baseline stimulus.

Patch-clamp studies: Recordings were performed in a submerged chamber continuously perfused at 2.5-3 ml/min flow rate by aCSF carbogenated with 95% O_2-5% CO_2 aCSF and warmed to 30±1 °C, containing kynurenic acid (KA, 3 mM) and GABA (5 mM). KA and GABA were added fresh as powder to the aCSF. CA1 pyramidal cells were visualized with 40x water immersion objective and IR-DIC video camera installed on BX50WI microscope (Olympus Imaging America Inc., Center Valley, PA). Patch-clamp recordings were amplified and low pass filtered at 4 kHz with MultiClamp 700B (Molecular Devices), then digitized on-line at 10 kHz using a Digidata 1322A (Molecular Devices). Borosilicate glass pipettes (O.D. 1.5 mm x I.D. 0.86 mm, Sutter Instruments, Novato, CA) were pulled to tip diameters of ~1 μm using a horizontal puller (P-97, Sutter Instruments, Novato, CA) then filled with an intracellular solution containing (in mM) 90 CsCl, 30 KCl, 5 NaCl, 10 NaHEPES, 5 EGTA, 4 Mg_2ATP 2, 0.4 Na_3GTP, 10 Na_2phosphocreatine, 4 QX-314, pH adjusted with 1M CsOH to 7.3 (290±5 mOsm). The resistances of the pipettes filled with internal solution were between 5-7 MΩ. Whole-cell, voltage-clamp recordings were performed at -60 mV holding potential. Cell capacitances and membrane resistances were measured using the membrane test algorithm provided in the acquisition software (Clampex 10.3, Molecular Devices). Series resistances were not compensated but were monitored, and recordings were discontinued if increased >25% through

the course of an experiment. Uncompensated series resistances varied between 8-18 MΩ.

LTP Measurement

Slices were incubated in either drug-free ACSF or ACSF containing etomidate for at least 1 hour prior initiating the experiment (Benkwitz et al., 2007). Following a stable baseline period, defined as less than a 10% change in fEPSP amplitude over 30 minutes, LTP was evoked using a theta burst stimulus (TBS) protocol consisting of 3 stimulus trains separated by 1 min. Each train consisted of five bursts of 10 pulses at 100 Hz, delivered every 300 ms (i.e. bursts at approximately 3.33 Hz), at baseline stimulus intensity. LTP was expressed as a percentage of the pre-tetanus baseline, calculated as the average fEPSP slope over the last 10 min of recording divided by the average fEPSP slope measured during the 10 min prior to TBS, times 100.

Detection and measurement of tonic inhibition

Tonic inhibition was assessed by applying the non-competitive $GABA_AR$ antagonist picrotoxin (PTX, 100 μM) and measuring the change in holding current. Holding current was derived from the Gaussian fit to an all-points amplitude histogram. Histograms (1 pA bin-width) were constructed using 1 min of data before PTX application and 20 sec of data following the attainment of a steady-state PTX effect, which required approximately 2 min. Before the application of

PTX, histograms were skewed towards larger negative values, reflecting the presence of inward sIPSCs. To exclude these sIPSCs in the measurement of the holding current, only to the upper half of the distribution was fit to the Gaussian function, and the resulting parameters were used to simulate a symmetric Gaussian curve for purposes of illustration. The difference between the peak values of the Gaussian fits before and after addition of PTX was used as the measure of the tonic current. The effect of etomidate on tonic current was measured in slices that had been pre-incubated at the desired anesthetic concentration for at least 1 hour (Benkwitz et al., 2007).

Detection and measurement of sIPSCs

To detect sIPSCs, the search protocol threshold was set at 3 times the root mean square (RMS) noise level, which typically was 3-6 pA. For each cell, at least 40 sIPSCs were averaged, normalized, and characterized by their 10-90% rise and weighted decay times. The sIPSCs used for averaging were chosen based on the presence of a stable baseline level and the lack of spontaneous events during the deactivation phase, and aligned at the time of half-maximal amplitude of the rising phase. The decay phases of averaged fast sIPSCs were fitted to mono- or bi-exponential functions using a Simplex fitting algorithm offered in Mini Analysis Program 6 (Synaptosoft Inc., Fort Lee, NJ) software.

Data analysis

Data analysis was performed in Clampfit 10.3 (Molecular Devices), Origin 9.0 (OriginLab Inc., Northampton, MA), custom-written R programming language scripts (R Foundation for Statistical Computing, Vienna, Austria), GraphPad Prism 5.04 (GraphPad Software Inc., La Jolla, CA), and Mini Analysis Program version 6 (Synaptosoft Inc.,) software.

Statistics

Data are presented as mean ± SEM unless indicated otherwise, with *n* specifying the number of mice, slices or recorded cells. Two-way ANOVA was used to test the effects of etomidate and genotype. Subsequent post-hoc comparisons of means were made using Tukey's test. Student's t-test was used to compare means as indicated, using the one-tailed alternative when prior information dictated a predicted outcome. The critical value for statistical significance was set at $P < 0.05$. All reported significant findings have survived correction for multiple comparisons using the Benjamini-Hochberg procedure (Benjamini and Hochberg, 1995).

Chemicals

For electrophysiological experiments *in vitro*, etomidate ((*R*)-1-(1-phenylethyl)-1*H*-imidazole-5-carboxylic acid ethyl ester) was purchased from Tocris (Bristol, United Kingdom) as a powder that was dissolved in DMSO and kept in aliquots at 50 mM concentration. For each experiment, an aliquot was

thawed and diluted appropriately in recording aCSF. For behavioral experiments *in vivo*, etomidate was purchased pre-dissolved in a 35% propylene glycol solution at a concentration of 2 mg etomidate/ml solution (Amidate, Hospira, Inc, Lake Forest, IL). All salts were obtained from Sigma-Aldrich, and kynurenic acid from Abcam Biochemicals® (Cambridge, MA), NaHEPES from ChemCruz™ Biochemicals, and $CaCl_2x2H_2O$ from Fisher Scientific.

Results

Etomidate impairs LTP in slices from WT but not gl-α5-KO mice

We investigated the effect of etomidate (0.5 μM and 1 mM) on LTP in slices from gl-α5-KO and *fl*-α5 (WT) mice. In the absence of etomidate, TBS induced LTP in both genotypes (WT: 157±13%, n=10, p=0.009; gl-α5-KO: 149±9%, n=10, p=0.0002; one-tailed t-tests, Fig. 2). In the presence of etomidate, the amplitude of LTP was strongly reduced in slices from WT mice (0.5 μM etomidate: 117±8%, n=5, p=0.012, one-tailed t-test; 1 μM etomidate: 110±10%, n=9, p=0.005, one-tailed t-test; Fig. 2a,d) but not in gl-α5-KO mice (165±8%, n=9, p=0.90, one-tailed t-test, Fig. 2b,d). These observations replicate previous reports that etomidate impairs LTP in WT but not gl-α5-KO mice (Cheng et al., 2006).

Etomidate enhances residual tonic inhibition in WT and gl-α5-KO mice

We also investigated the effect of etomidate on tonic inhibition in CA1 pyramidal neurons, in brain slices bathed in aCSF supplemented with 5 μM GABA and held at 30°C. Tonic current was present in both WT (16.8±2.3 pA, n=9, p<0.0001) and gl-α5-KO mice (10.4±2.2 pA, n=5, p=0.009, Fig. 3), though there was a trend toward reduced amplitude in the gl-α5-KO vs. WT mice (62±15%,

p=0.9, Fig. 3d). Nevertheless, etomidate increased tonic currents to comparable levels in both genotypes (WT 0.5 μM 36.4±2.9 pA, n=9; gl-α5-KO 0.5 μM: 30.8±5.3 pA, n=6, p=0.76 vs. WT; 1 μM 39.7±4.1 pA, n=5, p=0.52 vs. WT, unpaired t-test). This percent increase in tonic current did not differ between genotypes (WT 218±19%, gl-α5-KO 297±62%, p=0.17, Fig. 3d).

These results showing that tonic inhibition is present (though perhaps at a reduced level) in gl-α5KO, and that it is enhanced to an extent that is comparable to WT, is somewhat surprising, given previous indications that α5-$GABA_A$Rs underlie tonic inhibition in CA1 pyramidal cells (McKernan et al., 1991; Sieghart and Sperk, 2002; Caraiscos et al., 2004b). To test whether GABA supplementation and experimental temperature might have influenced our results (Houston et al., 2012; Bright and Smart, 2013), we repeated these experiments at room temperature and without GABA added to the aCSF. As before, tonic current was present in both WT and gl-α5-KO mice (11.3±2.3 pA, p=0.002, n=7; gl-A5-KO 5.5±1.1 pA, p=0.01 n=8; Fig. 3d), again with a trend toward smaller amplitude tonic current in gl-A5-KO *vs.* WT mice (p=0.2). In the presence of etomidate (0.5 mM), tonic currents were again enhanced in slices from both genotypes (WT 224±81%, p=0.07 n=7; gl-α5-KO 294±82%, p=0.005, n=8; Fig. 3d), with no difference between genotypes in percent increase (p=0.56, unpaired t-test).

We conclude that global knockout of the *Gabra5* gene might reduce, but does not eliminate, tonic inhibition in CA1 pyramidal cells. Furthermore, the tonic inhibition that remains is enhanced by etomidate to an equal or greater extent compared to the WT. These conclusions are independent of experimental temperature and whether 5 μM GABA is added to the perfusate. This dissociation between the enhancement of tonic current by etomidate and its ability to impair LTP in gl-α5-KO mice, which is similar to the dissociation observed in β3-N265M mice, provides further evidence that etomidate suppresses LTP in CA1 pyramidal neurons through a mechanism other than enhancement of tonic current.

Etomidate impairs LTP in slices from CA1-pyr-α5-KO mice

The evidence presented above indicates that etomidate suppresses LTP by targeting α5-$GABA_A$Rs, but not those that give rise to tonic inhibition in pyramidal neurons. We therefore considered two other possibilities: 1) etomidate might impair LTP by modulating other forms of α5-$GABA_A$R-medidated inhibition on CA1 pyramidal neurons, such as $GABA_{A,slow}$, a slowly decaying (~50 ms) synaptic response that is mediated in part by a5-$GABA_A$Rs (Pearce, 1993; Banks et al., 1998; Zarnowska et al., 2009); 2) etomidate might impair LTP by targeting α5-$GABA_A$Rs present on non-pyramidal cells, such as those that underlie slow synaptic inhibition on OL-M interneurons (Chamberland and Topolnik, 2012).

To evaluate this second possibility, we tested whether removing α5 subunits from pyramidal neurons but not interneurons (CA1-pyr-α5-KO) would interfere with the ability of etomidate to suppress LTP. In the absence of etomidate, TBS produced robust LTP in CA1-pyr-α5-KO mice (140±8%, n=8, p=0.0009; one-tailed t-test, Fig. 2C, filled circles), as it had in WT and gl-α5-KO mice (Fig. 2A,B, filled circles). However, unlike gl-α5-KO mice, etomidate reduced the amplitude of LTP in CA1-pyr-α5-KO mice (120±6%, n=8, p=0.0384, one-tailed t-test vs. WT, Fig. 2C,D).

The ability of etomidate to reduce LTP in CA1-pyr-α5-KO mice thus supports the second possibility – i.e. that etomidate acts through a mechanism that is independent of pyramidal neuron α5-$GABA_A$Rs. However, since the expression of CaMKIIα is developmentally regulated, and at 8 weeks of age the elimination of α5 subunits may not have been complete, we performed an additional set of experiments using CA1-pyr-α5-KO mice that were 16 weeks old, an age at which CaMKIIα has reached full expression (Tsien et al., 1996), and which our immunocytochemical results indicated that α5 subunit knockout was complete (Fig. 1). In these older animals, etomidate also blocked LTP (99±9%, n=5, p=0.0073 vs. drug-free, two-tailed t-test, Fig. 2D). We conclude, therefore, that etomidate blocks LTP independently of α5-$GABA_A$Rs on pyramidal neurons.

Characterization of inhibition in pyramidal cells of CA1-pyr-α5-KO mice

Although the results presented above point toward non-pyramidal cells as the target of etomidate, we examined other aspects of inhibition onto CA1 pyramidal cells of CA1-pyr-α5-KO mice to test for any unexpected changes that might have occurred and influenced our results.

Tonic current under control conditions was similar to levels seen in WT and gl-α5-KO mice (12.1±1.1 pA, Fig. 3, p=0.80 vs. WT and p=0.99 vs. gl-α5-KO). As in gl-α5-KO mice, etomidate increased the amplitude of this residual current (p=0.28, 0.5 μM etomidate CA1-pyr-α5-KO vs. 0.5 μM etomidate gl-α5-KO). Characteristics of fast synaptic inhibition, including IPSC frequency, amplitude, 10-90% rise time (RT), and weighted time constant of deactivation ($t_{deact.}$), were not different between genotypes under drug-free conditions (p=0.3-0.9, Table 1), and etomidate prolonged t_{deact} to a similar extent in all genotypes (WT 129±13%, gl-α5-KO 132±31%, CA1-pyr-α5-KO 126±13% *vs.* respective controls for all, Table 1). Because the recording conditions for these experiments produced high rates of ongoing fast spontaneous IPSCs with substantial baseline noise due to tonic current, we were unable to separate and characterize slow spontaneous IPSCs, which occur infrequently *in vitro* even under optimized conditions (Zarnowska et al., 2009). We are therefore unable to provide a detailed analysis of this inhibitory component. Nevertheless, we did not observe

any overt changes in $GABA_{A,slow}$, such as a strong increase in frequency or amplitude, that might have influenced our ability to induce LTP in these mice.

Thus, we conclude that characteristics of inhibition in pyramidal neurons of gl-α5-KO and CA1-pyr-α5-KO mice were similar, and cannot account for differences in the ability of etomidate to suppress LTP in the two genotypes.

Discussion

The results presented above support the now-well-established concept that α5-GABA$_A$Rs serve to constrain hippocampus-dependent learning and memory, and that modulation of these receptors underlies anesthetic-induced amnesia. However, rather than α5-GABA$_A$Rs on pyramidal neurons, which until now have been considered the most likely anesthetic targets, our results point to α5-GABA$_A$Rs receptors on non-pyramidal cells – most likely inhibitory interneurons – as the essential effectors controlling plasticity in this *in vitro* model of learning and memory. This conclusion is based on the finding that removing a5 subunits from hippocampal pyramidal cells (CA1-pyr-α5-KO) did not reproduce the effect of removing them from all cells (gl-α5-KO).

Whereas clinically relevant concentrations of etomidate suppressed LTP in brain slices from *fl*-α5 (WT) mice (Fig. 2A), brain slices from gl-α5-KO mice were resistant (Fig. 2B), as reported previously by other investigators (Cheng et al., 2006). When combined with other experiments showing that selective pharmacological or genetic manipulation of α5-GABA$_A$Rs alters learning and memory *in vivo* as well as LTP *in vitro* (Collinson et al., 2002; Martin et al., 2009; Martin et al., 2010), the accumulated evidence points strongly toward a causal role for α5-GABA$_A$Rs in suppression of LTP and memory by etomidate. Our finding that etomidate suppresses LTP in CA1-pyr-α5-KO but not in gl-α5-KO

mice (Fig. 2) demonstrates that α5-GABA$_A$Rs on pyramidal neurons are dispensable, and indicates that α5-GABA$_A$Rs on non-pyramidal cells are the critical targets.

The prevalent concept that enhancement of tonic inhibition in pyramidal neurons mediates the ability of etomidate to suppress synaptic plasticity was based on some of the prior studies cited above, plus immunocytochemical evidence that α5 subunits are found at extrasynaptic sites on pyramidal neuron dendrites (Crestani et al., 2002), pharmacological evidence that tonic inhibition in pyramidal neurons is mediated by α5-GABA$_A$Rs (Caraiscos et al., 2004b; Prenosil et al., 2006), and electrophysiological evidence that tonic inhibition is enhanced by etomidate and other anesthetics that impair memory (Caraiscos et al., 2004a). Taken together, these findings led to the intuitively appealing notion that these drugs impair memory by increasing membrane conductance, making dendrites 'leaky' and preventing the depolarization necessary to relieve Mg++ block of NMDA receptors, and thereby impairing synaptic plasticity.

Given this strong and well-reasoned narrative, we were surprised, therefore, to discover the dissociation between enhancement of tonic current and block of LTP in β3-N265M mice (Zarnowska et al., 2014), which carry a mutation in the GABA$_A$R β3 subunit that make these receptors insensitive to etomidate (Jurd et al., 2003). In those mice, etomidate failed to increase tonic current in

pyramidal neurons, yet it still blocked LTP. Our present experiments revealed two further dissociations: i) in gl-α5-KO mice, etomidate increased tonic current, yet it failed to block LTP; ii) enhancement of tonic current was greater in gl-α5-KO than CA1-pyr-α5-KO mice, but suppression of LTP was greater in CA1-pyr-α5-KO than gl-α5-KO mice (Fig. 2, 3). We presume that the reason that tonic current was not completely eliminated in these α5-KO mice involves compensatory substitution by other etomidate-sensitive $GABA_A$Rs. The most likely candidate is $GABA_A$Rs that incorporate δ subunits, which in many other cell types are also found at extrasynaptic sites and mediate tonic current (Sperk et al., 1997; Nusser and Mody, 2002). Indeed, δ-$GABA_A$Rs have been shown to undergo compensatory upregulation in hippocampal CA3 neurons of α5-KO mice (Glykys and Mody, 2006). It is also possible that the tonic current was carried by residual α5 subunits, but this explanation seems less likely given the strong reduction in immunocytochemical staining that we observed (Fig. 1). In either case, the results present a clear dissociation between effects of etomidate on tonic current and LTP, and indicate that other mechanisms must be considered. The proposal that etomidate impairs LTP by targeting non-pyramidal cells provides a ready explanation for this lack of correlation.

What might these non-pyramidal targets be? In the CA1 region, GABAergic inhibitory neurons and glial cells comprise the two major classes of non-pyramidal cells. Glial cells do express multiple isoforms of $GABA_A$Rs

(Schwarzer et al., 1997; Renzel et al., 2013), and it is clear that they can influence synaptic plasticity (Allen, 2014). Therefore, they represent a plausible target. However, α5-GABA$_A$Rs have not been described in these cells to date. By contrast, combined pharmacological and electrophysiological have shown experiments have shown that α5 subunits exist on some types of interneurons (Patenaude et al., 2001; Salesse et al., 2011), and that they mediate slowly decaying IPSCs in these cells (Banks et al., 2000).

Since interneurons are generally thought to reduce pyramidal cell excitability through feedforward and feedback inhibitory pathways, it is somewhat counterintuitive to propose that enhancing α5-GABA$_A$R-mediated inhibition onto interneurons might impair LTP, since this would then remove their constraining influence and produce the opposite effect. Indeed, it has long been recognized that LTP is more easily elicited, and more robust, in the presence of GABA$_A$ receptor antagonists such as picrotoxin. One way to reconcile these potentially conflicting views is through disinhibitory circuits. In this scenario, interneurons that inhibit other interneurons create positive feedback loops that support the induction of LTP. By suppressing the activity of interneurons that inhibit other interneurons, this positive feedback loop is interrupted, and activation of pyramidal neurons is more effectively quenched by conventional feedforward or feedback inhibitory inputs. In this way, anesthetic enhancement of both conventional feedforward/feedback inhibition, and interruption of disinhibitory

loops, would work together to more effectively suppress LTP. Indeed, there is an emerging consensus that interneurons can control memory either through direct inhibition of pyramidal cells or through disinhibitory circuits (Freund and Gulyas, 1997; Leao et al., 2012; Pi et al., 2013; Groen et al., 2014; Lovett-Barron et al., 2014; Wolff et al., 2014).

If interruption of essential disinhibitory circuitry is the mechanism by which etomidate exerts its control of LTP, our recent finding that this drug suppresses LTP through β2 subunit-containing $GABA_A$Rs (Zarnowska et al., 2014) provides a clear test of relevance for candidate interneurons and synapses. Biochemical and electrophysiological evidence support the existence of a5b2- as well as a5b3-containing $GABA_A$Rs in the CA1 region of hippocampus (Belelli et al., 1997; Sanna et al., 1997; Ju et al., 2009), and b2- and a5-containing $GABA_A$Rs mediate a portion of $GABA_{A,slow}$ synaptic currents (Benkwitz et al., 2007; Zarnowska et al., 2009). However, the relative sparsity of α5β2-$GABA_A$Rs compared to α5β3-$GABA_A$Rs (Burgard et al., 1996; Sur et al., 1998; Caraiscos et al., 2004b) suggests that there may quite specific cells or synapses that play a critical role in anesthetic impairment of memory circuits. Identifying those cells and synapses will be the next step toward furthering our understanding of the mechanisms of this essential general anesthetic action.

Figures and Figure Legends

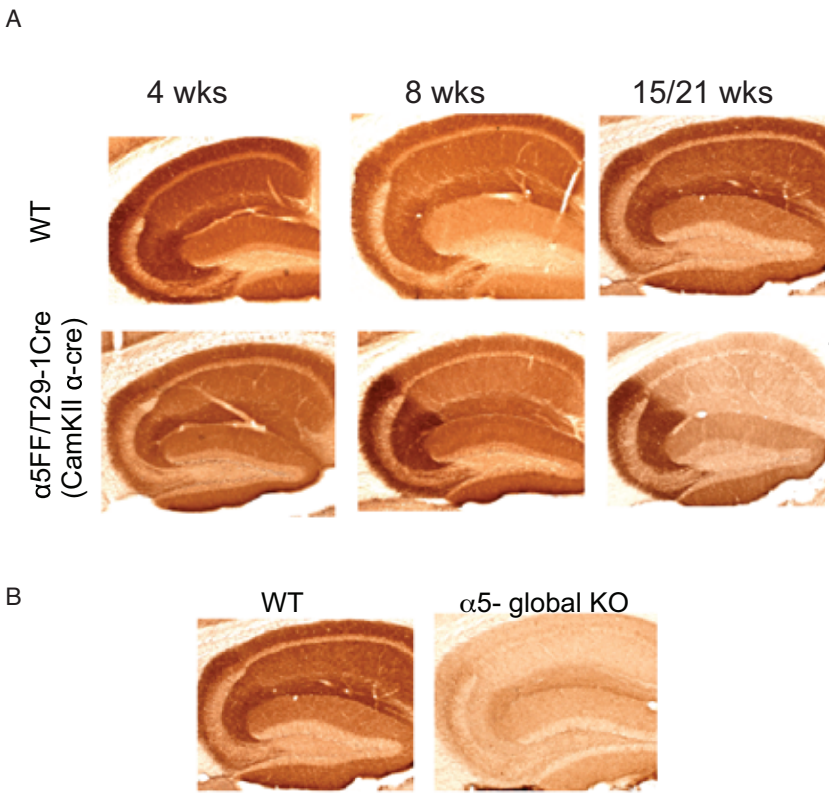

Fig. 1. Immunocytochemistry. (A), Upper: Immunohistochemical detection of the $GABA_A$Rs α5-subunit in the hippocampus of WT and hemizygous for T29-1Cre transgene (α5-CA1 KO). (B), Lower: Immunohistochemical detection of the $GABA_A$Rs α5-subunit in the hippocampus of 21-week-old WT and homozygous knockout mice.

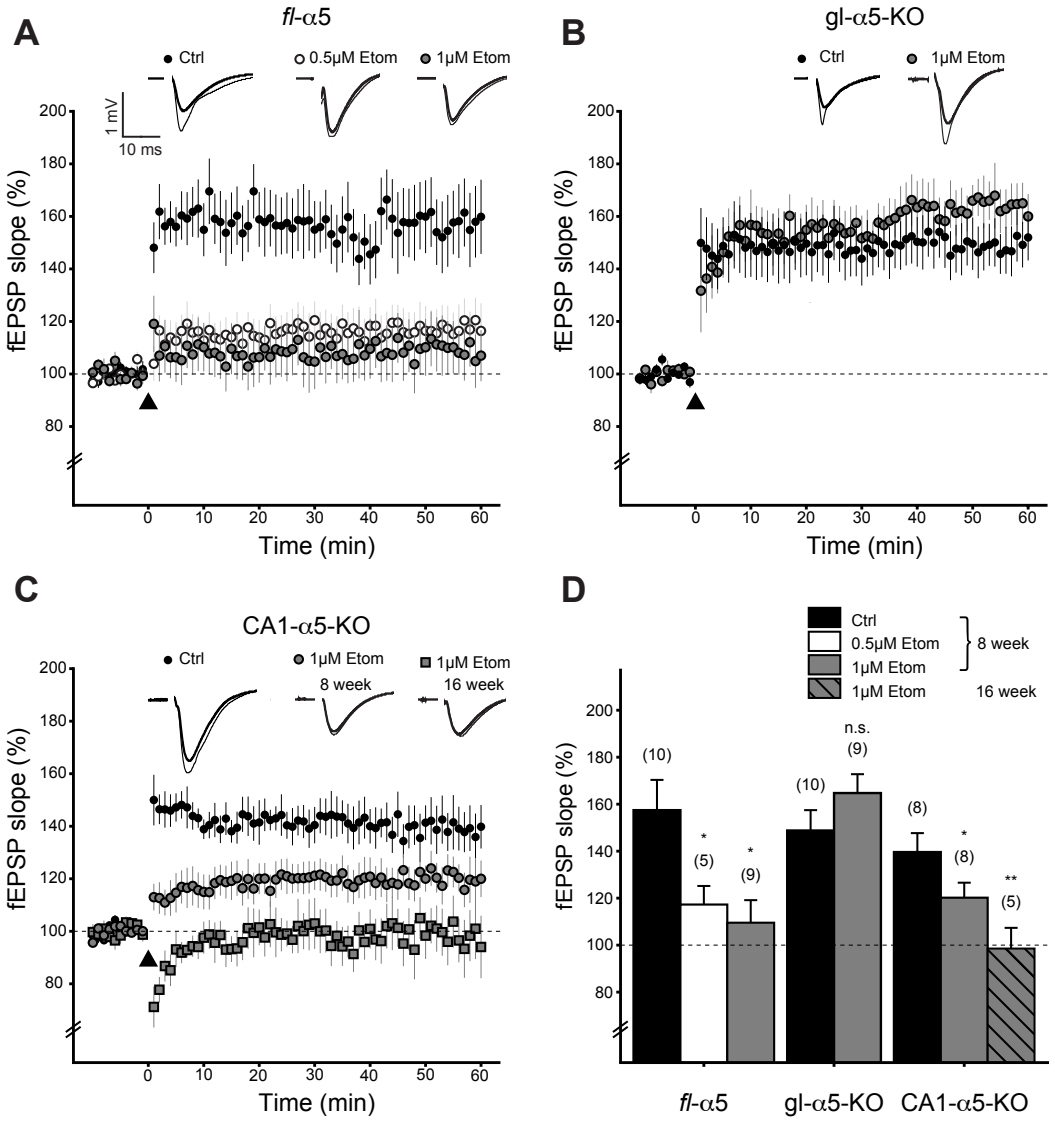

Fig. 2. Long-term potentiation (LTP) is suppressed by etomidate in *fl*-α5 and CA1-pyr-α5-KO, but not gl-α5-KO. (A), Data from slices from *fl*-α5 animals show that etomidate suppresses LTP. LTP-inducing tetanus was delivered at t = 0. Points indicate means and error bars indicate SEM. Black filled circles represent data recorded in the absence of drug, dark grey filled circles represent data recorded in the presence of 1 mM etomidate, and light grey empty circles represent data recorded in the presence of 0.5 mM etomidate. Inset traces show representative fEPSP traces recorded at the indicated times. (B), Data from slices from gl-α5-KO animals show that etomidate does not suppress LTP. (C), Data from slices from CA1-pyr-α5-KO show that etomidate suppresses LTP moderately in slices from young (8 week old; dark grey filled circles) animals and fully in slices from older (16 week old; dark grey filled squares) animals. (D),

Summary averaged data from the last 10 minutes (50 - 60 min) of recording. Bars indicate means and error bars indicate SEM. *p<0.05, **p<0.01.

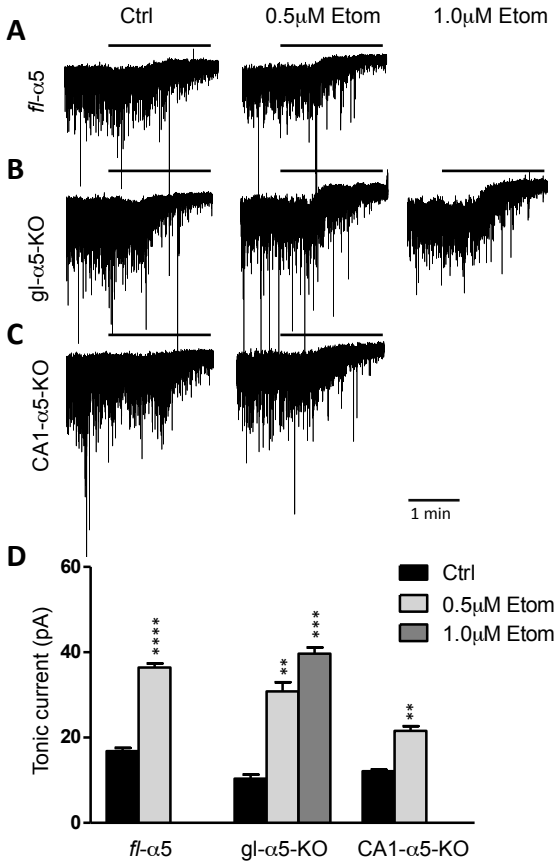

Fig.3. Etomidate potentiates tonic inhibition in wild type, and in mice lacking α5-GABA$_A$Rs. (A) Representative traces containing spontaneous inhibitory currents recorded in *fl*-α5, (B) gl-α5-KO and (C) CA1-pyr-α5-KO mice in the absence (Ctrl) and presence of etomidate (0.5 and 1 μM Etom). Bars above traces represent application of non-competitive GABA$_A$Rs channel-blocker, picrotoxin (PTX, 100 μM). (D) Summary bar plot of average amplitudes of tonic inhibition measured in the three genotypes under different conditions. Comparisons were made between controls and etomidate effect within single genotype (**P<0.001, ****P<0.0001, *n*=5-9 (mostly 9 cells per group)).

Genotype	Condition	Frequency	Amplitude	10-90% Rise time	Weighted t_{decay}
		(s^{-1})	(pA)	(ms)	(ms)
fl-α5	Ctrl	14.1 ± 1.4	41.8 ± 3.2	0.56 ± 0.07	6.6 ± 0.5
	0.5 μM Etom	19.1 ± 3.1	39 ± 3.8	0.63 ± 0.06	8.5 ± 0.8*
gl-α5-KO	Ctrl	18.2 ± 4.2	46.4 ± 4.7	0.63 ± 0.05	8.2 ± 1.0
	0.5 μM Etom	14.6 ± 2.6	42.6 ± 3.7	0.56 ± 0.05	10.8 ± 2.1
CA1-α5-KO	Ctrl	11.8 ± 1.2	37.8 ± 3.6	0.55 ± 0.07	7.2 ± 0.5
	0.5 μM Etom	16.6 ± 2.6	41.6 ± 3.8	0.56 ± 0.06	9.1 ± 0.9

Tab.1. $GABA_{A,fast}$ IPSCs recorded from pyramidal cells located in CA1 area. Comparisons were made between controls and etomidate effect within one genotype (*P<0.05), *n*=5-9 (mostly 8 cells per group).

References

Allen NJ (2014) Astrocyte regulation of synaptic behavior. Annu Rev Cell Dev Biol 30:439-463.

Banks MI, Li TB, Pearce RA (1998) The synaptic basis of GABAA,slow. J Neurosci 18:1305-1317.

Banks MI, White JA, Pearce RA (2000) Interactions between distinct GABA(A) circuits in hippocampus. Neuron 25:449-457.

Belelli D, Lambert JJ, Peters JA, Wafford K, Whiting PJ (1997) The interaction of the general anesthetic etomidate with the gamma-aminobutyric acid type A receptor is influenced by a single amino acid. Proc Natl Acad Sci U S A 94:11031-11036.

Benjamini Y, Hochberg Y (1995) Controlling the False Discovery Rate: A Practical and Powerful Approach to Multiple Testing. Journal of the Royal Statistcal Society 57:289-300.

Benkwitz C, Liao M, Laster MJ, Sonner JM, Eger EI, 2nd, Pearce RA (2007) Determination of the EC50 amnesic concentration of etomidate and its diffusion profile in brain tissue: implications for in vitro studies. Anesthesiology 106:114-123.

Bright DP, Smart TG (2013) Methods for recording and measuring tonic GABAA receptor-mediated inhibition. Front Neural Circuits 7:193.

Burgard EC, Tietz EI, Neelands TR, Macdonald RL (1996) Properties of recombinant gamma-aminobutyric acid A receptor isoforms containing the alpha 5 subunit subtype. Mol Pharmacol 50:119-127.

Capogna M, Pearce RA (2011) GABA A,slow: causes and consequences. Trends Neurosci 34:101-112.

Caraiscos VB, Newell JG, You-Ten KE, Elliott EM, Rosahl TW, Wafford KA, MacDonald JF, Orser BA (2004a) Selective enhancement of tonic GABAergic inhibition in murine hippocampal neurons by low concentrations of the volatile anesthetic isoflurane. J Neurosci 24:8454-8458.

Caraiscos VB, Elliott EM, You-Ten KE, Cheng VY, Belelli D, Newell JG, Jackson MF, Lambert JJ, Rosahl TW, Wafford KA, MacDonald JF, Orser BA (2004b) Tonic inhibition in mouse hippocampal CA1 pyramidal neurons is mediated by alpha5 subunit-containing gamma-aminobutyric acid type A receptors. Proc Natl Acad Sci U S A 101:3662-3667.

Chamberland S, Topolnik L (2012) Inhibitory control of hippocampal inhibitory neurons. Front Neurosci 6:165.

Cheng VY, Martin LJ, Elliott EM, Kim JH, Mount HTJ, Taverna FA, Roder JC, MacDonald JF, Bhambri A, Collinson N, Wafford KA, Orser BA (2006) alpha 5GABA(A) receptors mediate the amnestic but not sedative-hypnotic effects of the general anesthetic etomidate. J Neurosci 26:3713-3720.

Collinson N, Kuenzi FM, Jarolimek W, Maubach KA, Cothliff R, Sur C, Smith A, Otu FM, Howell O, Atack JR, McKernan RM, Seabrook GR, Dawson GR, Whiting PJ, Rosahl TW (2002) Enhanced learning and memory and altered GABAergic synaptic transmission in mice lacking the alpha 5 subunit of the GABAA receptor. J Neurosci 22:5572-5580.

Crestani F, Keist R, Fritschy JM, Benke D, Vogt K, Prut L, Bluthmann H, Mohler H, Rudolph U (2002) Trace fear conditioning involves hippocampal alpha5 GABA(A) receptors. Proc Natl Acad Sci U S A 99:8980-8985.

Forman SA (2011) Clinical and molecular pharmacology of etomidate. Anesthesiology 114:695-707.

Freund TF, Gulyas AI (1997) Inhibitory control of GABAergic interneurons in the hippocampus. Can J Physiol Pharmacol 75:479-487.

Glykys J, Mody I (2006) Hippocampal network hyperactivity after selective reduction of tonic inhibition in GABA A receptor alpha5 subunit-deficient mice. J Neurophysiol 95:2796-2807.

Groen MR, Paulsen O, Perez-Garci E, Nevian T, Wortel J, Dekker MP, Mansvelder HD, van Ooyen A, Meredith RM (2014) Development of dendritic tonic GABAergic inhibition regulates excitability and plasticity in CA1 pyramidal neurons. J Neurophysiol 112:287-299.

Houston CM, McGee TP, Mackenzie G, Troyano-Cuturi K, Rodriguez PM, Kutsarova E, Diamanti E, Hosie AM, Franks NP, Brickley SG (2012) Are extrasynaptic GABAA receptors important targets for sedative/hypnotic drugs? J Neurosci 32:3887-3897.

Jones MV, Harrison NL (1993) Effects of volatile anesthetics on the kinetics of inhibitory postsynaptic currents in cultured rat hippocampal neurons. J Neurophysiol 70:1339-1349.

Jones MV, Brooks PA, Harrison NL (1992) Enhancement of gamma-aminobutyric acid-activated Cl- currents in cultured rat hippocampal neurones by three volatile anaesthetics. J Physiol 449:279-293.

Ju YH, Guzzo A, Chiu MW, Taylor P, Moran MF, Gurd JW, MacDonald JF, Orser BA (2009) Distinct properties of murine alpha 5 gamma-aminobutyric acid type a receptors revealed by biochemical fractionation and mass spectroscopy. J Neurosci Res 87:1737-1747.

Jurd R, Arras M, Lambert S, Drexler B, Siegwart R, Crestani F, Zaugg M, Vogt KE, Ledermann B, Antkowiak B, Rudolph U (2003) General anesthetic actions in vivo strongly attenuated by a point mutation in the GABA(A) receptor beta3 subunit. FASEB J 17:250-252.

Leao RN, Mikulovic S, Leao KE, Munguba H, Gezelius H, Enjin A, Patra K, Eriksson A, Loew LM, Tort AB, Kullander K (2012) OLM interneurons differentially modulate CA3 and entorhinal inputs to hippocampal CA1 neurons. Nat Neurosci.

Lovett-Barron M, Kaifosh P, Kheirbek MA, Danielson N, Zaremba JD, Reardon TR, Turi GF, Hen R, Zemelman BV, Losonczy A (2014) Dendritic inhibition in the hippocampus supports fear learning. Science 343:857-863.

Martin LJ, Oh GH, Orser BA (2009) Etomidate targets alpha5 gamma-aminobutyric acid subtype A receptors to regulate synaptic plasticity and memory blockade. Anesthesiology 111:1025-1035.

Martin LJ, Zurek AA, MacDonald JF, Roder JC, Jackson MF, Orser BA (2010) Alpha5GABAA receptor activity sets the threshold for long-term potentiation and constrains hippocampus-dependent memory. J Neurosci 30:5269-5282.

McKernan RM, Quirk K, Prince R, Cox PA, Gillard NP, Ragan CI, Whiting P (1991) GABAA receptor subtypes immunopurified from rat brain with alpha subunit-specific antibodies have unique pharmacological properties. Neuron 7:667-676.

National Research Council (2011) Guide for the Care and Use of Laboratory Animals, Eighth Edition Edition. Washington, DC: The National Academies Press.

Nusser Z, Mody I (2002) Selective modulation of tonic and phasic inhibitions in dentate gyrus granule cells. J Neurophysiol 87:2624-2628.

Olsen RW, Sieghart W (2008) International Union of Pharmacology. LXX. Subtypes of gamma-aminobutyric acid(A) receptors: classification on the basis of subunit composition, pharmacology, and function. Update. Pharmacol Rev 60:243-260.

Orser BA (2007) Lifting the fog around anesthesia. Sci Am 296:54-61.

Patenaude C, Nurse S, Lacaille JC (2001) Sensitivity of synaptic GABA(A) receptors to allosteric modulators in hippocampal oriens-alveus interneurons. Synapse 41:29-39.

Pearce RA (1993) Physiological evidence for two distinct GABAA responses in rat hippocampus. Neuron 10:189-200.

Pi HJ, Hangya B, Kvitsiani D, Sanders JI, Huang ZJ, Kepecs A (2013) Cortical interneurons that specialize in disinhibitory control. Nature 503:521-524.

Prenosil GA, Schneider Gasser EM, Rudolph U, Keist R, Fritschy JM, Vogt KE (2006) Specific subtypes of GABAA receptors mediate phasic and tonic forms of inhibition in hippocampal pyramidal neurons. J Neurophysiol 96:846-857.

Renzel R, Sadek AR, Chang CH, Gray WP, Seifert G, Steinhauser C (2013) Polarized distribution of AMPA, but not GABAA , receptors in radial glia-like cells of the adult dentate gyrus. Glia 61:1146-1154.

Rudolph U, Antkowiak B (2004) Molecular and neuronal substrates for general anaesthetics. Nat Rev Neurosci 5:709-720.

Salesse C, Mueller CL, Chamberland S, Topolnik L (2011) Age-dependent remodelling of inhibitory synapses onto hippocampal CA1 oriens-lacunosum moleculare interneurons. J Physiol 589:4885-4901.

Sanna E, Murgia A, Casula A, Biggio G (1997) Differential subunit dependence of the actions of the general anesthetics alphaxalone and etomidate at gamma-aminobutyric acid type A receptors expressed in Xenopus laevis oocytes. Mol Pharmacol 51:484-490.

Schwarzer C, Tsunashima K, Wanzenbock C, Fuchs K, Sieghart W, Sperk G (1997) GABA(A) receptor subunits in the rat hippocampus II: altered distribution in kainic acid-induced temporal lobe epilepsy. Neuroscience 80:1001-1017.

Sieghart W, Sperk G (2002) Subunit composition, distribution and function of GABA(A) receptor subtypes. CurrTopMedChem 2:795-816.

Sperk G, Schwarzer C, Tsunashima K, Fuchs K, Sieghart W (1997) GABA(A) receptor subunits in the rat hippocampus I: immunocytochemical distribution of 13 subunits. Neuroscience 80:987-1000.

Sur C, Quirk K, Dewar D, Atack J, McKernan R (1998) Rat and human hippocampal alpha5 subunit-containing gamma-aminobutyric AcidA receptors have alpha5 beta3 gamma2 pharmacological characteristics. Mol Pharmacol 54:928-933.

Tsien JZ, Chen DF, Gerber D, Tom C, Mercer EH, Anderson DJ, Mayford M, Kandel ER, Tonegawa S (1996) Subregion- and cell type-restricted gene knockout in mouse brain. Cell 87:1317-1326.

Uchida I, Kamatchi G, Burt D, Yang J (1995) Etomidate potentiation of GABAA receptor gated current depends on the subunit composition. Neurosci Lett 185:203-206.

Velez-Fort M, Audinat E, Angulo MC (2012) Central role of GABA in neuron-glia interactions. Neuroscientist 18:237-250.

Wolff SB, Grundemann J, Tovote P, Krabbe S, Jacobson GA, Muller C, Herry C, Ehrlich I, Friedrich RW, Letzkus JJ, Luthi A (2014) Amygdala interneuron subtypes control fear learning through disinhibition. Nature 509:453-458.

Zarnowska ED, Keist R, Rudolph U, Pearce RA (2009) GABAA receptor alpha5 subunits contribute to GABAA,slow synaptic inhibition in mouse hippocampus. J Neurophysiol 101:1179-1191.

Zarnowska ED, Rodgers FC, Oh I, Rau V, Jurd R, Rudolph U, Eger EI, 2nd, Pearce RA (2014) Etomidate blocks LTP and impairs learning but does not enhance tonic inhibition in mice carrying the N265M point mutation in the beta3 subunit of the GABAA receptor submitted to Neuropharmacology or refer to chapter 3.

CHAPTER 5
Etomidate modulation of LTP in hippocampal CA1 region evaluated by CSD

Etomidate modulation of LTP in hippocampal CA1 region evaluated by CSD.

F. Clifford Rodgers[1,2] and Robert A. Pearce[2]

[1]Neuroscience Training Program, University of Wisconsin, Madison, WI 53705

[2]Department of Anesthesiology, University of Wisconsin, Madison, WI 53705

Corresponding author

Robert A. Pearce at rapearce@wisc.edu, University of Wisconsin, 1111 Highland Ave, WIMR II, Madison, WI 53705, +1 608 263 4429

Acknowledgments

This research was supported by a grant form the National Institutes of Health (NIH P01-GM47818) to RAP and a grant to the University of Wisconsin-Madison Neuroscience Training Program (NIH/NIGMS T32-GM007507).

Abstract

Excitatory synaptic transmission in the hippocampus has been studied extensively using extracellular and intracellular recording techniques. The current source density method allows for the reconstruction of current information from extracellular measures of voltage. Previous work has shown that measures of current source density reflect changes in synaptic transmission as a result of the induction of long-term potentiation (LTP). In the present work we compared the changes in CSD-derived peak amplitude of the synaptic sink (SyS) and field excitatory post-synaptic potential (fEPSP) slope in the hippocampal CA1 region during LTP induction using a theta burst protocol (TBS), in the absence and presence of amnestic concentrations of the clinically-used anesthetic etomidate.

We compared changes in average response amplitudes and stimulus-to-stimulus variability for the two measures, and examined the spatiotemporal profiles of CSD responses before, during, and after LTP induction. We show, for the first time, that suppression of LTP of the fEPSP slope corresponds to a suppression of LTP of the SyS in the presence of etomidate and that a measure of the CSD during the TBS corresponds to the measure of the fEPSP slope.

Introduction

The current source density (CSD) method estimates the net current flux in the extracellular space for voltage signals sampled synchronously or asynchronously by a linear array of electrodes across laminar cellular structures (Nicholson and Freeman, 1975; Pettersen et al., 2006). The currents of CA1 pyramidal cells in hippocampus are an ideal substrate to analyze using this method, resulting in the identification of a number of distinct sinks and sources that contribute to the generation of field excitatory postsynaptic potentials (fEPSPs) and population spikes (PS).

The physiological features of excitatory synaptic transmission in the hippocampus have been extensively characterized. Despite thorough investigations using intracellular and extracellular recording techniques, the origin, dynamics, and function of the currents evoked by excitatory synaptic transmission are still controversial (London and Hausser, 2005; Spruston, 2008). There are several currents that contribute to the generation of extracellular voltages in response to electrical stimulation of CA1 pyramidal cell afferents.

The synaptic sink (SyS) located in the apical dendrites that likely represents synaptic currents associated with excitatory transmission from CA3 to CA1 and thus corresponds to extracellular fEPSPs (Taube and Schwartzkroin, 1988; Herreras, 1990; Vida et al., 1995; Kloosterman et al., 2001). The

propagating dendritic sink (PrS) is a sink that actively progresses from the apical dendrites to the soma upon orthodromic stimulation, which is thought to represent the activation of voltage-dependent conductances in the dendrites that integrate dendritic signals and trigger action potentials at the soma (Herreras, 1990; Vida et al., 1995; Kloosterman et al., 2001; Kasuga et al., 2003). However there some data indicate a PrS that propagates from the soma to the dendrites in response to orthodromic stimulation (Richardson et al., 1987) and some were inconclusive (Miyakawa and Kato, 1986; Taube and Schwartzkroin, 1988).

Synaptic plasticity at excitatory synapses on hippocampal pyramidal cells is a commonly used cellular model for learning and memory (Hebb, 1949; Bliss and Collingridge, 1993; Martin and Morris, 2002; Martin et al., 2010). Long-term potentiation (LTP) and depotentiation (LTD) are mechanisms by which synaptic plasticity is changed over time, both of which can be induced in *in vitro* slice preparations through a variety of electrical and pharmacological paradigms (Bliss and Lomo, 1973; Larson et al., 1986; Bliss and Collingridge, 1993; Markram et al., 1997; Hyman et al., 2003; Otmakhov et al., 2004; Martin et al., 2010; Bliss and Collingridge, 2013). Since the influx of Ca^{2+} through NMDARs leading to a local increase in [Ca^{2+}] in the postsynaptic cell is necessary for the induction of LTP, characterizing dendritic excitability is critical for understanding the induction and expression of LTP (Collingridge et al., 1983; Tsien et al., 1996; Volianskis and Jensen, 2003; MacDonald et al., 2006).

The present investigation sought to assess changes in the amplitude of the SyS and the propagation velocity PrS following LTP induction using a theta-burst protocol (TBS). Since amnestic concentrations of anesthetics have previously been shown to suppress synaptic plasticity at CA1 pyramidal cell synapses (Rudolph and Antkowiak, 2004; Cheng et al., 2006; Benkwitz et al., 2007; Martin et al., 2009; Perouansky and Pearce, 2011), we used etomidate to suppress LTP of the fEPSP slope and looked for a similar suppression of SyS amplitude and PrS propagation velocity indicating changes in extrinsic synaptic strength and intrinsic dendritic excitability, respectively. We acquired data synchronously across the entire CA1 field, thus we were able to analyze the acute induction phase of LTP during the TBS.

Materials & Methods

All experiments were performed in accordance with the National Institutes of Health *Guide for the Care and Use of Laboratory Animals* (National Research Council, 2011) and were approved by the University of Wisconsin Institutional Animal Care and Use Committee, Madison, Wisconsin. All efforts were made to minimize the suffering of animals and to reduce the number of animals used. Mice used for these experiments were on the C57BL/6J background.

Slice preparation

The methods used in these experiments have previously been described (Blake et al., 2010). In brief, transverse (500 μm thick) hippocampal slices were prepared from mice aged 64 ± 2 days (10 mice total). Slices were recovered in carbogenated (95% O_2/5% CO_2) artificial cerebrospinal fluid (aCSF) containing (in mM) 127 NaCl, 1.9 KCl, 1.2 KH_2PO_4, 26 $NaHCO_3$, 1.4 $MgSO_4x7H_2O$, 2.2 $CaCl_2x2H_2O$, 2.5 ascorbic acid, 15 glucose and kept at room temperature (21-23 °C) until the recording.

Electrophysiology

Extracellular recordings were obtained using a 16-channel linear recording electrode (50 μm separating recording sites; NeuroNexus Technologies, Ann Arbor, MI) inserted orthogonal to the hippocampal layers in the middle of CA1 (Fig. 1A, B, and C). Slices were bathed in aCSF at a flow rate of 2.5-3.0 mL/min at an elevated temperature of 30 ± 0.5 °C. Field excitatory postsynaptic potentials (fEPSPs) were electrically evoked by a tungsten stereotrode stimulating electrode (0.5 MΩ, World Precision Instruments, Sarasota, FL) placed in *stratum radiatum*, activating Schaffer collateral/commissural fibers (SC). Recorded signals were digitized at 10 kHz using an analog-to-digital converter (Digidata 1440A, Molecular Devices, Sunnyvale, CA), amplified 1000x, band-pass filtered between

1-3000 Hz (Model Lynx-8 amplifiers, Neuralynx Inc., Tucson, AZ), and acquired using pClamp software (Version 10.2, Molecular Devices, Sunnyvale, CA). Stimuli of 0.1 ms duration were delivered using a constant current stimulus isolator (Model A365D, World Precision Instruments) at 0.03 Hz using stimulus intensity ("baseline") adjusted to evoke responses below half-maximal fEPSP amplitude. Baseline stimulus amplitude was typically between 50-90 μA and was not significantly different when chosen in the presence of etomidate (Drugfree: 76 ± 7 μA; 1μM etomidate: 125 ± 27 μA; $p = 0.1358$). The stimulus amplitude used to assess propagation velocity of the PrS was typically between 150-300 μA. The recording electrode site used for LTP analysis of the fEPSP was selected by choosing the site with the largest amplitude fEPSP in response to baseline stimulus.

CSD analysis

CSD analysis was performed using a custom-written analysis pipeline in MATLAB (MATLAB R2012a, The Mathworks Inc., Natick, MA), based on the cubic spline iCSD method (Pettersen et al., 2006), and was previously described (Blake et al., 2010). While there is heterogeneity in conductivity across the layers of laminated cortical structures, it only has a minor effect on the spatial profiles of

derived sinks and sources (Holsheimer, 1987; Kloosterman et al., 2001). Therefore we assumed uniform conductivity throughout our slices.

The peak amplitude of the CSD was used for LTP analysis of the CSD, measured in arbitrary units of $\mu A/mm^3$. The spatial features of the CSD were registered anatomically based on features of the fEPSP waveform recorded at each electrode position. Specifically, the electrode showing a characteristic PS waveform with a prominent left upward-going shoulder followed by a downward-going sharp spike and an upward-going right shoulder was used as the reference for the location of *stratum pyramidale* (Fig. 2B).

PrS measurement

The propagation velocity of the PrS was measured by visually inspecting CSD plots and selecting two points along the PrS with the computer mouse. The points were then used to compute the slope of the PrS, indicating the propagation velocity in m/s (Fig. 2D).

LTP Measurement

LTP was assessed at the electrode site showing maximum depolarization following baseline stimulation. Following a stable baseline period of less than

10% change in fEPSP amplitude over 30 minutes, LTP was evoked using a theta burst stimulus (TBS) protocol consisting of 3 trains, with 1 min between trains (ITI), of 150 total pulses. Each train consisted of bursts of 10 pulses at 100 Hz, delivered every 300 ms (i.e. bursts at approximately 3.33 Hz) at baseline stimulus intensity (Fig. 1D). LTP was analyzed as a ratio of the average fEPSP slope or peak amplitude of the SyS measured during the 10 min prior to TBS compared to the average fEPSP slope or peak of amplitude of the SyS over the last 10 min of recording, expressed as a percentage of the pre-tetanus baseline. Stimulus-to-stimulus response variation of these measures is expressed as a coefficient of variation (ssCV = SD/mean).

TBS analysis

Responses during TBS were analyzed for fEPSP slope, peak amplitude of the SyS, and total sink current. The total sink current was computed as the sum of the extracellular sinks during the TBS. Responses were normalized to the first burst of the TBS (Fig. 1D) and averaged for each burst.

Data analysis

Data analysis was performed using Clampfit (Version 10.2, Molecular Devices), MATLAB software and custom-written scripts (MATLAB R2012a), and custom-written R programming language scripts (R Foundation for Statistical Computing, Vienna, Austria).

Statistics

Data are presented as mean ± SEM unless indicated otherwise, with *N* specifying the number of slices. Two-tailed Student's t-test was used to compare means. The critical value for statistical significance was set at $p < 0.05$. All reported significant findings have survived correction for multiple comparisons using the Benjamini-Hochberg procedure (Benjamini and Hochberg, 1995).

Results

Profile of evoked currents

In response to baseline stimulation, a strong SyS was generated at positions along the electrode axis corresponding to the apical dendrites with a maximum sink amplitude ~150 *μ*m from *stratum pyramidale* (Fig. 2C and D). There was a corresponding passive source detected at positions along the

electrode axis corresponding to basal dendrites and somata and a smaller source centered ~450 μm from *stratum pyramidale* (Fig. 2C and D).

In response to suprathreshold stimulation, a PrS was generated in the at electrode positions corresponding to the apical dendrites ~175-300 μm from *stratum pyramidale* (Fig. 2D). Similarly to the subthreshold SyS, the PrS generated a passive source at electrode positions corresponding to basal dendrites and somata (Fig. 2D). There was an apparent SyS following suprathreshold stimulation, but it is partially obscured by the superimposed PrS (Fig. 2D). There was a brief sharp incision corresponding to a focal source in the dendrites following the PrS starting at ~250 μm away from *stratum pyramidale* and extending toward the hippocampal fissure (Fig. 2D).

LTP measured by CSD has reduced variability

In the absence of etomidate, TBS induced LTP of the fEPSP slope (166 ± 15%, N = 8, p = 2.2e-16; Fig. 3A) and the peak amplitude of the SyS (147 ± 7%, N = 6, p = 2.2e-16; Fig. 3B) which was reduced in the presence of 1 μM etomidate by 77% and 68%, respectively (fEPSP: 115 ± 12%, N = 8, p = 4.671e-16; SyS: 115 ± 17%, N = 6, p = p = 7.398e-8; vs. respective controls; Fig. 3A and B).

In the absence of etomidate, ssCV of the fEPSP slope (6.2 ± 2.2, N = 8; Fig. 4A) is not significantly different from the ssCV of the peak amplitude of the SyS (2.4 ± 0.8, N = 6, p = 0.038; Fig. 4A). There is a trend toward reduced variability in the SyS measure, but it does not survive correction for multiple comparisons. In the presence of etomidate there is no difference between the ssCVs (fEPSP: 5.8 ± 2.4, N = 8; SyS: 3.5 ± 1.4, N = 6, p = 0.15; Fig. 4A). The application of etomidate did not significantly alter ssCV for either measure compared to the absence of drug (fEPSP: p = 0.8234; SyS: 0.4297).

Examining the time course of the SyS revealed that there was an increase in the heterogeneity of synaptic strength in the presence of 1μM etomidate that stood out from the average, as indicated by the larger error bars (Fig. 3B). Although on average LTP of the SyS was reduced in the presence of etomidate, 2 of the slices showed decrease in SyS amplitude compared to the average, 2 slices showed change around the average, and 2 slices showed an increase.

Measures of synaptic transmission during the TBS did not reveal the source of the heterogeneity in LTP expression. During induction, the fEPSP slope in the dendrites was reduced in presence of etomidate (p = 9.72e-12; Fig. 6A), but the peak amplitude of the SyS was not (p = 0.1199; Fig. 6B). Similarly to the fEPSP slope, the total sink current during TBS was reduced in the presence of etomidate (p = 1.232e-6; Fig. 6C). We detected no significant differences between the absence and presence of etomidate among the raw values for the

initial burst used for normalization (fEPSP slope: p = 0.5901; SyS peak amplitude: p = 0.5125; total sink current: p = 0.4914).

Propagation velocity of PrS does not change following LTP-inducing stimulus

In order to investigate whether changes in dendritic excitability influenced the heterogeneity in LTP expression we observed, we measured propagation velocities of the PrS from 0.27 - 0.18 m/s (mean ± SEM: 0.22 ± 0.02 m/s, N = 5) in the absence of drug (Fig. 2D). In the presence of 1 μM etomidate the propagation velocity is not significantly changed (0.31 ± 0.05 m/s, N = 5, p = 0.2001). Following the induction of LTP, propagation velocity was not significantly altered in the absence (0.24 ± 0.05, N = 5, p = 0.7618; 2 out of 5 slices showed an increase in PrS velocity) or presence of 1 μM etomidate (0.49 ± 0.08, N = 5, p = 0.09214; 4 out of 5 slices showed an increase in PrS velocity).

The PrS propagated from the distal dendrites to the soma, in response to orthodromic electrical stimulation of SC inputs of CA1 pyramidal cells. The PrS initiated between 200-400 μm distal from *stratum pyramidale* and terminated between 0-50 μm toward the *stratum oriens*. During the TBS, a similar PrS was apparent, typically occurring on the second shock of a burst (Fig. 5A and C).

Discussion

Benefits of the current experimental preparation

The use of linear electrodes in the present experiments required careful and consistent placement to derive good CSD measurements. We were able to produce reliable CSD measurements from 6 of the 8 slices used in this study. While the use of optical measurements may allow for robust assessment of CSD (Kasuga et al., 2003), simultaneous acquisition of extracellular voltage and CSD using a linear electrodes in the middle of sliced hippocampal tissue rather than near the surface allows for better approximation of the conditions of *in vivo* recordings (Kloosterman et al., 2001) without the disturbance of repeated serial electrode penetrations (Miyakawa and Kato, 1986; Richardson et al., 1987; Taube and Schwartzkroin, 1988; Herreras, 1990; Vida et al., 1995). Additionally, recording *in vitro* in the absence of surgical anesthesia allowed for novel investigation of the effects of anesthetics on the SyS and PrS.

We did not detect several of the currents reported by others, such as a late sink (LS) centered ~150 μm ventral from the somata in *stratum pyramidale* (Herreras, 1990; Vida et al., 1995). Although the terminology is unclear with one report describing a propagating LS with characteristics similar to the PrS described here (Vida et al., 1995), we do not know whether the particular recording arrangement or analysis method precludes the detection of those

currents. These currents could be induced or revealed by serial electrode penetrations or the addition of surgical anesthesia, which were not performed in these experiments.

LTP of the SyS

A CSD analysis of LTP of excitatory synapses from SC revealed two intriguing properties of the SyS. Consistent with previous reports (Taube and Schwartzkroin, 1988; Vida et al., 1995), the peak amplitude of the SyS expresses a similar LTP following TBS, and displayed a trend toward relatively reduced response variation when compared to the measure of fEPSP slope. Furthermore, analyzing the peak amplitude of SyS reveals a variation in changes in synaptic strength in the presence of concentrations of etomidate that have been shown to suppress learning and memory and synaptic plasticity *in vivo* and *in vitro* (Cheng et al., 2006; Benkwitz et al., 2007; Martin et al., 2009). The CSD-derived measurement of the SyS allowed for the observation of a novel effect of etomidate: conversion of a reliable increase to a more variable increase, or even decrease, in synaptic strength following TBS. It is unsurprising that measuring the current reveals this heterogeneity because the size, kinetics, timing, and location of transient currents, such as Ca^{2+}, can affect the induction and

expression of LTP and LTD (Huerta and Lisman, 1995; Hyman et al., 2003; Volianskis and Jensen, 2003; MacDonald et al., 2006; Martin et al., 2010).

Function of the SyS

The SyS likely corresponds to depolarizing synaptic currents arising at SC synapses onto CA1 pyramidal cell dendrites in SR mediated by AMPA and NMDA receptors because the SyS has similar kinetics, location, and mechanisms (e.g. susceptibility to LTP and sensitivity anesthetics; Taube and Schwartzkroin 1988; Herreras 1990; Vida et al., 1995). The finding that total sink charge passed during TBS correlates with the amnestic effect of etomidate (Fig. 6C) likely reflects an increase in inhibition that blunts depolarization by the influx of Na^+ through AMPA and NMDA receptors leading to a relative decrease in influx of Ca^{2+}, and thus to the suppression of LTP (Jurd et al., 2003; Reynolds et al., 2003; Cheng et al., 2006; Benkwitz et al., 2007).

It is likely that the heterogeneity in synaptic strength we observed in the presence of etomidate revealed by analyzing the SyS reflects subtle variations in the synaptic plasticity over the CA1 pyramidal cell field that is lost when sampling voltage with sub-optimal electrode placement, and reflects a modulation of Ca^{2}+ entry that may show up in subtle ways during the TBS. Our analysis did not reveal the basis for the heterogeneity in synaptic strength, but we did observe

drug-dependent differences in measures of voltage and current during the induction of LTP.

We analyzed the peak amplitude of the SyS, total sink (inward) current (Gong et al., 2009) and fEPSP for each burst (Fig. 6). Whereas there was no clear indication of a source for the heterogeneity of synaptic plasticity, it is interesting that the total sink current evoked during the TBS correlates with the amnestic effects of etomidate and with the fEPSP slope measured during TBS, considering that the rise slope of the fEPSP is thought to primarily reflect synaptic currents which should be captured in the CSD by the peak of the SyS. It is our opinion that a more systematic and holistic investigation of the currents active during the TBS may reveal the source of increased heterogeneity in synaptic plasticity of the SyS in the presence of etomidate.

Propagation velocity of the PrS

We were able to detect PrS in 5 of 8 slices used for CSD analysis in the absence of drug. The propagation velocity measured in this report (0.22 ± 0.02 m/s) is consistent with previous reports (0.2 m/s, Herreras, 1990; 0.18 m/s, Vida et al., 1995; 0.14 m/s, Kloosterman et al., 2001; 0.17 m/s, Kasuga et al., 2003). In contrast with a previous report (Vida et al., 1995) we did not detect a significant change in the propagation velocity of the PrS following LTP induction,

although there is a trend toward an increase in propagation velocity following LTP induction in the presence of etomidate.

Function of the PrS

The PrS may underlie the coincidence detection function of dendrites, causing synaptic plasticity in response to coincident activation of multiple synaptic inputs along the dendrite. Dendritic Ca^{2+} spikes have been suggested to underlie the coincidence detection mechanism, and they follow a similar time course to the PrS (London and Hausser, 2005). The time course of the PrS is also consistent with mediation by fast voltage-dependent Na^{+} currents. It is likely that the PrS observed in our data reflects some combination of dendritic and somatic spikes, which also contribute to the population spike.

We did not see a change in the propagation velocity of the PrS following LTP induced by TBS. While we do replicate their finding that there is a change in the amplitude of the SyS corresponding to the change in the fEPSP slope following LTP induction, the lack of detecting a change in PrS could be due to differences in LTP induction protocol, smaller sample size, the stimulus intensity, and/or a failure to examine the EPSP-spike (E-S) potentiation as the earlier report failed to detect change in 5 out of 14 slices that did not show an E-S shift following LTP induction (Andersen et al., 1980; Vida et al., 1995). Our data are

consistent with an E-S shift occurring in most of the slices in the presence of etomidate, however we did not directly investigate E-S shift.

We observed an apparent incision in the distal dendrites at suprathreshold stimulus intensities and a smaller source at subthreshold stimulus intensities that are consistent with a previous report (Vida et al., 1995). At suprathreshold stimulus intensities, the incision follows the initiation of the PrS and overlaps with the SyS, which is consistent with a dendritic initiation of the currents leading to the generation of the PS. It is also possible that the currents generating the incision are passive sources superimposed on the existing dendritic SyS in conjunction with the large influx of positive charge at the soma during the PS.

It appears that PS amplitude depends on the amplitude and propagation velocity of the PrS, and therefore the stimulus intensity (Richardson et al., 1987; Herreras, 1990; Vida et al., 1995; Kloosterman et al., 2001). Accordingly in the present work we investigated corresponding stimulus intensities prior to and following LTP induction. No steps were taken to scale currents prior to and following LTP induction, but it is possible that early currents, such as the rise slope of the SyS could be used as a scaling factor to ensure comparisons of aspects of the CSD are not affected by E-S shift. Similarly, we took no steps to isolate the PrS from the underlying SyS during TBS, which we think complicated the interpretation of peak synaptic sink amplitude during the TBS (Fig. 6B).

Finally, it is possible that the mechanisms underlying the SyS and other

spatiotemporally overlapping dendritic sinks could be potentiated separately (Vida et al., 1995), obscuring shifts in E-S potentiation, however we observed no dendritic sinks separate from the SyS, which may be due to the smoothing caused by the use of the cubic spline iCSD method in the present investigation.

Conclusion

Our results are largely consistent with the prevailing explanation for the mechanisms underlying the SyS and PrS. While we did not detect any changes in the propagation velocity of the PrS following LTP induction using a TBS protocol, we were able to detect LTP of the SyS and the amplitude of the SyS had reduced variability compared to the fEPSP slope. Amnestic concentrations of the anesthetic etomidate were able to suppress the potentiation of the SyS analogous to the suppression of the fEPSP slope.

References

Andersen P, Sundberg SH, Sveen O, Swann JW, Wigstrom H (1980) Possible mechanisms for long-lasting potentiation of synaptic transmission in hippocampal slices from guinea-pigs. J Physiol 302:463-482.

Benjamini Y, Hochberg Y (1995) Controlling the False Discovery Rate: A Practical and Powerful Approach to Multiple Testing. Journal of the Royal Statistcal Society 57:289-300.

Benkwitz C, Liao M, Laster MJ, Sonner JM, Eger EI, 2nd, Pearce RA (2007) Determination of the EC50 amnesic concentration of etomidate and its diffusion profile in brain tissue: implications for in vitro studies. Anesthesiology 106:114-123.

Blake AJ, Rodgers FC, Bassuener A, Hippensteel JA, Pearce TM, Pearce TR, Zarnowska ED, Pearce RA, Williams JC (2010) A microfluidic brain slice perfusion chamber for multisite recording using penetrating electrodes. J Neurosci Methods 189:5-13.

Bliss TV, Lomo T (1973) Long-lasting potentiation of synaptic transmission in the dentate area of the anaesthetized rabbit following stimulation of the perforant path. J Physiol 232:331-356.

Bliss TV, Collingridge GL (1993) A synaptic model of memory: long-term potentiation in the hippocampus. Nature 361:31-39.

Bliss TV, Collingridge GL (2013) Expression of NMDA receptor-dependent LTP in the hippocampus: bridging the divide. Molecular brain 6:5.

Cheng VY, Martin LJ, Elliott EM, Kim JH, Mount HTJ, Taverna FA, Roder JC, MacDonald JF, Bhambri A, Collinson N, Wafford KA, Orser BA (2006) alpha 5GABA(A) receptors mediate the amnestic but not sedative-hypnotic effects of the general anesthetic etomidate. J Neurosci 26:3713-3720.

Collingridge GL, Kehl SJ, McLennan H (1983) Excitatory amino acids in synaptic transmission in the Schaffer collateral-commissural pathway of the rat hippocampus. J Physiol 334:33-46.

Gong N, Li Y, Cai GQ, Niu RF, Fang Q, Wu K, Chen Z, Lin LN, Xu L, Fei J, Xu TL (2009) GABA transporter-1 activity modulates hippocampal theta oscillation and theta burst stimulation-induced long-term potentiation. J Neurosci 29:15836-15845.

Hebb DO (1949) The organization of behavior; a neuropsychological theory. New York,: Wiley.

Herreras O (1990) Propagating dendritic action potential mediates synaptic transmission in CA1 pyramidal cells in situ. J Neurophysiol 64:1429-1441.

Holsheimer J (1987) Electrical conductivity of the hippocampal CA1 layers and application to current-source-density analysis. Exp Brain Res 67:402-410.

Huerta PT, Lisman JE (1995) Bidirectional synaptic plasticity induced by a single burst during cholinergic theta oscillation in CA1 in vitro. Neuron 15:1053-1063.

Hyman JM, Wyble BP, Goyal V, Rossi CA, Hasselmo ME (2003) Stimulation in hippocampal region CA1 in behaving rats yields long-term potentiation when delivered to the peak of theta and long-term depression when delivered to the trough. J Neurosci 23:11725-11731.

Jurd R, Arras M, Lambert S, Drexler B, Siegwart R, Crestani F, Zaugg M, Vogt KE, Ledermann B, Antkowiak B, Rudolph U (2003) General anesthetic actions in vivo strongly attenuated by a point mutation in the GABA(A) receptor beta3 subunit. FASEB J 17:250-252.

Kasuga A, Enoki R, Hashimoto Y, Akiyama H, Kawamura Y, Inoue M, Kudo Y, Miyakawa H (2003) Optical detection of dendritic spike initiation in hippocampal CA1 pyramidal neurons. Neuroscience 118:899-907.

Kloosterman F, Peloquin P, Leung LS (2001) Apical and basal orthodromic population spikes in hippocampal CA1 in vivo show different origins and patterns of propagation. J Neurophysiol 86:2435-2444.

Larson J, Wong D, Lynch G (1986) Patterned Stimulation at the Theta-Frequency Is Optimal for the Induction of Hippocampal Long-Term Potentiation. Brain Res 368:347-350.

London M, Hausser M (2005) Dendritic computation. Annu Rev Neurosci 28:503-532.

MacDonald JF, Jackson MF, Beazely MA (2006) Hippocampal long-term synaptic plasticity and signal amplification of NMDA receptors. Crit Rev Neurobiol 18:71-84.

Markram H, Lubke J, Frotscher M, Sakmann B (1997) Regulation of synaptic efficacy by coincidence of postsynaptic APs and EPSPs. Science 275:213-215.

Martin LJ, Oh GH, Orser BA (2009) Etomidate targets alpha5 gamma-aminobutyric acid subtype A receptors to regulate synaptic plasticity and memory blockade. Anesthesiology 111:1025-1035.

Martin LJ, Zurek AA, MacDonald JF, Roder JC, Jackson MF, Orser BA (2010) Alpha5GABAA receptor activity sets the threshold for long-term potentiation and constrains hippocampus-dependent memory. J Neurosci 30:5269-5282.

Martin SJ, Morris RG (2002) New life in an old idea: the synaptic plasticity and memory hypothesis revisited. Hippocampus 12:609-636.

Miyakawa H, Kato H (1986) Active properties of dendritic membrane examined by current source density analysis in hippocampal CA1 pyramidal neurons. Brain Res 399:303-309.

National Research Council (2011) Guide for the Care and Use of Laboratory Animals, Eighth Edition Edition. Washington, DC: The National Academies Press.

Nicholson C, Freeman JA (1975) Theory of current source-density analysis and determination of conductivity tensor for anuran cerebellum. J Neurophysiol 38:356-368.

Otmakhov N, Khibnik L, Otmakhova N, Carpenter S, Riahi S, Asrican B, Lisman J (2004) Forskolin-induced LTP in the CA1 hippocampal region is NMDA receptor dependent. J Neurophysiol 91:1955-1962.

Perouansky M, Pearce RA (2011) How we recall (or don't): the hippocampal memory machine and anesthetic amnesia. Can J Anaesth 58:157-166.

Pettersen KH, Devor A, Ulbert I, Dale AM, Einevoll GT (2006) Current-source density estimation based on inversion of electrostatic forward solution: effects of finite extent of neuronal activity and conductivity discontinuities. J Neurosci Methods 154:116-133.

Reynolds DS, Rosahl TW, Cirone J, O'Meara GF, Haythornthwaite A, Newman RJ, Myers J, Sur C, Howell O, Rutter AR, Atack J, Macaulay AJ, Hadingham KL, Hutson PH, Belelli D, Lambert JJ, Dawson GR, McKernan R, Whiting PJ, Wafford KA (2003) Sedation and anesthesia mediated by distinct GABA(A) receptor isoforms. J Neurosci 23:8608-8617.

Richardson TL, Turner RW, Miller JJ (1987) Action-potential discharge in hippocampal CA1 pyramidal neurons: current source-density analysis. J Neurophysiol 58:981-996.

Rudolph U, Antkowiak B (2004) Molecular and neuronal substrates for general anaesthetics. Nat Rev Neurosci 5:709-720.

Spruston N (2008) Pyramidal neurons: dendritic structure and synaptic integration. Nat Rev Neurosci 9:206-221.

Taube JS, Schwartzkroin PA (1988) Mechanisms of long-term potentiation: a current-source density analysis. J Neurosci 8:1645-1655.

Tsien JZ, Chen DF, Gerber D, Tom C, Mercer EH, Anderson DJ, Mayford M, Kandel ER, Tonegawa S (1996) Subregion- and cell type-restricted gene knockout in mouse brain. Cell 87:1317-1326.

Vida I, Czopf J, Czeh G (1995) A current-source density analysis of the long-term potentiation in the hippocampus. Brain Res 671:1-11.

Volianskis A, Jensen MS (2003) Transient and sustained types of long-term potentiation in the CA1 area of the rat hippocampus. J Physiol 550:459-492.

Figure legends

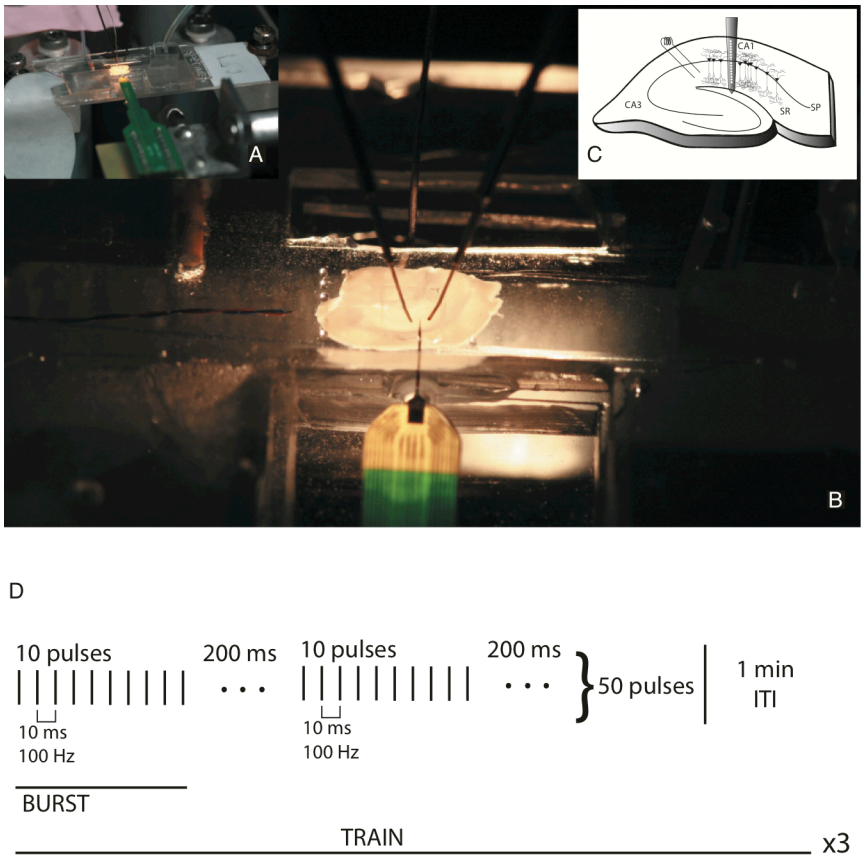

Fig. 1. Experimental setup and LTP induction protocol. (A) Photograph of the experimental setup showing the recording chamber and recording electrode. (B) Photograph of the experimental setup at higher magnification showing the placement of stimulating electrodes and the recording electrode. (C) Diagram showing the typical stimulating and recording electrode placement relative to the slice. (D) Diagram showing the theta burst stimulus (TBS) used to induce LTP. Vertical tick marks denote single electrical stimuli delivered to the Schaffer collateral axons synapsing on CA1 pyramidal cells. The tetanus delivers a total of 150 pulses. See accompanying methods for further description.

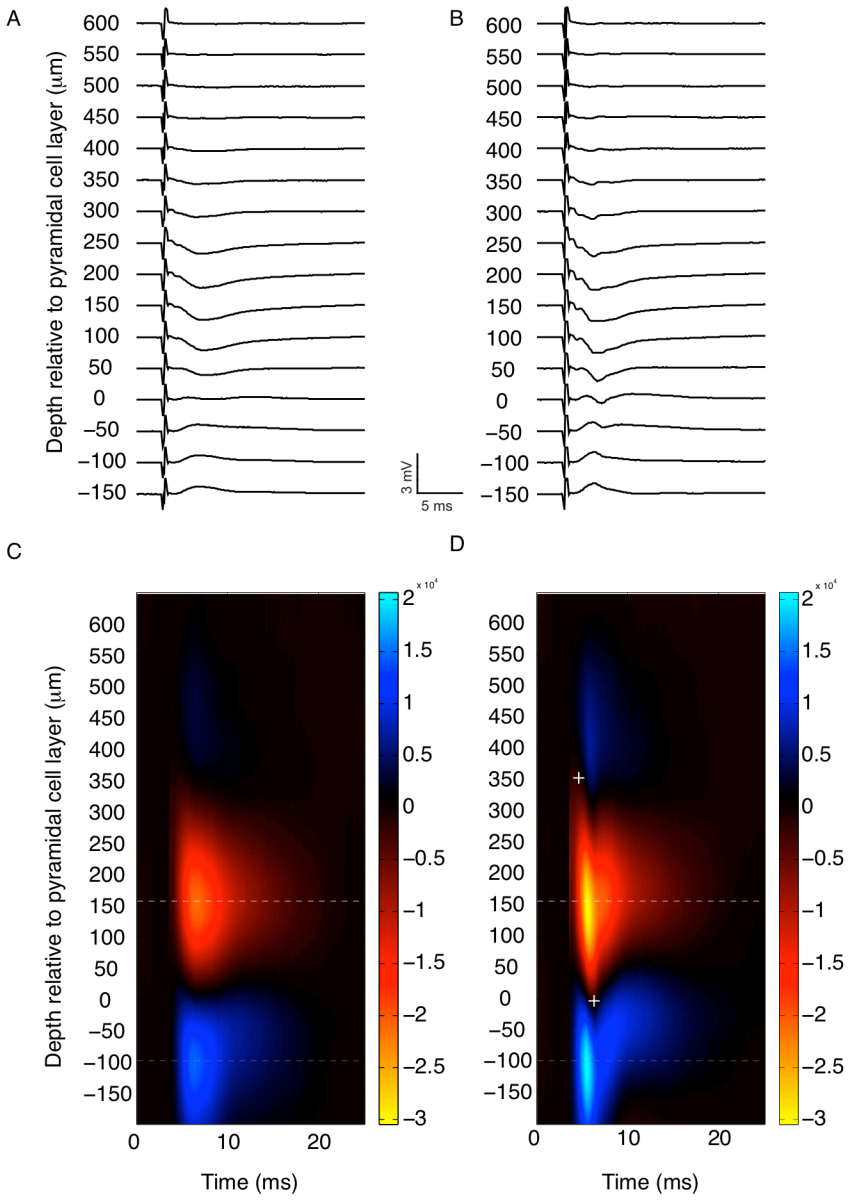

Fig. 2. Laminar profiles of evoked field potentials and corresponding current source density (CSD). (A and B) Evoked field potentials from CA1 pyramidal cells just below and just above threshold for evoking a population spike (See panel B, depth = 0 μm). Scale bar represents 3 mV by 5 ms. (C and D) Corresponding CSD profiles with warm colors representing current sinks and cool colors representing current sources (μA/mm^3, arbitrary units). A light gray dotted line and a dark gray line indicate the spatial location of the peak current sink in the synaptic sink and the corresponding peak current source in response to subthreshold stimulation, respectively. (D) White + symbols indicate the positions used for measurement of the propagation velocity of the propagating dendritic sink.

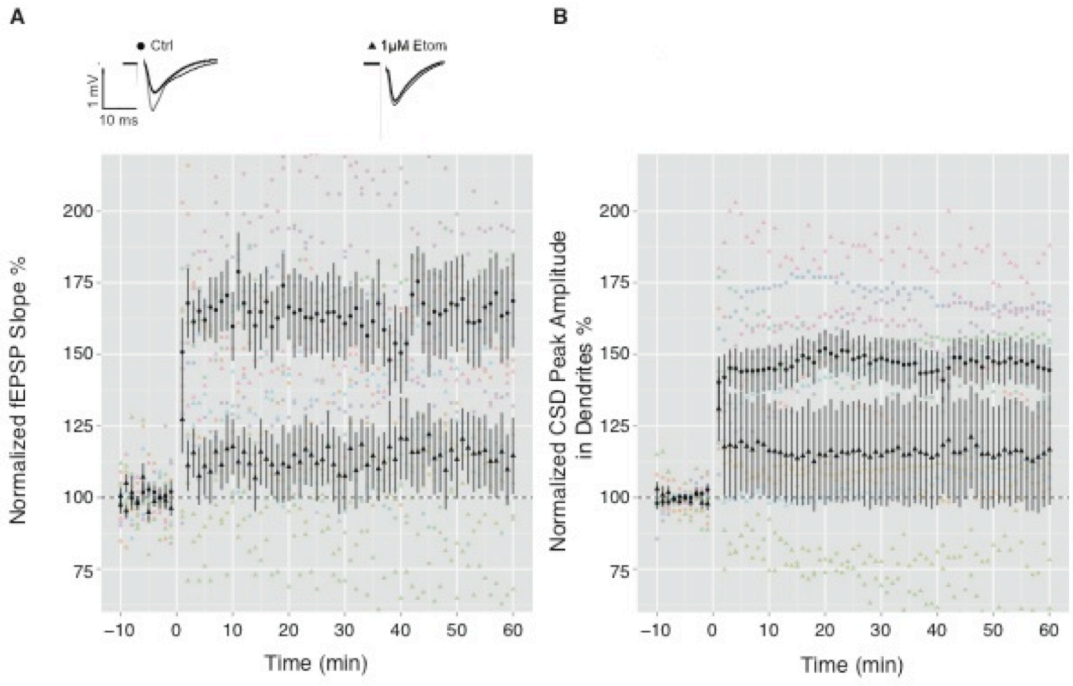

Fig. 3. Time course of long-term potentiation (LTP). (A and B) Summary time series showing LTP evoked by theta burst stimulus (TBS) assessed as average field excitatory postsynaptic potential (fEPSP) slope (A) or peak amplitude of the synaptic sink (SyS) (B) acquired 10 min prior to TBS and the last 10 min (51-60) following TBS in the absence (circles) and presence of 1μM etomidate (triangles). TBS occurred at time = 0. N = 6-8 slices per group. (A inset) Representative traces showing fEPSP measured in *stratum radiatum* of CA1 in the absence (Ctrl) and presence of etomidate (1 μM Etom). Traces show average fEPSPs acquired pre-TBS (thick line) and post-TBS (thin line). Scale bars indicate 1 mV and 10 ms.

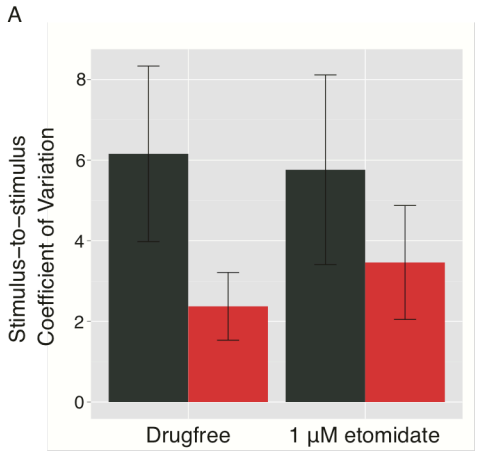

Fig. 4. Stimulus-to-stimulus coefficient of variation (ssCV). (A) Summary bar plots showing the stimulus-to-stimulus response variation expressed as a coefficient of variation (ssCV = SD / mean) between 50-60 min following theta burst stimulus (TBS). There are no significant differences between ssCV of the fEPSP slope measure (black bars) and ssCV of the peak amplitude of the synaptic sink (red bars) in the absence or presence of etomidate.

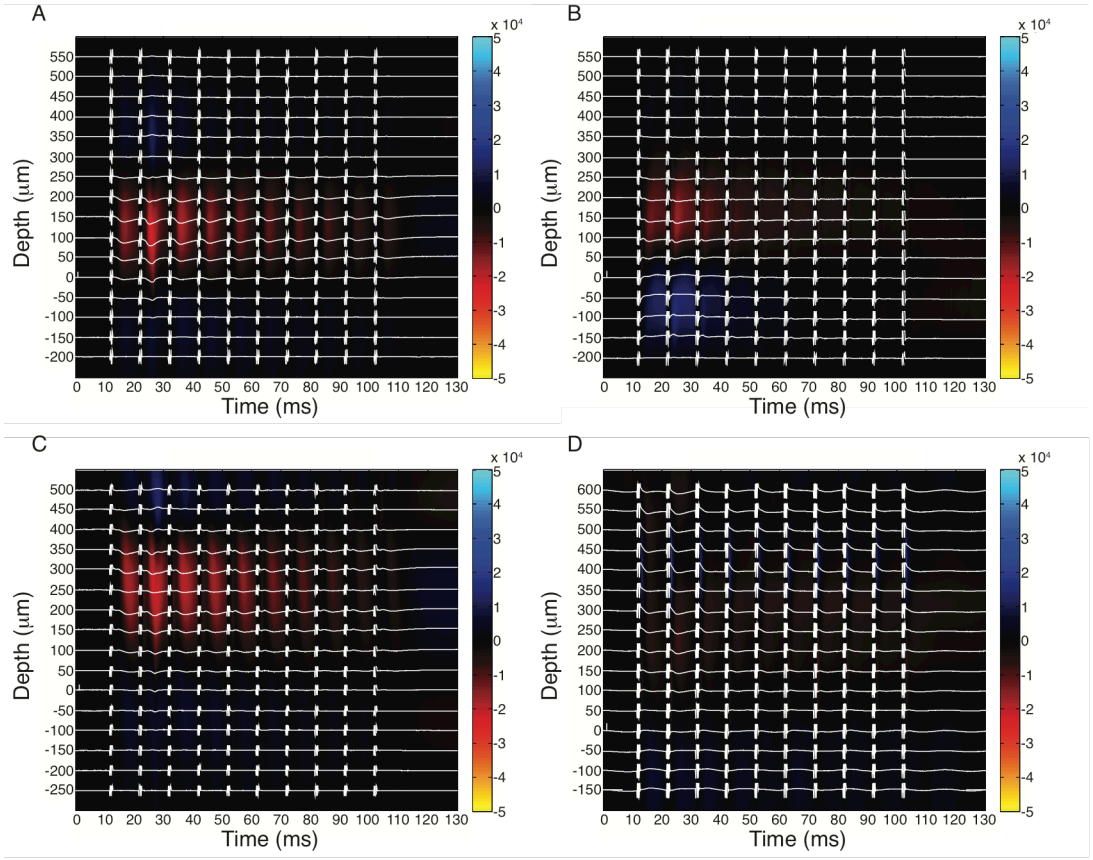

Fig. 5. Laminar profiles of the field excitatory post-synaptic potential (fEPSP) evoked during the first burst of theta burst stimulus (TBS) and the corresponding current source density (CSD). Evoked fEPSP response from CA1 pyramidal cells (white traces) superimposed on corresponding CSD profiles. Depth on the y-axis is expressed relative to *stratum pyramidale*, with positive depth indicating the direction of *stratum lacunosum moleculare* and the hippocampal fissure, and negative depth indicating the direction of *stratum oriens*. Warm colors represent current sinks; cool colors represent current sources (μA/mm^3, arbitrary units). Examples show TBS from a variety of recording conditions and LTP outcomes: (A) drugfree, large increase in synaptic strength; (B) 1μM etomidate, large increase in synaptic strength; (C) 1μM etomidate, average change in synaptic strength; (D) 1μM etomidate, decrease in synaptic strength. A propagating dendritic sink is apparent on the second stimulus of the burst in two of the examples (A and C). Scale bar near time = 0 at depth = 0 in all laminar profiles indicates 1 mV.

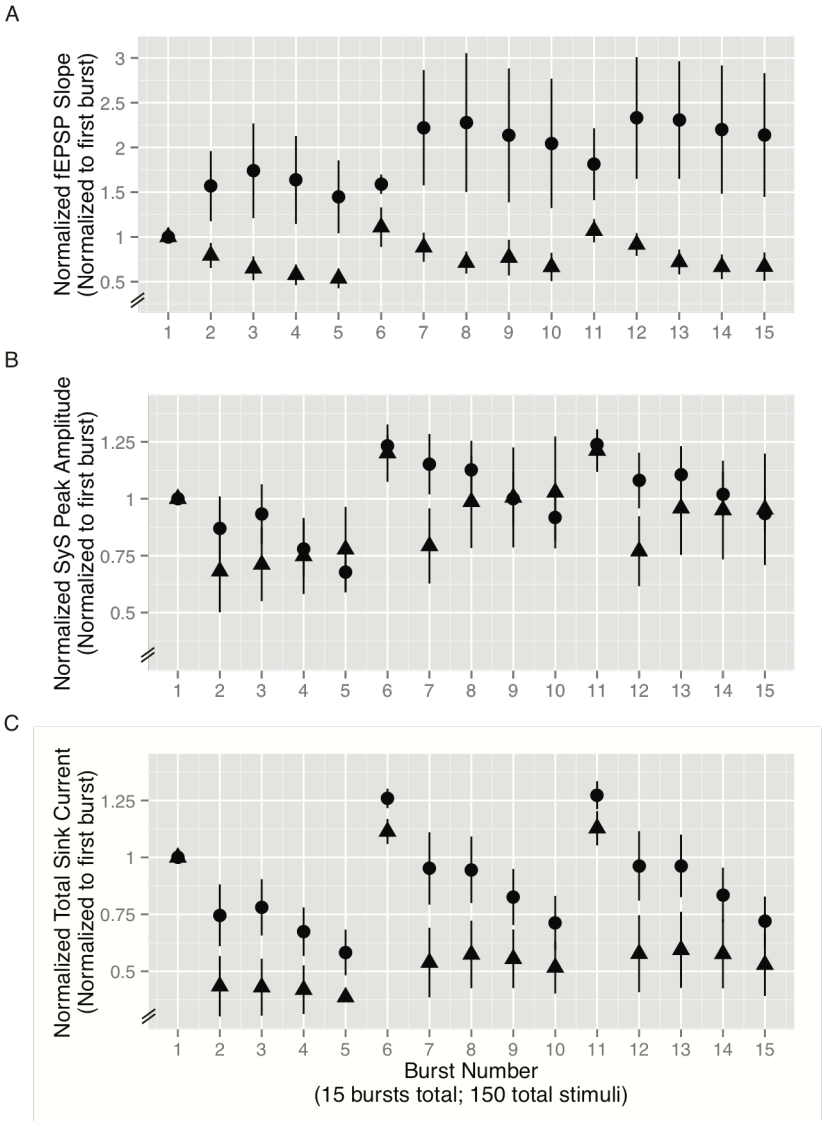

Fig. 6. Measures of synaptic transmission during TBS. Summary plots showing the (A) field excitatory post-synaptic slope (fEPSP), (B) peak amplitude of synaptic sink, and (C) total sink current for each of the bursts during the theta burst stimulus (TBS) normalized to the value derived from the initial burst in the absence (circle) and presence of 1μM etomidate (triangles).

CHAPTER 6
Conclusions & Future Directions

Conclusions

The work in this thesis demonstrates new evidence about the source of the inhibition that controls synaptic plasticity in CA1 of the mouse hippocampus. Using a novel recording setup that more closely mimics *in vivo* electrophysiology recording arrangements, I have narrowed down the targets of a commonly used anesthetic. By using an anesthetic with a relatively well-characterized pharmacology for $GABA_A$Rs as a tool to perturb the synaptic plasticity machinery, my research elucidates a mechanism for the control of synaptic plasticity by GABAergic inhibition in hippocampus.

It was previously thought that β3 subunit-containing $GABA_A$Rs were likely targets of etomidate to control anesthesia. However, the evidence presented here shows that etomidate is still able to suppress LTP evoked by TBS in CA1 of β3N265M mice expressing point-mutated etomidate-insensitive β3 subunits. These results are consistent with previous findings that demonstrate similar persistent sensitivity to anterograde amnesia produced by the anesthetics propofol and isoflurane *in vivo* in these β3N265M mice (Liao et al., 2005; Zeller et al., 2007) but a forebrain-specific knockout of β3 subunits suggests a partial contribution (Rau et al., 2011). These data suggest that β3-containing $GABA_A$Rs are not part of the population that controls LTP in CA1 pyramidal cells. Since β3-containing $GABA_A$Rs are rendered insensitive to etomidate in mutated animals, based on the likely $GABA_A$R subunit synthesis (and possibly expression) in CA1

pyramidal cells (Wisden et al., 1992) and the subunit profile of etomidate efficacy (Belelli et al., 1997; Sanna et al., 1997; Janssen et al., 2009), I infer that the persistent effects of etomidate in the animals mutated to express etomidate-insensitive β3-containing $GABA_ARs$ are likely mediated by β2-containing $GABA_ARs$ or β1-containing $GABA_ARs$.

These findings that implicate β2- or β1-containing $GABA_ARs$ are surprising, given the abundance of $\alpha5\beta3\gamma$ $GABA_ARs$ in CA1 pyramidal cells and evidence supporting a role for $\alpha5$-containing $GABA_ARs$ in controlling learning and memory (Martin et al., 2010). In fact, the data presented in this thesis replicate previous findings that etomidate targets $\alpha5$-containing $GABA_ARs$ to control synaptic plasticity induced by TBS in CA1 (Martin et al., 2009). Using a novel mouse line in which $\alpha5$-containing $GABA_ARs$ are selectively removed from excitatory cells in CA1 in conjunction with a mouse line in which $\alpha5$-containing $GABA_ARs$ are removed globally, the research presented in this thesis demonstrates that etomidate targets a population of $\alpha5$-containing $GABA_ARs$ on non-neuronal cells in CA1 to control synaptic plasticity. It is likely that this population of receptors resides on specific populations of interneurons.

The evidence suggests that etomidate targets a specific population of $\alpha5\beta2\gamma$ and/or $\alpha5\beta1\gamma$ $GABA_ARs$ on interneurons, which constitute a minority of the receptors present in CA1 relative to the more abundant $\alpha5\beta3\gamma$ $GABA_ARs$ (Sperk et al., 1997; Pirker et al., 2000). This would imply that the location of a small

population of receptors in the CA1 cellular network contributes to a disproportionately large impact on the dynamics of plasticity in the cells of CA1. The findings presented in this thesis fit into a larger body of work contributing to an emerging consensus for the role of inhibitory interneurons to control through direct inhibition on principal cells or through disinhibitory circuits (Freund and Gulyas, 1997; Leao et al., 2012; Lovett-Barron and Losonczy, 2013; Pi et al., 2013; Groen et al., 2014; Lovett-Barron et al., 2014; Wolff et al., 2014).

Future Directions

The data presented in this thesis provide several avenues for continuing research. Given the recent evidence that α5β2- and α5β3-containing $GABA_A$Rs show similar sensitivities to etomidate (Janssen et al., 2009), determining the β subunit partner for the α5-containing $GABA_A$Rs targeted by etomidate to control synaptic plasticity is paramount. Also determining the location of the non-pyramidal cells expressing these α5-containing $GABA_A$Rs will be necessary to develop a more complete picture of the mechanism of etomidate-induced amnesia, in addition to showing the type of inhibition modulated by etomidate. Finally, the majority evidence presented in this thesis comes from *in vitro* slice preparations. It would be nice to demonstrate a role for the circuit in mediating etomidate's effects on circuit dynamics and learning and memory *in vivo* to link these levels of investigation.

There are similar point mutations that render β2-containing $GABA_AR$s insensitive to etomidate (Desai et al., 2009). So directly testing etomidate's effects on LTP in mice expressing mutated β2 $GABA_AR$ subunits is one approach to characterizing the identity of the β subunit partner of the α5-containing $GABA_AR$s targeted by etomidate to control synaptic plasticity. However, there is still a possibility that β1-containing $GABA_AR$s are still sensitive in β2N265M mutant animals. The lack of a similar point mutation for β1 subunits necessitates a pharmacological investigation of the relative sensitivities of expressed α5β2-, α5β3-, and α5β1-containing $GABA_AR$s to etomidate. These experiments could demonstrate the likely target of etomidate at the low amnestic concentrations that are presented in this thesis.

It is more difficult to directly demonstrate the circuit location of the α5-containing $GABA_AR$s targeted by etomidate to control synaptic plasticity. It seems likely that interneurons in CA1 are cells that express the receptors, but it is not impossible that $GABA_AR$s on glia could affect synaptic transmission in CA1. To investigate the most likely possibility that interneurons express the $GABA_AR$s targeted by etomidate to control synaptic plasticity, one approach is to start by knocking the receptors out of the broadest possible class of interneurons and subsequently narrow the investigation to more specific classes (e.g. somatostatin-expressing interneurons) until a single likely type of interneuron emerges (e.g., restricting knockout to OLM cells using an α2-nicotinic ACh

receptor driver of Cre). Accordingly, pairing the evidence that etomidate targets α5-containing $GABA_A$Rs with mutation selective all interneurons (e.g. GAD-Cre) allows for the broadest knockout of these receptors from all interneurons in the brain. This approach would allow for the reuse of animals generated to derive the selective knockout of α5 subunits from CA1 pyramidal cells. The same line of mice could be used for subsequent tapering of the set of interneurons studied. At each step in the process, evidence to confirm the role of interneurons would consist of a lack of etomidate's ability to block TBS-induced LTP, similar to the results from mice lacking α5-containing $GABA_A$Rs globally. Of course it would be best to demonstrate that etomidate has no effect in mice lacking only the specific α5β2- and/or α5β1-containing $GABA_A$Rs implicated by the previously described research to determine the identity of the β subunit partner.

Even if there is strong evidence implicating a specific type of interneuron in mediating the amnestic effects of etomidate *in vitro*, there is no guarantee that the same circuits control synaptic plasticity and learning and memory in the intact animal. The data presented in this thesis present one step on the path of connecting *in vitro* studies to *in vivo* behavioral effects of etomidate on learning and memory. Subsequent behavioral studies using any new lines of knockout mice would serve to underscore the conclusions drawn at the *in vitro* cellular and network levels of investigation. Additionally, *in vivo* electrophysiology in behaving animals, specifically behaving animals undergoing learning and memory tasks,

would provide a more dynamic picture of the functioning of the putative interneuron circuit targeted by etomidate to control learning and memory. For example, there may be different populations of $GABA_ARs$ that control properties of ongoing oscillations that crucially support learning and memory in the hippocampus. There are possibilities that the described mechanism of etomidate targeting interneurons could affect the timing of theta oscillations or the relative strength of theta or gamma oscillations (Quilichini et al., 2010). The same approach used in this thesis, using an anesthetic to perturb the system in conjunction with genetic manipulations designed to remove specific targets of that anesthetic, could elucidate the underlying controlling circuits. These experiments, if undertaken, would represent an ideal link between the *in vitro* electrophysiological and *in vivo* behavioral studies.

References

Belelli D, Lambert JJ, Peters JA, Wafford K, Whiting PJ (1997) The interaction of the general anesthetic etomidate with the gamma-aminobutyric acid type A receptor is influenced by a single amino acid. Proc Natl Acad Sci U S A 94:11031-11036.

Desai R, Ruesch D, Forman SA (2009) Gamma-amino butyric acid type A receptor mutations at beta2N265 alter etomidate efficacy while preserving basal and agonist-dependent activity. Anesthesiology 111:774-784.

Freund TF, Gulyas AI (1997) Inhibitory control of GABAergic interneurons in the hippocampus. Can J Physiol Pharmacol 75:479-487.

Groen MR, Paulsen O, Perez-Garci E, Nevian T, Wortel J, Dekker MP, Mansvelder HD, van Ooyen A, Meredith RM (2014) Development of dendritic tonic GABAergic inhibition regulates excitability and plasticity in CA1 pyramidal neurons. J Neurophysiol 112:287-299.

Janssen MJ, Ade KK, Fu Z, Vicini S (2009) Dopamine modulation of GABA tonic conductance in striatal output neurons. J Neurosci 29:5116-5126.

Leao RN, Mikulovic S, Leao KE, Munguba H, Gezelius H, Enjin A, Patra K, Eriksson A, Loew LM, Tort AB, Kullander K (2012) OLM interneurons differentially modulate CA3 and entorhinal inputs to hippocampal CA1 neurons. Nat Neurosci.

Liao M, Sonner JM, Jurd R, Rudolph U, Borghese CM, Harris RA, Laster MJ, Eger EI, 2nd (2005) Beta3-containing gamma-aminobutyric acidA receptors are not major targets for the amnesic and immobilizing actions of isoflurane. Anesth Analg 101:412-418, table of contents.

Lovett-Barron M, Losonczy A (2013) Behavioral consequences of GABAergic neuronal diversity. Curr Opin Neurobiol 26C:27-33.

Lovett-Barron M, Kaifosh P, Kheirbek MA, Danielson N, Zaremba JD, Reardon TR, Turi GF, Hen R, Zemelman BV, Losonczy A (2014) Dendritic inhibition in the hippocampus supports fear learning. Science 343:857-863.

Martin LJ, Oh GH, Orser BA (2009) Etomidate targets alpha5 gamma-aminobutyric acid subtype A receptors to regulate synaptic plasticity and memory blockade. Anesthesiology 111:1025-1035.

Martin LJ, Zurek AA, MacDonald JF, Roder JC, Jackson MF, Orser BA (2010) Alpha5GABAA receptor activity sets the threshold for long-term potentiation and constrains hippocampus-dependent memory. J Neurosci 30:5269-5282.

Pi HJ, Hangya B, Kvitsiani D, Sanders JI, Huang ZJ, Kepecs A (2013) Cortical interneurons that specialize in disinhibitory control. Nature 503:521-524.

Pirker S, Schwarzer C, Wieselthaler A, Sieghart W, Sperk G (2000) GABA(A) receptors: immunocytochemical distribution of 13 subunits in the adult rat brain. Neuroscience 101:815-850.

Quilichini P, Sirota A, Buzsaki G (2010) Intrinsic circuit organization and theta-gamma oscillation dynamics in the entorhinal cortex of the rat. J Neurosci 30:11128-11142.

Rau V, Oh I, Liao M, Bodarky C, Fanselow MS, Homanics GE, Sonner JM, Eger EI, 2nd (2011) Gamma-aminobutyric acid type A receptor beta3 subunit forebrain-specific knockout mice are resistant to the amnestic effect of isoflurane. Anesth Analg 113:500-504.

Sanna E, Murgia A, Casula A, Biggio G (1997) Differential subunit dependence of the actions of the general anesthetics alphaxalone and etomidate at gamma-aminobutyric acid type A receptors expressed in Xenopus laevis oocytes. Mol Pharmacol 51:484-490.

Sperk G, Schwarzer C, Tsunashima K, Fuchs K, Sieghart W (1997) GABA(A) receptor subunits in the rat hippocampus I: immunocytochemical distribution of 13 subunits. Neuroscience 80:987-1000.

Wisden W, Laurie DJ, Monyer H, Seeburg PH (1992) The distribution of 13 GABAA receptor subunit mRNAs in the rat brain. I. Telencephalon, diencephalon, mesencephalon. J Neurosci 12:1040-1062.

Wolff SB, Grundemann J, Tovote P, Krabbe S, Jacobson GA, Muller C, Herry C, Ehrlich I, Friedrich RW, Letzkus JJ, Luthi A (2014) Amygdala interneuron subtypes control fear learning through disinhibition. Nature 509:453-458.

Zeller A, Arras M, Jurd R, Rudolph U (2007) Identification of a molecular target mediating the general anesthetic actions of pentobarbital. Mol Pharmacol 71:852-859.